

การจำลองเชิงตัวเลขของกระแสน้ำในอ่าวไทยเปรียบเทียบข้อมูลจากภาพถ่ายดาวเทียม



นางสาวปัทมา สิงห์รักษ์

สถาบันวิทยบริการ  
จุฬาลงกรณ์มหาวิทยาลัย

วิทยานิพนธ์นี้เป็นส่วนหนึ่งของการศึกษาตามหลักสูตรปริญญาวิทยาศาสตรมหาบัณฑิต

สาขาวิชาวิทยาศาสตร์ทางทะเล ภาควิชาวิทยาศาสตร์ทางทะเล


คณะวิทยาศาสตร์ จุฬาลงกรณ์มหาวิทยาลัย

ปีการศึกษา 2545

ISBN 974-17-2835-2

ลิขสิทธิ์ของจุฬาลงกรณ์มหาวิทยาลัย

NUMERICAL MODELING OF EDDIES IN THE GULF OF THAILAND  
COMPARING WITH SATELLITE REMOTE SENSING DATA



Miss Patama Singhruck

A Thesis submitted in Partial Fulfillment of the Requirements  
for the degree of Master of Science in Marine Science

Department of Marine Science

Faculty of Science  
Chulalongkorn University

Academic Year 2002

ISBN 974-17-2835-2

จุฬาลงกรณ์มหาวิทยาลัย



ปีทมา สิงหาคม : การจำลองเชิงตัวเลขของกระแสน้ำในอ่าวไทยเปรียบเทียบกับข้อมูลจาก  
 ภาพดาวเทียม. (NUMERICAL MODELING OF EDDIES IN THE GULF OF  
 THAILAND COMPARING WITH SATELLITE REMOTE SENSING DATA)  
 อ.ที่ปรึกษา : ดร.ศุภิชัย ตั้งใจตรง, อ. ที่ปรึกษาร่วม : ดร.อานนท์ สนิทวงศ์ ณ อยุธยา,  
 94 หน้า. ISBN 974-17-2835-2.

การศึกษาระแสนน้ำในอ่าวไทยช่วงเดือนมกราคม 2543 ถึงเดือนกุมภาพันธ์ 2544 โดยใช้แบบ  
 จำลองทางคณิตศาสตร์ Princeton Ocean Model มีข้อมูลนำเข้าที่สำคัญคือ ข้อมูลลมราย 12  
 ชั่วโมงจากแบบจำลองสำหรับพยากรณ์อากาศของ Navy Operational Global Atmospheric  
 Prediction System และองค์ประกอบฮาร์โมนิกของน้ำขึ้นน้ำลงที่สำคัญ 4 ตัวคือ M2, S2, K1  
 และ O1 พบกระแสน้ำทั้งแบบหมุนตามเข็มนาฬิกาและหมุนทวนเข็มนาฬิกา ขนาดเส้นผ่าน  
 ศูนย์กลางระหว่าง 100 ถึง 200 กิโลเมตร กระแสน้ำที่เกิดขึ้นมีระยะเวลาประมาณ 2 วัน ถึง 2  
 สัปดาห์ เกิดขึ้นใน 2 บริเวณคือ อ่าวไทยตอนบนระหว่างละติจูดที่ 10 - 11 องศาเหนือและลองจิจูด  
 ที่ 101 - 102 องศาตะวันออก และบริเวณอ่าวไทยตอนล่างระหว่างละติจูดที่ 8 - 9 องศาเหนือและ  
 ลองจิจูดที่ 101.5 - 102.5 องศาตะวันออก จากการทำการทดลองเพื่อศึกษาอิทธิพลของลมและ  
 น้ำขึ้นน้ำลงต่อการเกิดกระแสน้ำพบว่า ลมเป็นปัจจัยหลักที่ทำให้เกิดกระแสน้ำ ขณะที่น้ำขึ้นน้ำลง  
 ไม่ใช่ปัจจัยที่จำเป็นต่อการเกิดกระแสน้ำ อย่างไรก็ตามพบว่าปฏิสัมพันธ์ระหว่างลมและน้ำขึ้น  
 น้ำลงส่งผลต่อลักษณะของกระแสน้ำที่เกิดขึ้น ข้อมูลจากดาวเทียม Sea-viewing Wide Field-of-  
 view Sensor (SeaWiFS) ระดับ 1A HRPT ในช่วงเวลาเดียวกันถูกนำมาแปลงให้เป็นภาพการ  
 กระจายของปริมาณความเข้มข้นของคลอโรฟิลล์เอในอ่าวไทยโดยใช้ความสัมพันธ์ตามสมการ  
 Ocean Chlorophyll 4 ไม่พบกระแสน้ำจากภาพดาวเทียมเนื่องจากข้อมูลในช่วงเวลาที่ศึกษา  
 ส่วนใหญ่ถูกเมฆบัง และช่วงความแตกต่างของคลอโรฟิลล์เอบริเวณกลางอ่าวมีค่าน้อย

ภาควิชา.....วิทยาศาสตร์ทางทะเล..... ลายมือชื่อนิสิต.....  
 สาขาวิชา.....วิทยาศาสตร์ทางทะเล..... ลายมือชื่ออาจารย์ที่ปรึกษา.....  
 ปีการศึกษา...2545..... ลายมือชื่ออาจารย์ที่ปรึกษาร่วม .....

# # 4272339023

:MAJOR MARINE SCIENCE

KEYWORD: EDDIES / GULF OF THAILAND / PRINCETON OCEAN MODEL / SeaWiFS

PATAMA SINGHRUCK : NUMERICAL MODELING OF EDDIES IN THE GULF OF THAILAND COMPARING WITH SATELLITE REMOTE SENSING DATA.

THESIS ADVISOR : SUPICHAJ TANGJAITRONG, Ph.D., THESIS CO-ADVISOR : ANOND SNIDVONGS, Ph.D., 94 pp. ISBN 974-17-2835-2.

Eddies in the Gulf of Thailand were studied using numerical ocean model in conjunction with satellite remote sensing. Princeton Ocean Model with 10-km spatial resolution was driven by combined 12-hour wind stress from Navy Operational Global Atmosphere Prediction System and 4 principal tidal constituents, M2, S2, K1 and O1 at open boundaries for the period between January 2000 to February 2001. Anticyclonic eddies and cyclonic eddies of 100 to 200 km spatial-scale are found. Eddies time scales are in the order of 2 days to 2 weeks. There are two main areas where eddies are recurrent. The first one locates at approximately between latitude 10-11 °N and longitude 101-102 °E. The other locates at approximately between latitude 8-9 °N and longitude 101.5-102.5 °E. Both areas lie in the middle of the Gulf where bottom depth exceeding 60 m. Numerical experiments show that wind is the major contributor to eddy generation in the Gulf of Thailand, while tide is not essential to eddy generation. However, interaction between wind and tide may account for the location and scale of eddies. Sea-viewing Wide Field-of-view Sensor (SeaWiFS) level 1A HRPT data of the concurrent period were analyzed for chlorophyll<sub>a</sub> concentration according to standard Ocean Chlorophyll 4 algorithm. Eddy is not detected from those images due to high cloud cover over the region and low chlorophyll<sub>a</sub> concentration in the middle of the Gulf where numerical results suggest existence of eddies.

Department.....Marine Science.....	Student's signature.....
Field of study.....Marine Science.....	Advisor's signature.....
Academic year.....2002.....	Co-advisor's signature.....

## ACKNOWLEDGEMENTS

I would like to express my sincere gratitude to Supichai Tangjaitrong, Ph.D., thesis advisor, for his advice and encouragement and Anond Snidvongs, Ph.D., thesis co-advisor, for his suggestion and support that I had received throughout my study. I am grateful to Assistant Professor Wilaiwan Utoomprurkporn, Ph.D., Associate Professor Absornsuda Siripong, Associate Professor Jack Asavanant, Ph.D., who served as thesis chairman and thesis committees respectively, for their suggestions. I am also thankful to Pramote Sojisuporn, Ph.D. for his advice.

The support provided by the following organizations are appreciated, namely, the Ministry of University Affairs for granting the scholarship; the Geo-Informatics and Space Technology Development Agency (Public Organization) for data from oceanographic buoys; the Hydrographic Department for data from tide gauge stations; the Department of Marine Science, Faculty of Science, Chulalongkorn University, for computer facilities; the Southeast Asia START Regional Center for computer facilities; SeaWiFS project (Code 970.2) and Distributed Active Archive Center (Code 902) at the Goddard Space Flight Center, Greenbelt, MD 20771 for production and distribution of the SeaWiFS data.

I would like to thank Lt. Viriya Luang-aram for technical help on numerical model and visualization software; Ms. Penjan Laongmanee for her help on visualization software; and friends at the Department of Marine Science for their helps and encouragements.

Lastly, I am indebted to my parents, brother and sister for their understanding and continuing support.

## CONTENTS

Thai abstract.....	iv
English abstract .....	v
Acknowledgements.....	vi
Contents.....	vii
List of tables .....	ix
List of figures .....	x
Chapter	
1 Introduction.....	1
1.1 Importance of the study.....	1
1.2 Objectives.....	2
1.3 Scope of the study.....	2
2 Literature review.....	3
2.1 Overview of the Gulf of Thailand oceanography.....	3
2.2 Eddy characteristics .....	5
2.3 Eddy generation mechanisms.....	6
2.4 Eddy detection by ocean color.....	9
3 Methodology.....	11
3.1 Numerical ocean model.....	11
3.2 Satellite remote sensing .....	24
4 Results.....	26
4.1 Model verification.....	26
4.2 Eddy characteristics in the Gulf of Thailand.....	40
4.3 Eddy generation mechanisms in the Gulf of Thailand.....	52
5 Discussion.....	63
5.1 Model verification.....	63
5.2 Eddy characteristics.....	64
5.3 Eddy generation mechanisms.....	64
5.4 Detection of eddy by ocean color images .....	66

	<b>viii</b>
6 Conclusions and recommendations.....	67
6.1 Conclusions.....	67
6.2 Recommendations.....	68
References.....	69
Appendices.....	75
Appendix A International Equation of state, 1980 .....	76
Appendix B Locations of tide gauge stations and oceanographic buoys .....	78
Appendix C Monthly mean wind stress and simulated current .....	80
Biography.....	94



สถาบันวิทยบริการ  
จุฬาลงกรณ์มหาวิทยาลัย



## LIST OF TABLES

Table 2.1	Spectral bands of SeaWiFS and their primary use.....	10
Table 3.1	Summary of numerical experiments.....	21
Table 4.1	Comparison of observed and calculated harmonic constants of the four principal tidal constituents M2, S2, K1 and O1.....	32
Table B.1	Location of coastal tide gauge stations and oceanographic buoys	78



สถาบันวิทยบริการ  
จุฬาลงกรณ์มหาวิทยาลัย

## LIST OF FIGURES

Figure 2.1	Current direction around high and low pressure centers in the northern and southern hemisphere.....	5
Figure 2.2	The effect of cyclonic wind in the northern hemisphere.....	8
Figure 3.1	Bathymetry of the Gulf of Thailand from ETOPO5 as used in the model .....	19
Figure 4.1	Computed elevation coamplitude and cophase for M2, S2, K1 and O1.....	28
Figure 4.2	Comparisons of M2 co-tidal charts.....	29
Figure 4.3	Comparisons of K1 co-tidal charts.....	30
Figure 4.4	Scatter diagrams for the amplitude and phase between the observed and calculated elevations for M2, S2, K1 and O1.....	31
Figure 4.5	Comparison of observed and calculated currents at Huahin from 23 August 2000 - 7 September 2000.....	35
Figure 4.6	Comparison of observed and calculated currents at Ko Sichang from 23 August 2000 - 7 September 2000.....	36
Figure 4.7	Comparison of observed and calculated currents at Ko Chang from 23 August 2000 - 7 September 2000.....	37
Figure 4.8	Comparison of observed and calculated currents at Huahin from 12-28 February 2001.....	38
Figure 4.9	Comparison of observed and calculated currents at Ko Sichang from 12-28 February 2001.....	39

Figure 4.10	Simulated daily averaged surface currents driven by NOGAPS wind and composite M2, S2, K1 and O1 tides at open boundaries on which eddies are present.....	43
Figure 4.11	Vertical structure of anticyclonic eddy on 12 September 2000.....	44
Figure 4.12	A time series of anticyclonic eddies in March 2000.....	45
Figure 4.13	A time series of anticyclonic eddies in September 2000.....	46
Figure 4.14	A time series of a dipole eddy in September 2000.....	47
Figure 4.15	A time series of a cyclonic eddies of January 2000.....	48
Figure 4.16	Chlorophyll_a concentration derived from SeaWiFS on 13 March 2000.....	50
Figure 4.17	Chlorophyll_a concentration derived from SeaWiFS on 3 April 2000.....	50
Figure 4.18	Chlorophyll_a concentration derived from SeaWiFS on 20 June 2000.....	51
Figure 4.19	Chlorophyll_a concentration derived from SeaWiFS on 25 February 2001.....	51
Figure 4.20	Comparison of simulated (a) wind-tidally driven current and (b) wind-driven current on 5 March 2000.....	52
Figure 4.21	Comparison of simulated (a) wind-tidally driven current and (b) wind-driven current on 12 September 2000.....	53
Figure 4.22	Comparison of simulated (a) wind-tidally driven current and (b) tide-induced residual current on 13 September 2000.....	54
Figure 4.23	Wind stress from NOGAPS and simulated current in March 2000 when an anticyclonic eddy was present and absent.....	57
Figure 4.24	Wind stress from NOGAPS and simulated current in September 2000 when a dipole eddy was present and absent .....	58
Figure 4.25	Wind stress from NOGAPS and simulated current in December 2000 when a cyclonic eddy was present and absent .....	59
Figure 4.26	Current driven by steady and uniform northeasterly wind.....	60

Figure 4.27	Current driven by steady and uniform easterly wind.....	61
Figure 4.28	Current driven by steady and uniform westerly wind.....	62
Figure 5.1	(a) current at 10 m depth driven by steady and uniform westerly wind of 5 m/s (b) current at 10 m depth driven by NOGAPS wind on 26 December 2000.....	66
Figure B.1	Location of coastal tide gauges and oceanographic buoys.....	79
Figure C.1	Monthly mean wind stress and simulated current in January 2000.....	80
Figure C.2	Monthly mean wind stress and simulated current in February 2000.....	81
Figure C.3	Monthly mean wind stress and simulated current in March 2000.....	82
Figure C.4	Monthly mean wind stress and simulated current in April 2000.....	83
Figure C.5	Monthly mean wind stress and simulated current in May 2000.....	84
Figure C.6	Monthly mean wind stress and simulated current in June 2000.....	85
Figure C.7	Monthly mean wind stress and simulated current in July 2000.....	86
Figure C.8	Monthly mean wind stress and simulated current in August 2000.....	87
Figure C.9	Monthly mean wind stress and simulated current in September 2000....	88
Figure C.10	Monthly mean wind stress and simulated current in October 2000.....	89
Figure C.11	Monthly mean wind stress and simulated current in November 2000....	90
Figure C.12	Monthly mean wind stress and simulated current in December 2000....	91
Figure C.13	Monthly mean wind stress and simulated current in January 2001.....	92
Figure C.14	Monthly mean wind stress and simulated current in February 2001.....	93

## CHAPTER 1

### INTRODUCTION

#### 1.1 Importance of the study

Eddy is a term describing a whirlpool-like rotating movement of fluids. It is the manifestation of turbulence motion. Eddies transport mass, momentum and energy (Robinson, 1983). Divergence and convergence of flow can be induced by eddies resulting in upwelling and downwelling respectively (Aristegui et al., 1997). Dissolved substance and particulate matter can be entrapped inside closed eddies (Bograd et al., 1994). As a result, their existence can affect distribution of physical and chemical properties as well as dispersion of some biological organisms or even pollutants (Robinson, 1983).

Although much knowledge of oceanographic processes in the Gulf of Thailand has been accumulated to date, those which pertain to eddy are still sketchy. Existence of eddies in the Gulf of Thailand was first suggested from pioneering oceanographic expedition in 1960 (Robinson, 1974). Since then, however, eddy has been given little attention. This may attribute to their characteristics of high variability both in space and in time. Accordingly, *in situ* observation may fail to detect it unless data are collected simultaneously over a certain period of time, adequately over eddy time scale (Robinson, 1983). Such a task is impossible by conventional observation. Therefore, other tools applicable to eddy investigation should be explored.

With the advent of satellite remote sensing technology, such long-term synoptic observations are made possible. While numerical model provides control environment where different eddy generation mechanism could be separated and studied its contribution which is otherwise not possible in the true ocean.

In order to manage the coastal environment soundly, sufficient knowledge on dynamical process such as eddy must be sought. The present study attempt to provide additional information on eddies in the Gulf of Thailand.

## 1.2 Objectives

1. To describe spatial and temporal characteristics of eddies in the Gulf of Thailand from numerical model and satellite remote sensing data
2. To identify major mechanism for eddy generation in the Gulf of Thailand

## 1.3 Scope of the study

1. Princeton Ocean Model, a three-dimensional model developed by Blumberg and Mellor (1987), was used to simulate eddies for the period between January 2000 to February 2001.
2. Sea-viewing Wide Field-of-view Sensor (SeaWiFS) data of the concurrent period were analyzed for chlorophyll<sub>a</sub> concentration to be used as a supplement in describing eddy patterns.
3. Numerical experiments were performed to identify eddy generation mechanisms.

## CHAPTER 2

### LITERATURE REVIEW

#### 2.1 Overview of the Gulf of Thailand oceanography

The Gulf of Thailand is a semi-enclosed basin located between latitude 6-14 °N and longitude 99-105 °E. Its major axis is 800 km and aligns in the northwest-southeast direction. Its minor axis is about 400 km. The Gulf of Thailand is essentially a part of the Sunda Shelf which is the shallow region to the southwest of the South China Sea. The averaged depth of the Gulf is about 50 m, with the deepest spot in the central part of about 83 m. The presence of a 40-m sill at the center of the mouth of the Gulf could restrict the exchange of the Gulf of Thailand bottom water with South China Sea water to a narrow channel, more than 60 m deep but only 50 km wide, at the center of the mouth (Snidvongs, 1998).

Circulation in the Gulf of Thailand is driven by the interplay of reversal monsoon wind, co-oscillation tide and density gradients (Robinson, 1974). The northeast monsoon prevails in November to February, while the southwest monsoon prevails in May to September. There are two periods of transition between the opposing monsoon winds. The first intermonsoon starts from March to April and the second intermonsoon occurs in October (Robinson, 1974). The major component of the circulation appears to be wind-induced motion (Robinson, 1974; Yanagi and Takao, 1998). However, circulation under different monsoon regimes reported by different authors using hydrographic data (Robinson, 1974) and numerical model (Buranapratheprat, 1997; Snidvongs and Sojisuporn, 1997; Lowwittayakorn, 1998; Yanagi and Takao, 1998) revealed great diversity. The discrepancy points out that the circulation in the Gulf is quite complex. The validity of each model result must be evaluated by taking into consideration each model assumptions as well as data used.

Stratification in the Gulf of Thailand varies seasonally (Yanagi et al., 2001). Large sea surface heating and weak wind during the intermonsoon period lead to most-developed stratification in March-May. Stratification is weakened during the SW

monsoon season due to stronger wind and vanishes in NE monsoon season due to sea surface cooling and intense vertical mixing by wind.

Density-driven current induced by the horizontal density difference between the head of the Gulf of Thailand and the South China Sea flows offshore in the upper layer and onshore in the lower layer during the stratified period from March to October. Water exchange between the Gulf of Thailand and the South China Sea is intensified in March-May when the stratification is developed (Yanagi et al., 2001).

Whether the Gulf of Thailand is characterized by barotropic or baroclinic flow is still on debate. Based on numerical results, Snidvongs and Sojisuporn (1997) proposed that currents in the mid-depth layer (10-40 m) flowed opposite to those of surface in every season. Water from mid-depth is the source of replenishment to surface water. In contrast, Yanagi and Takao (1998) proposed that circulations in the Gulf were nearly barotropic based on results from diagnostic numerical model in spite of inclusion of observed stratification. This fact led them to conclude that monsoon wind and tidal stress governed the circulation while density field only strengthened the magnitude of residual flow.

Tides in the Gulf of Thailand are the result of tidal waves propagation from the South China Sea, which are known as co-oscillation tides (Wyrcki, 1961). In general, diurnal components have larger amplitudes than semidiurnal components. The diurnal amplification in the Gulf is attributed to the resonance (Choi et al., 1997; Fang et al., 1999). Cotidal charts drawn from numerical model results (Choi et al., 1997; Fang et al., 1999) and TOPEX/POSEIDON altimeter data (Yanagi et al., 1997) show that semidiurnal (M2 and S2) tidal regimes are different from those of diurnal (K1 and O1) constituents. Cotidal charts of semidiurnal constituents are dominated by a clockwise rotating amphidromic system. This pattern rarely occurs in the northern hemisphere. Their nodal bands lie in NW-SE direction or major axis. Cotidal charts of diurnal components are dominated by counterclockwise rotating amphidromic system. Their nodal bands run in NE-SW direction or minor axis. Based on observation, mixed diurnal-dominated tide is prevalent in the Inner Gulf whereas diurnal tide is prevalent along the upper eastern



coast of Thailand and the upper part of Malay Peninsular. At the southern part of the Malay Peninsular, mixed semidiurnal-dominated tide prevails. Based on numerical model results (Hatamaya et al., 1996; Choi et al., 1997; Fang et al., 1999), K1 tidal currents are strong in the Gulf of Thailand in the order of 0.25 m/s. The major semi-axis of K1 tidal ellipses aligns along the Gulf major axis. M2 tidal ellipses are smaller in the order of 0.1 m/s.

## 2.2 Eddy characteristics

Eddy characteristics vary geographically. Their horizontal scales range from tens of kilometers to the low hundreds of kilometers. Their time scales range from weeks to months (Robinson, 1983; Kamenkovich et al., 1986).

Eddies can be categorized into cyclonic eddy and anticyclonic eddy (Kamenkovich et al., 1986). Flow around eddy is in approximate geostrophic equilibrium (Robinson, 1983). Conforming to geostrophic balance between horizontal pressure gradient force and Coriolis force, cyclonic eddy rotates around center of low pressure, while anticyclonic eddy rotates around center of high pressure in both hemispheres. In the northern hemisphere, cyclonic motion is anti-clockwise, while anticyclonic motion is clockwise. In the southern hemisphere, cyclonic motion is clockwise, while anticyclonic motion is anti-clockwise (Tomczak, 1996).

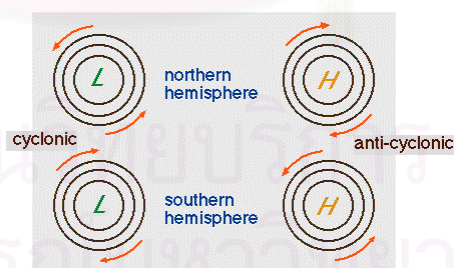


Figure 2.1 Current direction around high and low pressure centers in the northern and southern hemisphere (Tomczak , 1996).

In the region where hydrostatic pressure is high, the thermocline is depressed. Thus in the hydrographic section across anticyclonic eddy, the isotherms or equivalently

the isopycnals are depressed, while they are bulged up across cyclonic eddy. These distinctive characters are used to identify eddy from observed temperature and salinity.

Since hydrostatic pressure at any depth is determined by the weight of the water above it, high and low pressure are equivalent to high and low sea level. Hence cyclonic eddy is characterized by depressed sea surface, whereas anticyclonic eddy is characterized by elevated sea surface. Such characteristics allow eddy to be detected by calculation of dynamic height from hydrographic data (Namba, 2000; Qu, 2000) and recently by observing sea surface height from satellite altimeter such as TOPEX/POSEIDON (Ho et al., 2000; Hwang and Chen, 2000; Liu et al., 2001).

In northern hemisphere, cyclonic eddy causes divergence and induces upwelling whereas anticyclonic eddy causes convergence and induces downwelling. Thus cyclonic eddy is characterized by lower sea surface temperature to the surrounding and shallow thermocline. While anticyclonic eddy is characterized by higher sea surface temperature and deepening thermocline. Their sea surface temperature anomalies can be detected by Advanced Very High Resolution Radiometer (AVHRR) infrared imagery (Ikeda et al., 1984; Johannessen et al., 1989).

Upwelled water is usually nutrient-rich, and therefore able to support larger population of phytoplankton. Thus in northern hemisphere, cyclonic eddy is associated with high chlorophyll<sub>a</sub> concentration. Ocean color images from Coastal Zone Color Scanner (CZCS) and Ocean Color Temperature Scanner (OCTS) show close correlation of high chlorophyll<sub>a</sub> concentration associated with cyclonic eddies (Aristegui et al., 1997; Yokouchi et al., 2000).

### 2.3 Eddy generation mechanisms

Eddy generation mechanisms are baroclinic instability, barotropic instability, topographic irregularities and non-uniformities with corresponding scales in the fields of the wind stress curl (Kamenkovich et al., 1986).

Eddies seem to be most commonly generated in regions of the ocean where there are marked lateral density discontinuities, i.e. boundaries between different water

masses or fronts. Such regions are intrinsically unstable. If there is significant change of velocity with depth, i.e. strong vertical velocity shear, eddies may form. This mechanism is called baroclinic instabilities since there are associated with marked lateral variations in density (Open University Course Team, 1989). The baroclinic process is said to convert energy, which would otherwise be stored in the mean flow potential energy field, to eddy energy while the barotropic process converts mean flow kinetic energy to eddy energy (Robinson, 1983). Current flow perturbation by islands leads to the generation of eddies in the wake of the obstacle (Aristegui et al., 1997). In a rugged coastal environment, eddies can be shed by tidal current obstructs by islands and headland (Davies et al., 1995).

Open sea eddies are associated with flow convergence and divergence which can be described by Sverdrup balance (Tomczak, 1996). Currents in the upper ocean are directly affected by wind. The layer in which currents involve frictional force is known as Ekman layer. Below this layer, all movement is friction free. Movement below Ekman layer is induced by transfer of water to and from Ekman layer and the depth below as a result of flow convergence or divergence in Ekman layer. In the case of flow convergence, water is forced downwards to the depth below which is known as Ekman pumping. In the case of flow divergence, water is pumped upwards into the Ekman layer. This process is known as Ekman suction (Tomczak, 1996). Convergences and divergence of the Ekman transport are associated with the presence of wind stress curl. The curl of a field of vectors measures the tendency of the vector fields to induce rotation. Cyclonic wind stress curl produces divergence in the surface water and upwelling. Anticyclonic wind stress curl produces convergence and downwelling. Upwelling brings cold water from the deep to the surface and hence creates cold-core eddies; downwelling deepens the thermocline and hence creates warm-core eddies (Hwang and Chen, 2000). Figure 2.2 illustrates the effect of cyclonic wind and anticyclonic wind in the northern hemisphere.

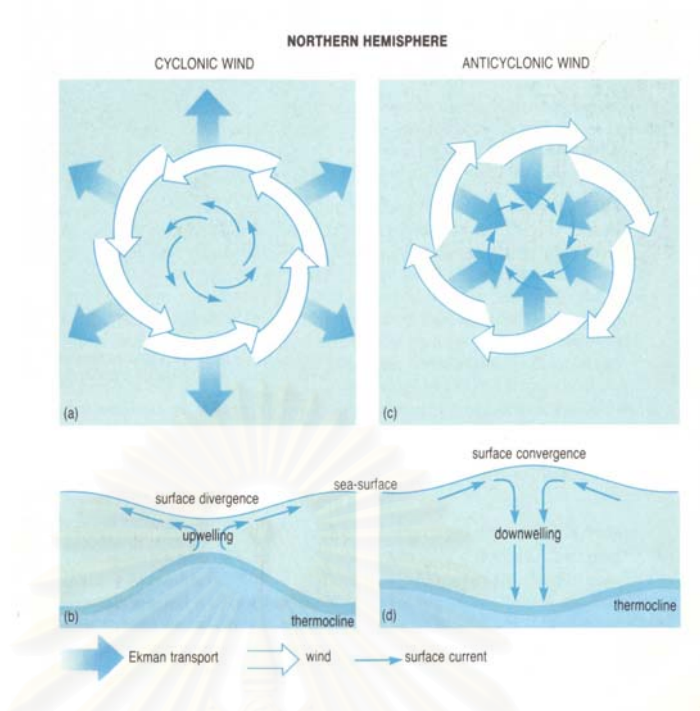


Figure 2.2 The effect of cyclonic wind in the northern hemisphere (a) on surface waters, (b) on the shape of the sea-surface and thermocline. Diagram (c) and (d) show the effects of an anticyclonic wind in the northern hemisphere. (Open University Course Team, 1989)

In different environment, these mechanisms contribute to eddies generation differently. Eddies in the Norwegian Coastal Current (Johannessen et al., 1989) are generated by the combined effect of topography and barotropic instability. Eddies in the California Current (Ikeda et al.; 1984, Pares-Sierra et al., 1993) are generated by local baroclinic instability and wind forcing adjacent to the coast. Eddies in the Alaska Coastal Current (Bograd et al., 1994) are generated by complex bottom topography and frontal activity at the interface of fresher and more saline waters leading to baroclinic instability. Wind stress curl, bottom topography and baroclinic instability are the mechanisms which generate eddies in the Black Sea (Rachev and Stanev, 1997). Wind stress curl causes the development of eddies by forcing strong Ekman pumping, which leads to water upwelling and downwelling (Longhurst, 1993). In South China Sea, wind stress curl is the main mechanism in eddy generation (Hwang and Chen, 2000). The location of cyclonic eddy and anticyclonic eddy in the surface and upper layers

correspond to areas with large positive (cyclonic) and negative (anticyclonic) curl of the wind stress (Namba, 2000; Qu, 2000).

## **2.4 Eddy detection by ocean color**

As already mentioned in section 2.2 that various satellite remote sensing can be applied to study eddy using its distinct characteristics, this study will explore whether ocean color can be used for eddy detection in the Gulf of Thailand.

### **2.4.1 Theory of measurement**

Ocean color remote sensing is based on the principle that particulate and dissolved substances suspended in water will interact with incident light. Where concentration of particulate matter and dissolved substances are low which is typical condition for the open ocean, water molecules scatter light similar to the way that the atmosphere scatters light, producing a characteristic deep blue color. The scattering of light by particulates and absorption of light by dissolved substances will alter this color. Chlorophyll, the photosynthetic pigment found in phytoplankton, absorbs strongly in red and blue regions of the visible light spectrum and reflects in the green. As the concentration of phytoplankton increases, the color of the water will therefore appear increasingly green. The absorption of light by chlorophyll can be quantified to determine the concentration of chlorophyll in water. The relationship between light absorption and chlorophyll concentration may be complicated by the presence of light-scattering inorganic particulate matter in the water. Particulate matter concentrations generally increase in coastal regions, such that the water color near the coast trends from green to brown or reddish brown. Even though chlorophyll may be present in higher concentrations near the coast, the presence of particulate matter makes it more difficult to extract the amount of light absorption due solely to chlorophyll (Kempner, 2000).

### **2.4.2 Ocean color sensor**

The Sea-viewing Wide Field-of-view Sensor (SeaWiFS) is an eight-channel visible light radiometer dedicated to global ocean color measurements. It is onboard the OrbView-2 satellite which orbits in a sun-synchronous, descending node orbit at an

altitude of 750 km. Local time of descending node is 12:05 PM  $\pm$  15 minutes. It provides regional data at a resolution of 1 kilometer. Table 2.1 lists the center wavelength for each of the eight SeaWiFS bands, along with the primary use of each wavelength. SeaWiFS bands 1-6 are 20 nm wide, and bands 7 and 8 are 40 nm wide (Kempfer, 2000).

Table 2.1 Spectral bands of SeaWiFS and their primary use.

Band	Center wavelength (nm)	Color	Primary use
1	412	violet	Dissolved organic matter
2	443	blue	Chlorophyll absorption
3	490	blue-green	Pigment absorption, Attenuation coefficient
4	510	blue-green	Chlorophyll absorption
5	555	green	Pigments, optical properties, sediment
6	670	red	Atmospheric correction and sediment
7	765	near IR	Atmospheric correction, aerosol radiance
8	865	near IR	Atmospheric correction, aerosol radiance

สถาบันวิทยบริการ  
จุฬาลงกรณ์มหาวิทยาลัย

## CHAPTER 3

### METHODOLOGY

The study of eddies in the Gulf of Thailand was based on two investigative tools. Numerical ocean model was used to reproduce the circulation in the Gulf under the influence of combined wind and tide for the period between January 2000 to February 2001. Characteristics of eddies were described from numerical model results. Satellite remote sensing data, specifically from SeaWiFS of concurrent period, were analyzed for chlorophyll\_a concentration. Eddies were identified by using chlorophyll\_a concentration as a tracer. Numerical experiments were subsequently performed to identify eddy generation mechanism.

#### 3.1 Numerical ocean model

The numerical model used in this study was the Princeton Ocean Model (POM) developed by Blumberg and Mellor (1987). It was originally constructed for predictions of the coastal ocean as well as estuarine circulation. It uses terrain-following sigma coordinate system to better represent variable bottom. The model predicts the evolution of the three-dimensional velocity, salinity and thermal structure in addition to the sea surface height. Parameterization of subgrid scale unresolved turbulent mixing is done by imbedded turbulence closure submodel.

##### 3.1.1 Governing equations

The model solves the Navier-Stokes equations of fluid dynamics with the gravitational buoyancy force (Archimedian force due to density stratification) and Coriolis force (from fictitious accelerations generated due to the non-inertial nature of the rotating coordinate frame). Two simplifying approximations are used. The first approximation exploits the fact that at certain scales of motion, the aspect ratio of the oceans is small and hence the vertical motions are small and are further inhibited by gravitational forces under stable density stratification. Thus vertical accelerations are small and the vertical frictional forces are also small, and the fluids acts as though it is

under static equilibrium as far as vertical motions are concerned. This is the so-called hydrostatic approximation, which yields an exact balance between the pressure gradient and the gravitational force in the vertical momentum equation. Second, density variations are neglected except where they are multiplied by gravity in the buoyancy force. In other words, changes in the mass or inertia of a fluid parcel due to changes in its density are negligible, while the same changes in density are consequential when a gravitational field is present. This is the so-called Boussinesq approximation and involves replacing density by a constant reference value everywhere except in terms involving the gravitational constant  $g$  (Kantha and Clayson, 2000).

Consider a system of Cartesian coordinates with  $x$  increasing eastward,  $y$  increasing northward, and  $z$  increasing upward. The free surface is located at  $z = \eta(x, y, t)$  and the bottom is at  $z = -H(x, y)$ . The velocity components  $(u, v, w)$  are in the  $(x, y, z)$  directions. Following Galperin and Mellor (1990), the entire set of the ensemble mean, primitive equations describing conservation of mass, momentum, temperature and salinity include, the continuity equation

$$\frac{\partial u}{\partial x} + \frac{\partial v}{\partial y} + \frac{\partial w}{\partial z} = 0. \quad (3.1)$$

For conservation of momentum, the Reynolds-averaged equations for mean quantities of turbulent flow are employed. They arise from the fact that flows in the ocean are turbulent and consist of random eddying motions superimposed on some statistical mean flow. It is therefore necessary to consider equations for average quantities, rather than instantaneous values. When such averaging is carried out, the nonlinear advection terms introduce additional terms in the momentum equations for the averaged quantities called Reynolds stresses or turbulent stresses (Kantha and Clayson, 2000).

$$\frac{\partial u}{\partial t} + \frac{\partial uu}{\partial x} + \frac{\partial uv}{\partial y} + \frac{\partial uw}{\partial z} - fv = -\frac{1}{\rho_0} \frac{\partial P}{\partial x} + \frac{\partial(-\overline{uw})}{\partial z} + F_u \quad (3.2)$$

$$\frac{\partial v}{\partial t} + \frac{\partial vu}{\partial x} + \frac{\partial vv}{\partial y} + \frac{\partial vw}{\partial z} + fu = -\frac{1}{\rho_0} \frac{\partial P}{\partial y} + \frac{\partial(-\overline{vw})}{\partial z} + F_v \quad (3.3)$$



where  $f$  is Coriolis parameter,  $\rho_0$  is reference density,  $P$  is pressure,  $(-\overline{uw})$  and  $(-\overline{vw})$  are turbulent stresses,  $F_u$  and  $F_v$  are related to small-scale mixing (describe below).

The integral of the hydrostatic equation is

$$P = P_{atm} + \rho_0 g \eta + g \int_z^0 \rho(x, y, s) ds$$

where  $P_{atm}$  is atmospheric pressure,  $g$  is gravitational acceleration and  $\rho$  is density.

The mean temperature equation is

$$\frac{\partial \theta}{\partial t} + \frac{\partial u \theta}{\partial x} + \frac{\partial v \theta}{\partial y} + \frac{\partial w \theta}{\partial z} = \frac{\partial(-\overline{w\theta})}{\partial z} + F_\theta \quad (3.5)$$

where  $\theta$  is potential temperature,  $(-\overline{w\theta})$  is turbulent heat flux and  $F_\theta$  is thermal diffusion.

The mean salinity equation is

$$\frac{\partial S}{\partial t} + \frac{\partial u S}{\partial x} + \frac{\partial v S}{\partial y} + \frac{\partial w S}{\partial z} = \frac{\partial(-\overline{wS})}{\partial z} + F_s \quad (3.6)$$

where  $S$  is salinity,  $(-\overline{wS})$  is turbulent salt flux and  $F_s$  is horizontal diffusion.

This set is completed by the equation of state (see Appendix A)

$$\rho = \rho(\theta, S). \quad (3.7)$$

The terms  $F_u, F_v, F_\theta$  and  $F_s$  are related to the small-scale mixing processes not directly resolved by the model and parameterized as horizontal diffusion:

$$F_u = \frac{\partial \tau_{xx}}{\partial x} + \frac{\partial \tau_{xy}}{\partial y}$$

$$F_u = \frac{\partial}{\partial x} (2A_M \frac{\partial u}{\partial x}) + \frac{\partial}{\partial y} [A_M (\frac{\partial u}{\partial y} + \frac{\partial v}{\partial x})] \quad (3.8)$$

$$F_v = \frac{\partial \tau_{xy}}{\partial x} + \frac{\partial \tau_{yy}}{\partial y}$$

$$F_v = \frac{\partial}{\partial y} (2A_M \frac{\partial v}{\partial y}) + \frac{\partial}{\partial x} [A_M (\frac{\partial u}{\partial y} + \frac{\partial v}{\partial x})] \quad (3.9)$$

$$F_{\theta, S} = \frac{\partial}{\partial x} [A_H \frac{\partial(\theta, S)}{\partial x}] + \frac{\partial}{\partial y} [A_H \frac{\partial(\theta, S)}{\partial y}] \quad (3.10)$$

where  $A_M$  and  $A_H$  are coefficients of horizontal viscosity and horizontal scalar diffusivity respectively.

The horizontal viscosity,  $A_M$ , is calculated according to Smagorinsky (1963, cited in Mellor, 1996):

$$A_M = C\Delta x\Delta y \frac{1}{2} [(\frac{\partial u}{\partial x})^2 + \frac{1}{2}(\frac{\partial v}{\partial x} + \frac{\partial u}{\partial y})^2 + (\frac{\partial v}{\partial y})^2]^{\frac{1}{2}} \quad (3.11)$$

where  $C$  is the coefficient of the Smagorinsky diffusivity.  $\Delta x$  and  $\Delta y$  are grid spacing.  $A_H$  is set equal to  $A_M$ .

Parameterization has been made for vertical turbulent momentum, heat and salt fluxes in the model where the vertical fluxes of horizontal turbulent momentum ( $-\overline{uw}$ ) and ( $-\overline{vw}$ ) are expressed in terms of the product of vertical eddy viscosity ( $K_M$ ) and vertical shear of the horizontal velocity. The vertical flux of heat ( $-\overline{w\theta}$ ) and salt ( $-\overline{wS}$ ) are given in terms of the product of vertical eddy diffusivity ( $K_H$ ) and vertical temperature gradient and vertical salinity gradient respectively.

$$-\overline{uw}, \overline{vw} = K_M \frac{\partial}{\partial z} (u, v) \quad (3.12)$$

$$-\overline{w\theta}, \overline{wS} = K_H \frac{\partial}{\partial z} (\theta, S) \quad (3.13)$$

The turbulent stresses and turbulent heat and salt fluxes are evaluated using the second-order turbulence closure scheme (level 2.5) developed by Mellor and Yamada (1982, cited in Mellor, 1996) wherein the vertical eddy viscosity coefficient ( $K_M$ ) and the vertical eddy diffusivity ( $K_H$ ) are parameterized based on turbulent energy and turbulent macroscale.

$$\begin{aligned} K_M &= S_M l q, \\ K_H &= S_H l q \end{aligned} \quad (3.14)$$

where  $l$  is the turbulence length scale and  $q$  is the turbulence velocity scale. The level 2.5 closure model adds two more prognostic equations to the model, describing the evolution of  $\frac{q^2}{2}$  and  $q^2 l$ . They are calculated from turbulence transport equation of the form

$$\frac{DF}{Dt} = (\text{diffusion of } F) + (\text{shear and buoyancy production of } F) + (\text{dissipation of } F) \quad (3.15)$$

where  $F$  denotes either  $\frac{q^2}{2}$  or  $q^2 l$ . The  $S_M$  and  $S_H$  are stability functions determined from algebraic relations derived analytically from small perturbation approximations to the full second-moment closure theory (Kantha and Clayson, 2000):

$$\begin{aligned} S_M &= A_1 \left\{ \frac{\left( 1 - \frac{6A_1}{B_1} - 3C_1 \right) + 9[2A_1 + A_2(1 - C_2)]S_H G_H}{(1 - 9A_1 A_2 G_H)} \right\}, \\ S_H &= A_2 \left\{ \frac{\left( 1 - \frac{6A_1}{B_1} \right)}{1 - 3A_2 G_H [6A_1 + B_2(1 - C_3)]} \right\}, \\ G_H &= \frac{l^2}{q^2} \frac{g}{\rho_0 D} \frac{\partial \rho}{\partial \sigma} \end{aligned} \quad (3.16)$$

The constants in (3.16) are mostly evaluated from near surface turbulence data and are found to be  $(A_1, A_2, B_1, B_2, C_1, C_2, C_3) = (0.92, 0.74, 16.6, 10.1, 0.08, 0.7, 0.2)$ .

The set of equations (3.1) - (3.16) is then transformed using the bottom and free-surface following sigma coordinate

$$\sigma = \frac{z - \eta}{D}, \quad D \equiv H + \eta \quad (3.17)$$

where  $\eta$  is the free surface elevation and  $H$  is the depth.

### 3.1.2 Boundary conditions

#### 3.1.2.1 Surface and bottom boundary conditions

The surface stress is set equal to the wind stress

$$K_M \frac{\partial}{\partial z}(u, v) = \frac{1}{\rho_0}(\tau_{0x}, \tau_{0y}) \quad (3.18)$$

where  $\tau_0 = (\tau_{0x}, \tau_{0y})$  is the wind stress vector and  $\rho_0$  is surface water density.

The surface wind stress is calculated using the quadratic drag law

$$(\tau_{0x}, \tau_{0y}) = \rho_a C_w |W|W \quad (3.19)$$

where  $\rho_a$  is the density of air,  $C_w$  is a drag coefficient and  $W$  is wind velocity vector.

$C_w$  is calculated from the observed wind speed.

$$C_w = 0.005 * (1.2 + \sqrt{1 + 0.02W^2}) \quad (3.20)$$

Parallel to the bottom, a quadratic bottom stress  $(\tau_{bx}, \tau_{by})$  is imposed

$$K_M \frac{\partial}{\partial z}(u, v) = \frac{1}{\rho_0}(\tau_{bx}, \tau_{by}) \quad (3.21)$$

$$(\tau_{bx}, \tau_{by}) = C_d \sqrt{u^2 + v^2}(u, v) \quad (3.22)$$

where the bottom drag coefficient is determined by matching a logarithmic bottom layer to the model at a height  $z_{ab}$  above the bottom

$$C_d = \text{MAX} \left[ \frac{k^2}{\left[ \ln\left(\frac{z_{ab}}{z_0}\right) \right]^2}, 0.0025 \right] \quad (3.23)$$

$k = 0.4$  is the von Karman constant and  $z_0$  is the bottom roughness,  $z_{,ab}$  is the height above the bottom of the first  $(u_b, v_b)$  grid node.

The surface boundary conditions for heat and salt are prescribed by surface heat flux  $Q_T$  and surface salinity flux  $Q_S$

$$K_H \left( \frac{\partial \theta}{\partial z}, \frac{\partial S}{\partial z} \right) = (Q_T, Q_S). \quad (3.24)$$

Zero flux boundary conditions for heat and salt are prescribed at the bottom

$$K_H \left( \frac{\partial \theta}{\partial z}, \frac{\partial S}{\partial z} \right) = (0, 0). \quad (3.25)$$

The surface and bottom boundary conditions for the turbulent kinetic energy and macroscale equations are

$$q^2 l = 0 \quad \text{and} \quad q^2 = B_1^{2/3} u_{\tau s}^2 \quad \text{at surface} \quad (3.26)$$

$$q^2 l = 0 \quad \text{and} \quad q^2 = B_1^{2/3} u_{\tau b}^2 \quad \text{at bottom} \quad (3.27)$$

where  $u_{\tau s}$  and  $u_{\tau b}$  are the friction velocities associated with the surface and bottom stresses, respectively, and  $B_1$  an empirical constant equals to 16.6.

### 3.1.2.2 Coastal boundary conditions

Perpendicular to any solid boundary, both the flux of mass and the velocity are set to zero. Since shear stress terms are included, a free-slip condition is applied on coastal boundaries by setting the gradient normal to the boundary of the tangential velocity to zero.

### 3.1.2.3 Open boundary conditions

On open boundaries a simple forced gravity wave radiation condition (Flather, 1988) on vertically integrated velocities is used,

$$U_n = \hat{U}_n \pm \frac{C}{H} (\eta - \hat{\eta}) \quad (3.28)$$

Here,  $C = \sqrt{gH} \cdot \hat{U}_n$  and  $\hat{\eta}$ , the input elevation and current, are prescribed functions of position and time, which may contain contributions of tidal and non-tidal origin. The tidal contribution is expressed in simple harmonic form,

$$\hat{\eta}(x, y, t) = H_i(x, y) * \cos\left(\frac{2\pi}{T_i}t - g_i(x, y)\right) \quad (3.29)$$

where  $T_i$  is the tidal period of constituent  $i$ ,  $H_i$  is the amplitude of constituent  $i$ ,  $g_i$  is the phase lag behind equilibrium constituent  $i$  on the Greenwich meridian with a similar expression for  $\hat{U}_n$ .

A gravity wave radiation condition is applied for three-dimensional velocities, while an upwind-advection scheme is applied for temperature and salinity.

### 3.1.3 Numerical scheme

The governing equations are discretized on staggered grids in which prognostic variables are calculated at alternate points. POM uses one particular arrangement out of five possible ones, called Arakawa C grids. Pressures are defined at the center of each cell and velocity components are defined at the cell faces. Such an arrangement makes the grid suitable for control volume discretization. All spatial derivatives are calculated using centered finite differences. The time integration marching uses leapfrog scheme. The scheme is explicit in the advective transport terms and, because of the generally finer mesh spacing in vertical direction, is implicit in the vertical diffusive flux terms. It is formally second-order accurate in space and time.

A mode splitting technique is used to integrate the governing equations in order to reduce the computational time, in which the calculation of depth-mean velocity and free surface (external mode) is separated from that of depth-dependent velocity and vertical structure of velocities, temperature, salinity and turbulence quantities (internal mode). Since the external mode represents the fast moving gravity waves, a small time step is required for the time integration of the free surface wave in order to satisfy the Courant-Friedrichs-Levy (CFL) condition. The internal mode is, however, integrated with

a much larger time step. A weak time filter of Asselin-Robert filter is included to prevent development of a computational mode with the leapfrog scheme.

### 3.1.4 Model grid and bathymetry

The Princeton Ocean Model domain for the Gulf of Thailand extended from latitude 5 - 14 ° N and longitude 99 - 107 ° E (Figure 3.1). The model used equally-spaced grids in the horizon with 0.1 degree resolution (approximately 11 km), and thus, contained 80x90 grids. The model uses bottom-following sigma coordinate grid in the vertical. There were 21 levels with finer resolution near the surface and the bottom. The bottom topography was obtained from the NOAA National Geophysical Data Center ETOPO5 database (5 minute by 5 minute resolution) by bilinear interpolation of the depth data onto the model grid.

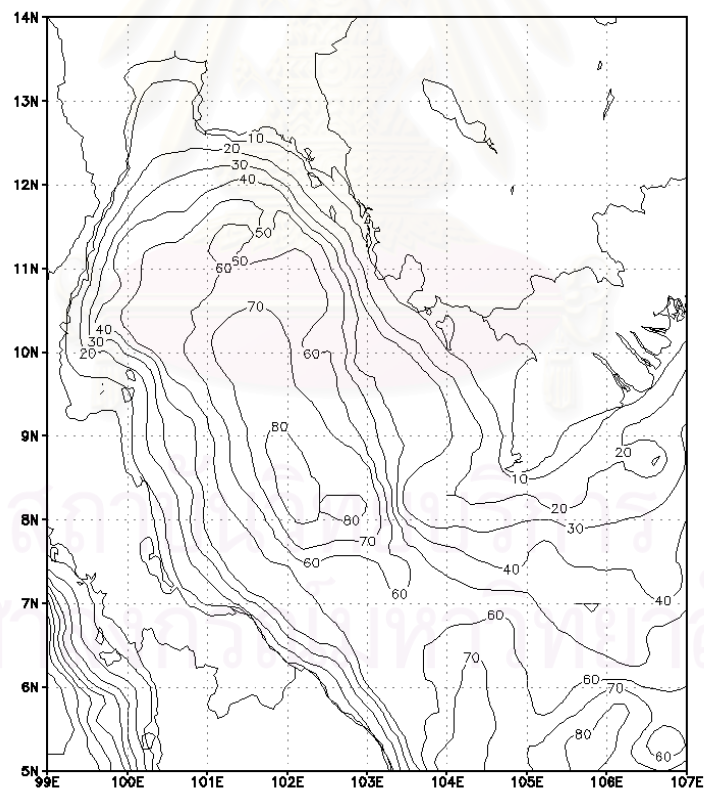


Figure 3.1 Bathymetry of the Gulf of Thailand from ETOPO5 as used in the model (contours in meter).

### 3.1.5 Details of numerical experiments

Eddy characteristics in the Gulf of Thailand were described from the point of view of numerical model simulation. Thus, first of all, numerical model results were verified with available *in situ* observations. Consequently, the model results were used to describe eddy characteristics. Numerical experiments were performed to identify eddy generation mechanisms. Table 3.1 summarizes numerical experiments performed in this study.

The prescribed tidal elevation and current at the East and South boundaries were derived from Oregon State University (OSU) Tidal Inversion Software (OTIS) regional-scale ( $1/6^\circ$ ) model of Indonesian Seas (Egbert and Erofeeva, 2002) in the form of harmonic constants. Four major tidal constituents used in this model compose of 2 semidiurnal constituents which are main lunar (M2) and main solar (S2) and 2 diurnal constituents which are lunisolar (K1) and main lunar (O1).

Wind stresses for the period between January 2000 to February 2001 were calculated from wind velocities at 10 m above mean sea level available from Navy Operational Global Atmospheric Prediction System (NOGAPS) (Hogan and Rosmond, 1991). The original data have 1 degree spatial resolution and 12 hour interval. They were interpolated to the model grids and the model time step by bilinear and linear interpolation respectively.

The model was integrated with all three components of velocity ( $u, v, w$ ) initially set to zero, and with temperature and salinity initialized by interpolating 1-degree-resolution climatology data (Levitus and Boyer, 1994; Levitus et al., 1994) to each model grid point. All simulations were initialized with Levitus's climatological temperature and salinity thus the model had horizontal density gradient and stratification. Temperature and salinity are prognostic variables, hence horizontal density gradient and stratification evolve in time.

There are two adjustable parameters in the model which are coefficient of Smagorinsky diffusivity (equation 3.11) and bottom roughness (equation 3.22). In this



study, the coefficient of Smagorinsky diffusivity was set to 0.01, while bottom roughness was set to 0.01 meter following the work of Thailand Research Fund.

Time integration is split into a two-dimensional external mode with a short time step of 10 seconds, and a three-dimensional internal mode with a longer time step of 10 minutes for all simulations.

Table 3.1 Summary of numerical experiments

Experiment	Purpose	Forcing variables	Integration (days)
V1	Verification (response to co-oscillation tide)	M2, S2, K1, and O1 tides	59
V2	Verification (response to combined wind and tide)	12-hour NOGAPS wind + M2, S2, K1, and O1 tides	425
EC	Eddy characteristics	12-hour NOGAPS wind + M2, S2, K1, and O1 tides	425
EM1	Eddy generation mechanism (contribution from tide)	12-hour NOGAPS winds	425
EM2	Eddy generation mechanism (contribution from non-uniform wind)	M2, S2, K1 and O1 tides	425
EM3	Eddy generation mechanism (contribution from uniform wind)	Uniform and steady wind of 2 m/s and 5 m/s from NE, E, SE, S, and W	15

### 3.1.5.1 Model verification

In this study, two major circulation driving terms in the Gulf of Thailand which are wind and tide were focused. To systematically investigate the model response to individual forcing term, the model was first driven by co-oscillation tide specified at the model open boundaries without wind stress at the model surface (experiment V1). Calculated tidal elevation constants were compared with observed ones at 18 coastal tide gauges (see Appendix B). Subsequently, the model was driven by inclusion of both wind stress at the model surface as well as prescribed tides at the open boundaries to simulate the current in the Gulf (experiment V2). Calculated current vectors were compared with observed current from oceanographic buoys (see Appendix B).

#### Experiment V1 (Model response to co-oscillation tide)

Tidal elevations and currents were computed by integrating the model forward in time from a state of rest with the composite M2, S2, K1 and O1 tidal elevations and transports specified at the East and South open boundaries (see details of calculation in section 3). Generally, the model needs some time before it approaches steady state. Five to nine day spin-up period are judged to be sufficient for the model to be independent of the initial condition for homogeneous water. Inclusion of stratification in the model results in longer spin-up period (Lee and Beardsley, 1999; Han, 2000). As the present model was initialized with climatological temperature and salinity, 30-day spin-up period was allowed. Then the model output from the following 29-day or 1 synodic month - from new moon to new moon (Pugh, 1987) – integration after the spin-up period was analyzed to retrieve amplitudes and phases of those constituents using harmonic analysis package.

#### Experiment V2 (Model response to a combination of wind and co-oscillation tide)

To simulate currents in the Gulf, wind stresses, calculated from NOGAPS wind, exerted at the model surface was included as well as co-oscillation tide at the open boundaries. Currents were computed by integrating the model forward in time from the state of rest starting from 1 January 2000. Calculated current vectors were compared

with available observed current measured by SEAWATCH buoys (Appendix B). Comparisons were done for two chosen periods to represent the different monsoon regimes. For each period, 15-days-comparison was chosen to account for variation due to spring-neap tidal cycle.

### 3.1.5.2 Eddy characteristics

#### Experiment EC

The analysis of eddy characteristics in the Gulf of Thailand for the period between January 2000 to February 2001 considered the current under the influence of wind from NOGAPS and composite M2, S2, K1 and O1 tides at the open boundaries. Daily-averaged currents were obtained by averaging current vectors at each grid over 25 hours to filter out tidal signal. In this study, eddy is defined as a closed circular path of current without predetermined spatial scales or time scales. However, the size of eddy which can be resolved by the present model is determined by the resolution of the model which is 0.1 degree (approximately 11 km).

### 3.1.5.3 Eddy generation mechanisms

As wind and tide are the two major circulation driving terms in the Gulf of Thailand, experiments were performed to investigate the contribution of individual term to eddy generation. The results of experiment EC were viewed as a control experiment against which the results from experiment EM1 and EM2 were compared. Experiment EC included various eddy generation terms which are wind forcing, tidal forcing, horizontal density gradient, stratification and topography. By excluding tidal forcing from the EC experiment while the rest was held unchanged (experiment EM1), contribution of tide to eddy generation was assessed. Likewise, by excluding wind forcing from the EC experiment while the rest was held unchanged (experiment EM2), contribution of wind to eddy generation was determined. Additional experiments were performed to investigate wind characteristics which could generate eddy in experiment EM3.

### Experiment EM1 (contribution from tide)

To investigate the contribution of tide on eddy generation in the Gulf of Thailand, the model was run by forcing wind stresses calculated from NOGAPS wind at the surface boundary while excluding tidal calculation at the open boundaries.

### Experiment EM2 (contribution from wind)

To investigate the contribution of wind on eddy generation in the Gulf of Thailand, the model was run by prescribing tide at the open boundaries without forcing wind stresses at the surface boundary.

### Experiment EM3 (uniform and steady wind)

Experiments were performed for the case of idealized uniform and constant wind blowing from northeast, east, southeast and west as they represent actual prevailing direction of wind in northeast monsoon season, the transition period and the southwest monsoon season respectively. For each wind direction, two experiments were carried out for wind magnitude of 2 m/s and 5 m/s representing the weak and strong wind conditions actually occurred. The model was integrated for 15 days.

## **3.2 Satellite remote sensing**

### **3.2.1 SeaWiFS image processing**

Sea-viewing Wide Field-of-view Sensor (SeaWiFS) level 1A HRPT data covering the area of the Gulf of Thailand spanning from September 1999 to February 2001 were obtained from NASA GSFC DAAC. Of nearly 400 scenes under the period of consideration, only one-fourth of those with cloud-free condition were processed to images of chlorophyll<sub>a</sub> concentration according to Ocean Chlorophyll 4 (OC4) algorithm (O'Reilly et al. 2000) using SeaDAS, the SeaWiFS Data Analysis System.

The fourth order polynomial equation for OC4 version 4 (maximum band ratio) is

$$C_a (\mu\text{g} / \text{l}) = 10.0^{(0.366 - 3.067R + 1.930R^2 + 0.649R^3 - 1.532R^4)} \quad (3.30)$$

where  $R = \log_{10} (R_{555}^{443} > R_{555}^{490} > R_{555}^{510})$ , where the argument of the logarithm is a shorthand representation for the maximum of the three values.

It should be noted that although OC4 algorithm used maximum band ratio of the three band ratios to account for wider ranges of chlorophyll\_a concentration in the ocean, it is still widely recognized as suitable for Case 1 water where phytoplankton are the prime constituent responsible for variations of optical properties of sea water. Certain parts of the Gulf of Thailand especially in the proximity of river mouths and shallow coastal zones belong to Case 2 water in which other substances such as suspended sediment and color dissolved organic matter may significantly contribute to the signal detected by the sensor. Thus the estimation of absolute value of chlorophyll\_a concentration in the Gulf is likely inexact. However, since this study was restricted to the use of variation of chlorophyll\_a concentration as a passive tracer to eddy rather than exact value of chlorophyll\_a concentration, the OC4 algorithm was then used without modification.

สถาบันวิทยบริการ  
จุฬาลงกรณ์มหาวิทยาลัย

## CHAPTER 4

### RESULTS

Eddy characteristics in the Gulf of Thailand were described from the point of view of numerical model simulation. Thus, first of all, numerical model results were verified with available *in situ* observations. Consequently, the model results were used to describe eddy characteristics. Ocean color images were used in supplement to identify eddy. Numerical experiments were performed to identify eddy generation mechanisms.

#### 4.1 Model verification

##### 4.1.1 Model response to co-oscillation tide

The model elevation from the 29-day integration after the 30-days spin-up period from experiment V1 was analyzed to retrieve amplitudes and phases of constituents using harmonic analysis package.

Co-amplitude and co-phase charts of the computed M2, S2, K1 and O1 constituents are presented in Figure 4.1. Simulated M2 co-tidal chart is dominated by an amphidromic point at the mouth of the Gulf near the eastern coast. The amphidrome rotates clockwise which rarely occurs in the Northern Hemisphere. At the middle of the Gulf, another tidal wave propagates northward toward the Inner Gulf in the form of standing wave. Simulated amplitudes usually remain below 10 cm except in two areas: the Inner Gulf where tidal amplification causes amplitude of more than 30 cm, and the area around Songkla of more than 20 cm. The M2 nodal axis aligns in NW-SE direction. The tidal regime of S2 is similar to that of M2.

Co-tidal chart of diurnal constituents, K1 and O1 exhibit similar spatial features. Counter-clockwise amphidromic points are located at the center of the Gulf near the western coast. The nodal axis run in NE-SW direction with tidal amplitude amplification toward the Inner Gulf.

These patterns of clockwise amphidromic system of semidiurnal components, counter-clockwise amphidromic system of diurnal components and diurnal amplification, are consistent with previous studies (Siripong, 1985; Choi et al., 1997; Yanagi et al., 1997; Fang et al., 1999) as shown in Figure 4.2 for M2 and Figure 4.3 for K1. Note that each model calculated phase refers to different meridians. This study use Thailand standard time (the meridian of  $105^{\circ}\text{E}$ ), while that of Choi et al. (1997) refers to the Greenwich and that of Fang et al. (1999) refers to the meridian of  $120^{\circ}\text{E}$ . Hence discrepancies of phase of the three models arise, eventhough the patterns of co-phase lines are similar.

Observed values of harmonic constants, amplitude and phase, of the four principal constituents, M2, S2, K1 and O1 tides at 18 coastal tide gauges (see Appendix B) were compared with those of computed values by the model as illustrated in Figure 4.4 and Table 4.1.

The amplitude comparison shows quite good agreement for the diurnal (K1 and O1) tides. However, discrepancies still exist for the semidiurnal (M2 and S2) tides. At the Inner Gulf (station 8-12 in Table 4.1), the present model underpredicts M2 amplitude by nearly 20 cm while overpredicts O1 amplitude by 10 cm. At the southwestern part of the Gulf (station 17-19), the model overpredicts S2 amplitude by more than 10 cm. Overall, the model biases toward underprediction for M2 and K1, while biases toward overprediction for S2 and O1.

Calculated phases of M2 and S2 lag observed phases by about 30-90 degree, or in other words, the calculated time of highest M2 and S2 tide at each place are 1-3 hours behind the actual time of occurrence. While calculated phases of K1 and O1 leads observed phases by about 90 degree, or, the calculated time of highest K1 and O1 tide at any place are 6 hours earlier than actual time of occurrence.

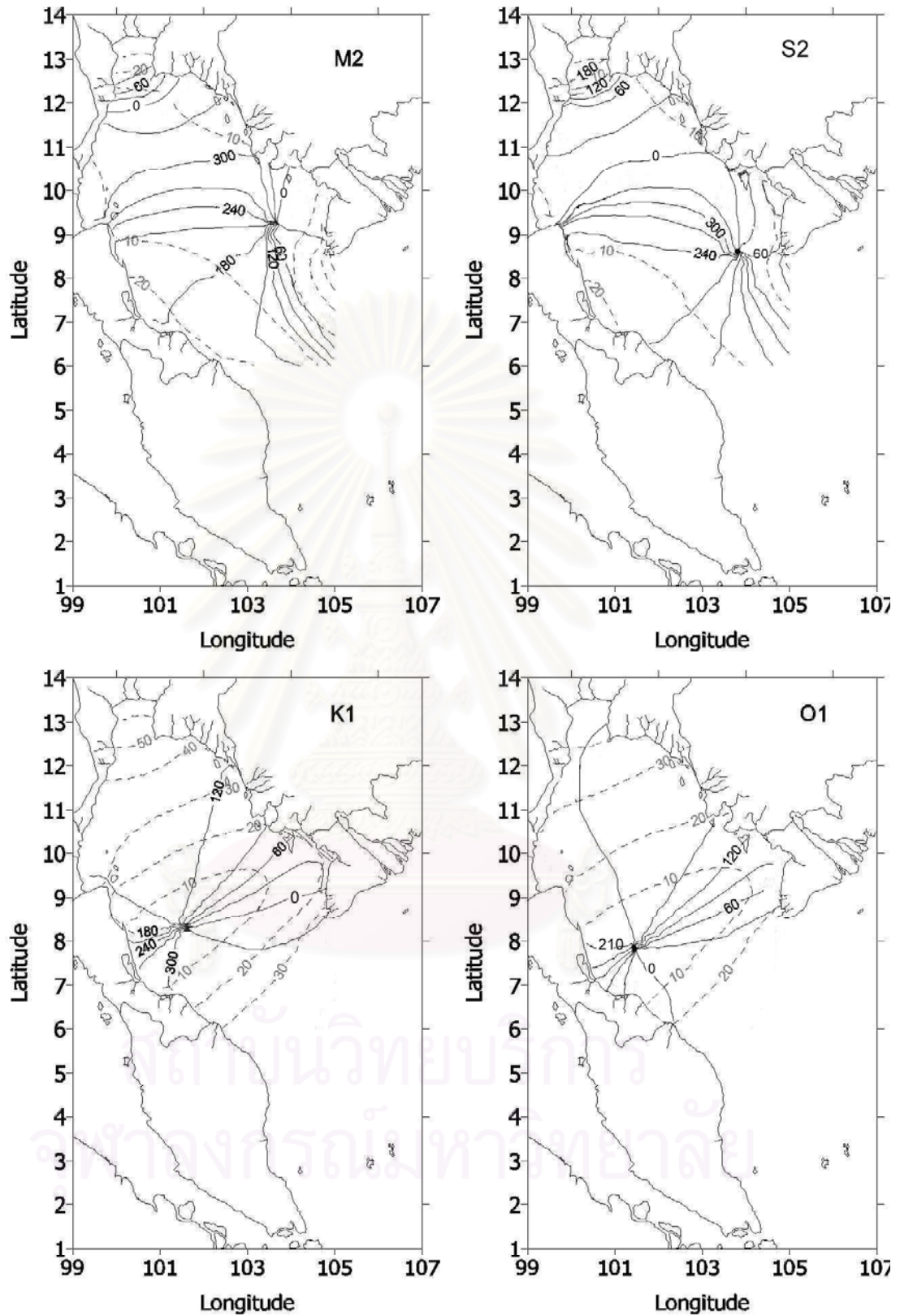


Figure 4.1 Computed elevation coamplitude (dash line, in centimeter) and cophase (in degree) for M2, S2, K1 and O1. Phase refers to the meridian of  $105^{\circ}$  E.



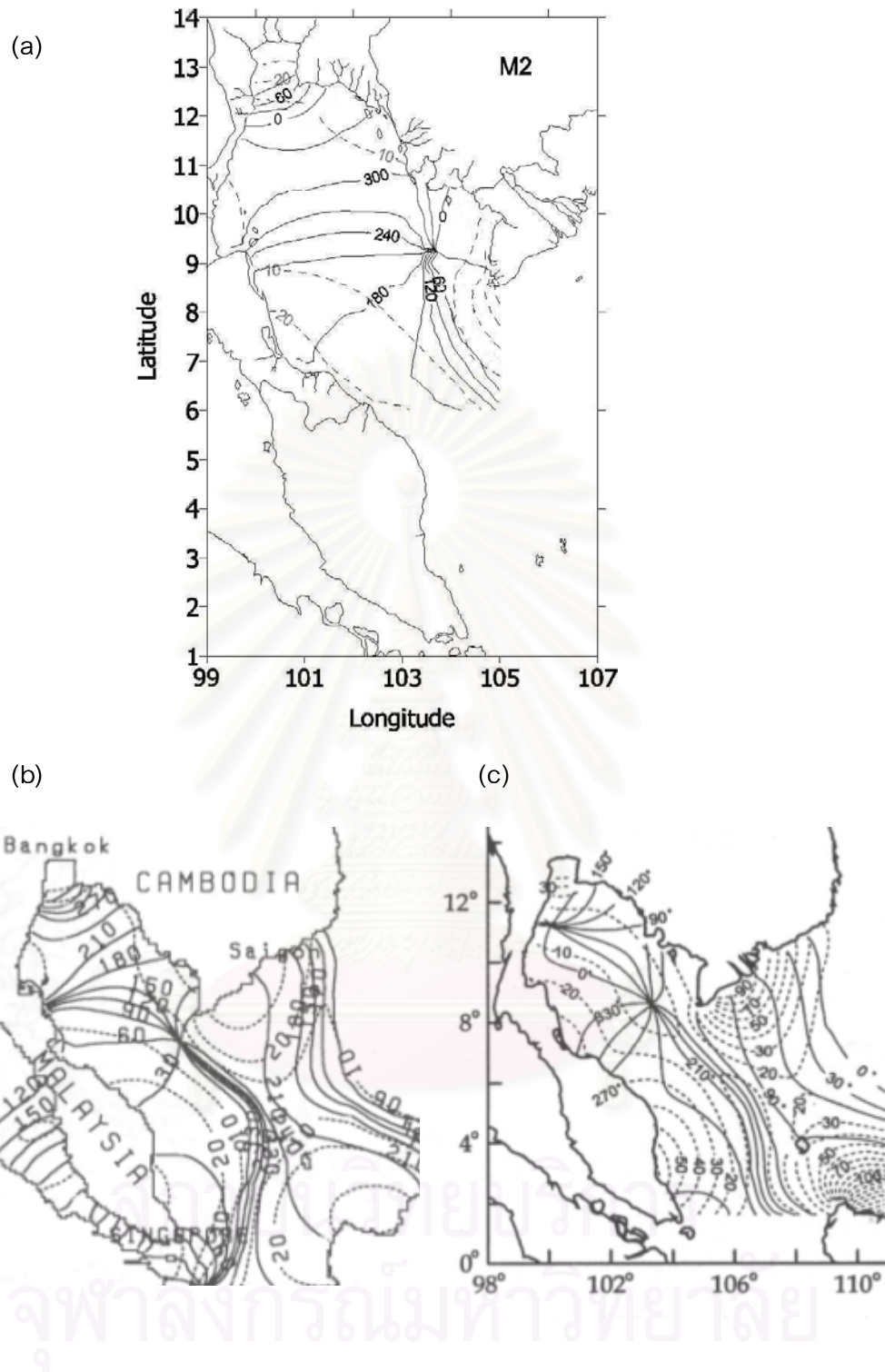


Figure 4.2 Comparison of M2 co-tidal charts (a) this study. Phase refers to the meridian of  $105^{\circ}$  E (b) that by Choi et al. (1997). Phase refers to Greenwich (c) that by Fang et al. (1999). Phase refers to the meridian of  $120^{\circ}$  E

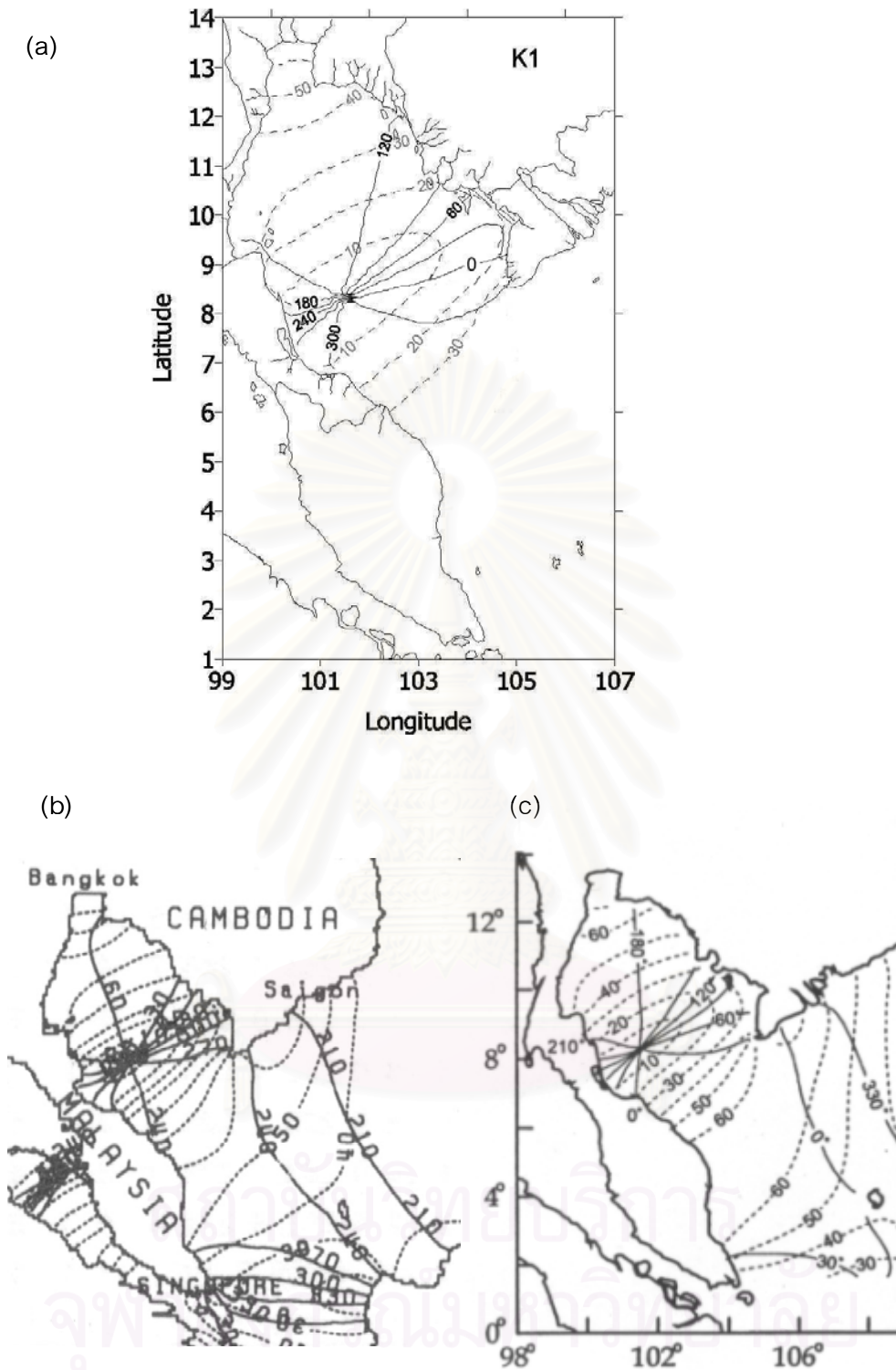


Figure 4.3 Comparison of K1 co-tidal charts (a) this study. Phase refers to the meridian of  $105^{\circ}$  E (b) that by Choi et al. (1997). Phase refers to Greenwich (c) that by Fang et al. (1999). Phase refers to the meridian of  $120^{\circ}$  E

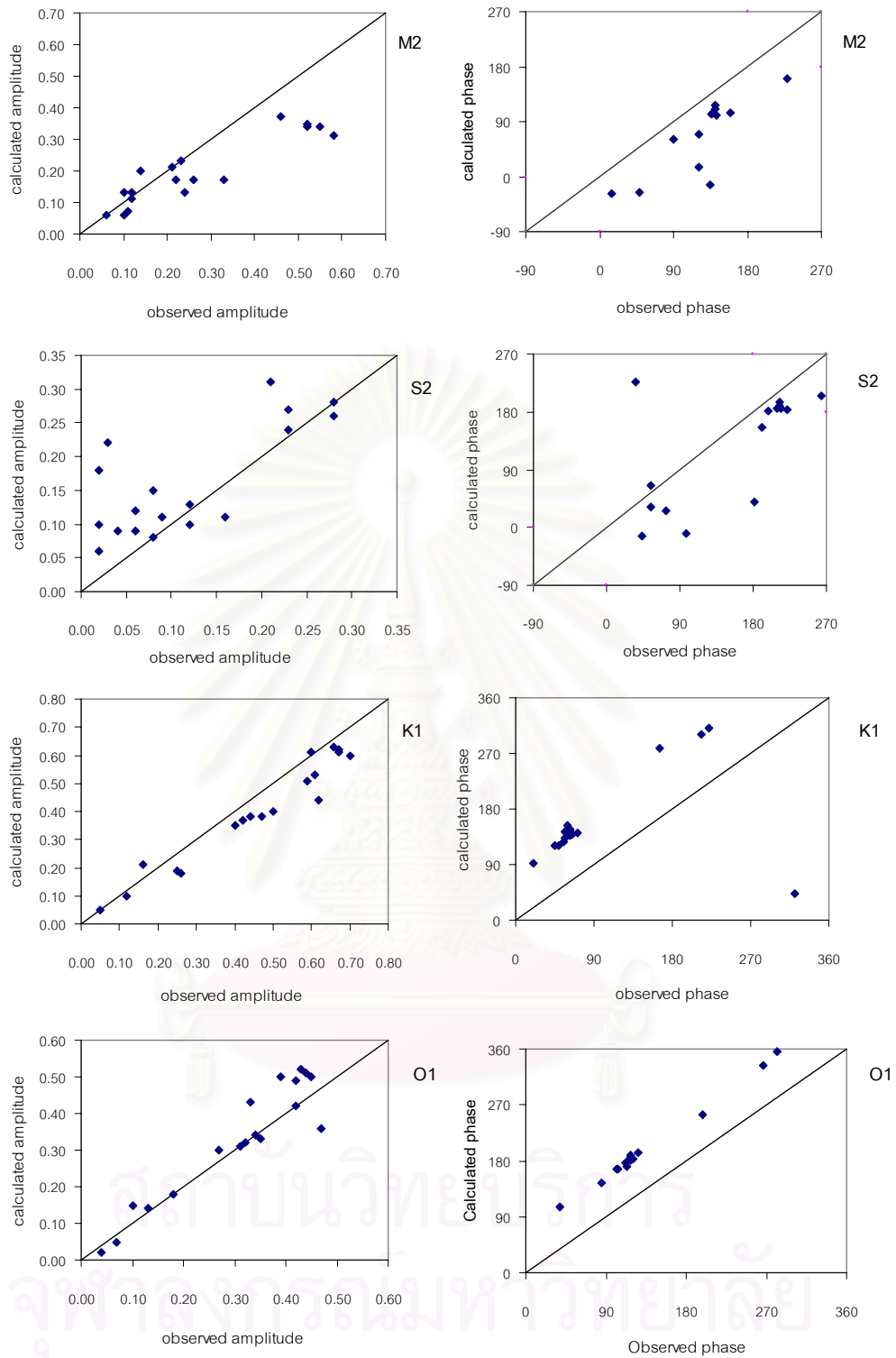


Figure 4.4 Scatter diagrams for the amplitude (in centimeter) and phase (in degree) between the observed and calculated elevations for M2, S2, K1 and O1.

Table 4.1 Comparison of observed and calculated harmonic constants of the four principal tidal constituents M2, S2, K1 and O1. Phase refers to the meridian of 105° E.

No.	Tide gauge site	M2		S2		K1		O1									
		Amplitude		Phase		Amplitude		Phase									
		Obs.	Calc.	Obs.	Calc.	Obs.	Calc.	Obs.	Calc.								
1	Hatien	0.10	0.06	90	61	0.02	0.10	323	43	0.26	0.18	321	42	0.13	0.14	38	105
2	Kampong Som	0.11	0.07	347	287	0.06	0.09	44	-13	0.25	0.19	21	92	0.18	0.18	85	145
3	Laem Ngob	0.12	0.13	14	-28	0.09	0.11	73	27	0.42	0.37	45	120	0.31	0.31	103	166
4	Laem Sing	0.10	0.13	49	-25	0.06	0.12	97	-10	0.47	0.38	49	120	0.32	0.32	102	166
5	Rayong	0.24	0.13	120	15	0.08	0.08	252	288	0.62	0.44	55	126	0.47	0.36	114	170
6	Ao Sattahip	0.26	0.17	121	70	0.12	0.10	191	155	0.59	0.51	56	133	0.42	0.42	112	176
7	Ko Si Chang	0.58	0.31	136	102	0.23	0.24	198	182	0.70	0.60	63	141	0.42	0.49	119	184
8	Bang Pakong	0.52	0.34	159	104	0.23	0.27	222	183	0.60	0.61	71	142	0.39	0.50	118	184
9	Bangkok Bar	0.55	0.34	138	105	0.28	0.26	209	185	0.67	0.61	56	143	0.45	0.50	118	185
10	Tachin	0.52	0.35	140	110	0.28	0.28	212	189	0.67	0.62	63	145	0.44	0.51	118	186
11	Mae Klong	0.46	0.37	140	117	0.21	0.31	212	195	0.66	0.63	63	148	0.43	0.52	118	189
12	Huahin	0.33	0.17	143	101	0.16	0.11	214	186	0.61	0.53	63	143	0.33	0.43	117	186
13	Ko Lak	0.06	0.06	134	-14	0.02	0.06	182	39	0.50	0.40	62	137	0.34	0.34	117	181
14	Ko Mattaphon	0.12	0.11	303	306	0.04	0.09	55	32	0.40	0.35	66	140	0.27	0.30	121	184
15	Ko Prap	0.22	0.17	318	320	0.12	0.13	54	66	0.44	0.38	59	153	0.35	0.33	126	194
16	Songkla	0.23	0.23	292	180	0.03	0.22	35	-134	0.05	0.05	165	279	0.04	0.02	198	255
17	Pattani	0.21	0.21	283	174	0.02	0.18	320	222	0.12	0.10	213	300	0.07	0.05	266	333
18	Bang Nara	0.14	0.20	228	160	0.08	0.15	264	206	0.16	0.21	222	310	0.10	0.15	282	356

#### 4.1.2 Model response to a combination of wind and co-oscillation tide

The model currents from experiment V2 were compared to observed currents at oceanographic buoys for two chosen periods to represent the different monsoon regimes. For each period, 15-days-comparison was chosen to account for variation due to spring-neap tidal cycle. The first was from 23 August 2000 – 7 September 2000 which coincided with the southwest monsoon season. There were 3 observations available in this period, namely Huahin, Ko Sichang and Ko Chang buoys. The latter was from 12-28 February 2001 which coincided with northeast monsoon season. There were 2 observations available namely, Huahin and Ko Sichang buoys.

Figure 4.5 compares the stick vector plots of hourly currents at Huahin (B1) buoy located 3.5 m below sea surface with calculated currents at the same level from 23 August 2000 - 7 September 2000. Observed currents exhibit a north-northwestward flow during flood and south-southeastward flow during ebb tide. This is clearly shown in the comparison of observed and calculated velocity in east-west and north-south velocity component. Note that the north-south velocity component has larger magnitude than east-west component. Currents due to mixed tide are seen by modulation of observed current from 1-cycle-per-day flood-ebb flow early in the time series to 2-cycle-per-day flow later in the time series. The calculated currents also reproduce such a pattern but with phase shift. The calculated current magnitudes are greater than observed ones by about 10 cm/s.

Observed currents at Ko Sichang (B2) (Figure 4.6) are characterized by intensified and chaotic pattern if not tidal rotation. Calculated currents are more or less constant in north-south direction. The model underestimated the east-west component magnitude by 30 cm/s.

Calculated currents at Ko Chang (B3) (Figure 4.7) are closely resemble to observed currents which are characterized by southeastward flow with diurnal fluctuation of current magnitude. There are some phase shifts in east-west and north-south velocity components.

Figure 4.8 compares the stick vector plots of observed currents at Huahin (B1) with calculated current from 12-28 February 2001. Observed currents are similar to that of southwest monsoon season for north-south direction. Calculated currents seem to be biased toward overestimation during neap cycle.

In contrast to pattern in southwest monsoon, observed currents at Ko Sichang (B2) (Figure 4.9) are characterized by weak tidal rotation current. Calculated currents were similar to observed currents in magnitude and direction. However, later in the time series the observed currents were of mixed tide while the calculated currents were of diurnal tide.



สถาบันวิทยบริการ  
จุฬาลงกรณ์มหาวิทยาลัย

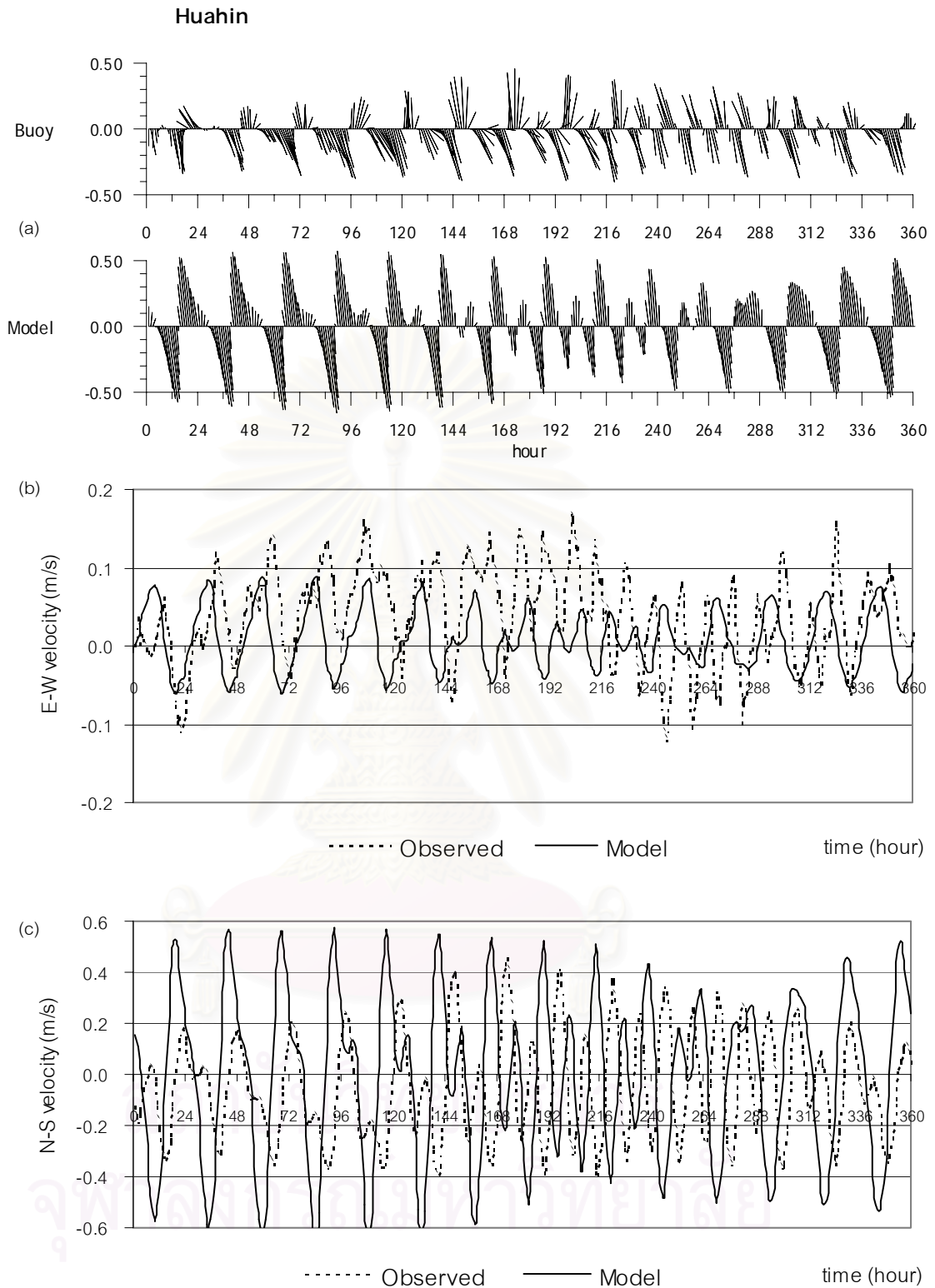


Figure 4.6 Comparison of observed and calculated currents at Ko Sichang from 23 August 2000 - 7 September 2000. (a) stick vector plots of hourly currents (b) east-west velocity component (c) north-south velocity component

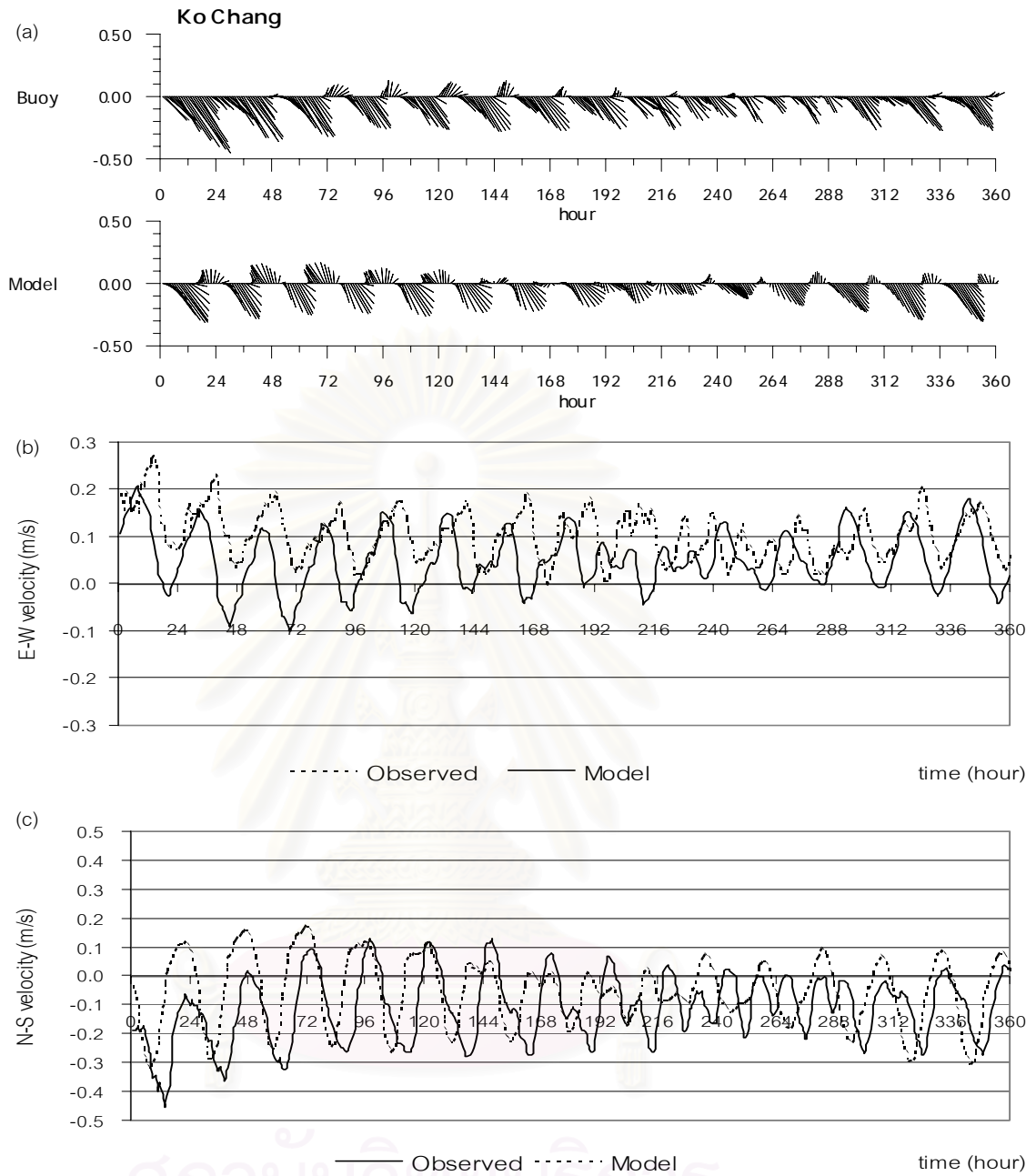


Figure 4.6 Comparison of observed and calculated currents at Ko Sichang from 23 August 2000 - 7 September 2000. (a) stick vector plots of hourly currents (b) east-west velocity component (c) north-south velocity component



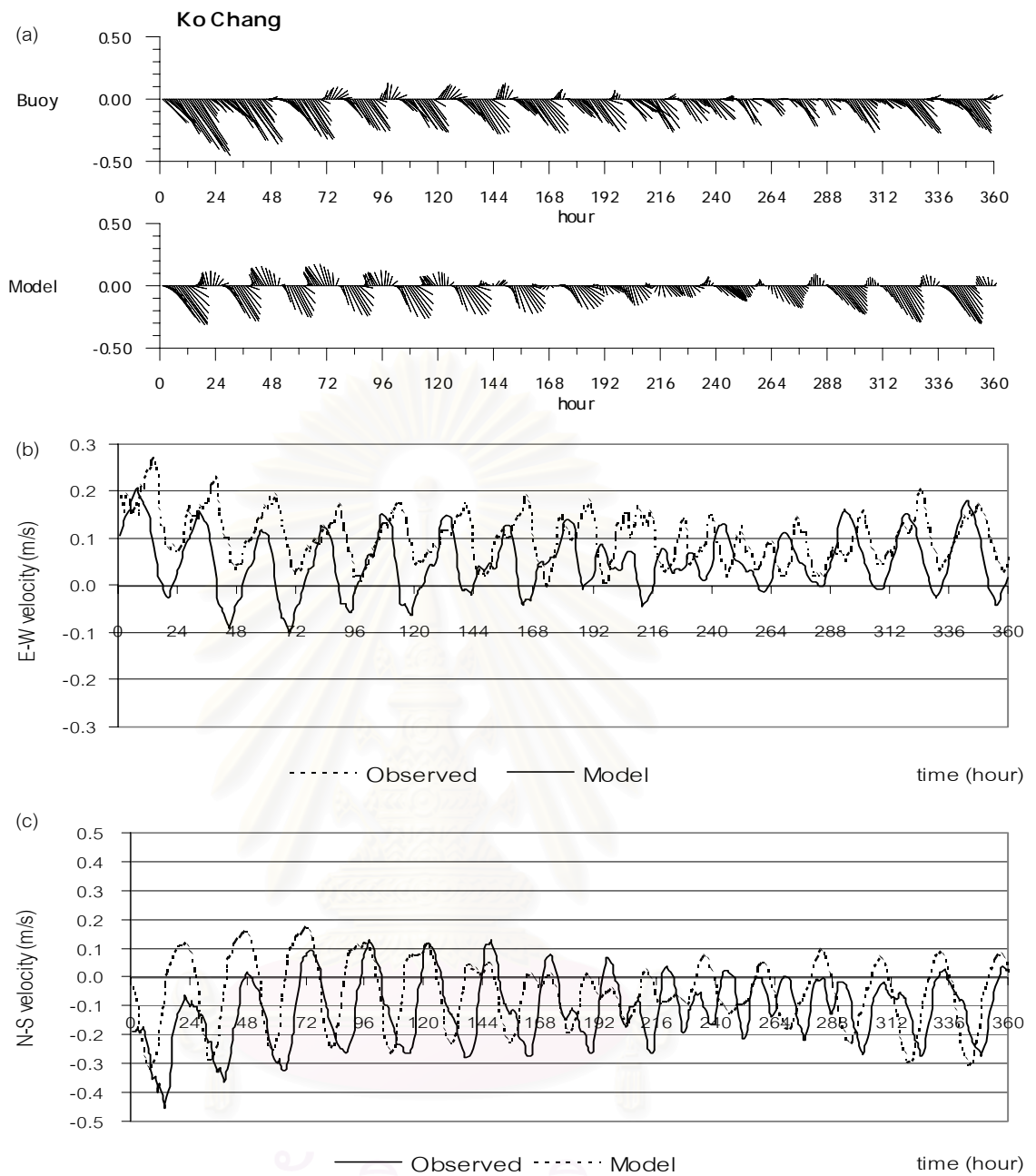


Figure 4.7 Comparison of observed and calculated currents at Ko Chang from 23 August 2000 - 7 September 2000. (a) Stick vector plots of hourly currents (b) east-west velocity component (c) north-south velocity component.

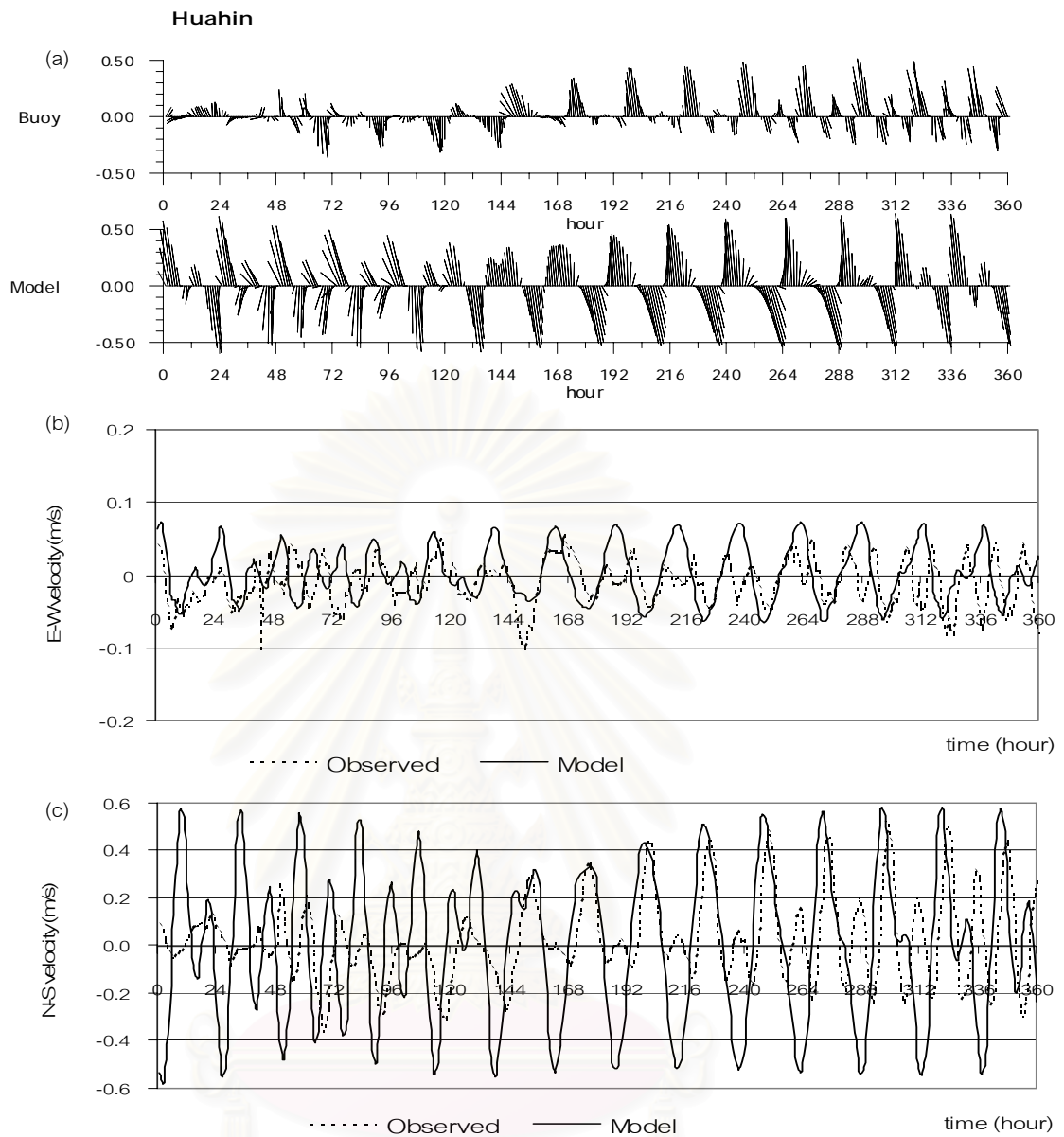


Figure 4.8 Comparison of observed and calculated currents at Huahin from 12-28 February 2001. (a) stick vector plots of hourly currents (b) east-west velocity component (c) north-south velocity component.

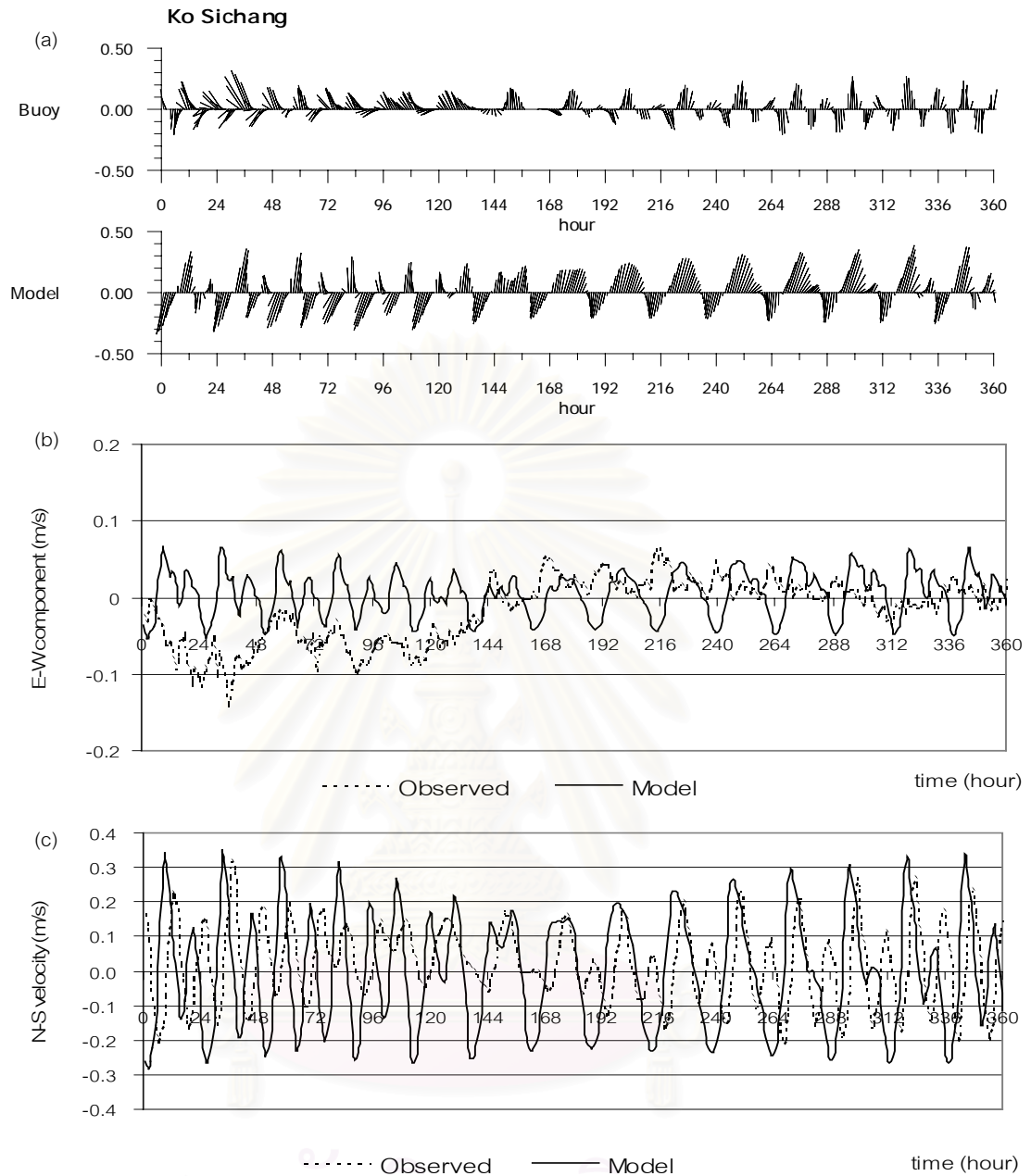


Figure 4.9 Comparison of observed and calculated currents at Ko Sichang from 12-28 February 2001. (a) stick vector plots of hourly currents (b) east-west velocity component (c) north-south velocity component

## 4.2 Eddy characteristics in the Gulf of Thailand

### 4.2.1 Eddy inferred from numerical ocean model

It is evident from the preceding section that accurate simulation of the model has not yet been achieved. Nevertheless, the model has demonstrated that it can reasonably respond to the two important circulation-driving terms in the Gulf which are wind and co-oscillation tide. The focus of this study is not to comprehensively predict existence of eddy in the Gulf, rather the model is viewed as a tool for study eddy characteristics under the influence of prescribed forcing as well as for eddy generation mechanism. Thus in this section, eddy characteristics were described based on results produced by this model.

The analysis of eddy characteristics in the Gulf of Thailand considered the current under the influence of wind from NOGAPS and composite M2, S2, K1 and O1 tides at open boundaries (experiment EC). Daily-averaged currents were obtained by averaging current vectors at each grid over 25 hours to filter out tidal signal.

Under the period of consideration from January 2000 – February 2001, both anticyclonic eddies and cyclonic eddies were found. Figure 4.10 depicts selected scenes of daily averaged surface current in which eddies were present. On 5 March 2000 two anticyclonic eddies were found. One occurred at the upper Gulf centered around  $10.5^{\circ}$  N, the other occurred at the lower Gulf centered around  $8.5^{\circ}$  N. Their spatial scales were approximately 200 km. On 12 September 2000, an anticyclonic eddy was present at the mouth of the Gulf. Its spatial scale was 100 km. Many meanders were observed in the surface current. On 24 September 2000 another cyclonic eddy occurred south of the existing anticyclonic eddy. Each eddy had a spatial scale of O (100 km). On 1 January 2001 a cyclonic eddy of O (200 km) was present at the upper Gulf. Vertical structures of all eddies found were barotropic type in which the direction of the current is the same over the entire water column as illustrated by anticyclonic eddies on 12 September 2000 (Figure 4.11).

Most eddies found were short-lived. Their time scales were 2-3 days. Figure 4.12 shows a sequence of an anticyclonic eddy of March 2000 event presented by daily averaged surface current. On 4 March 2000, a large anticyclonic gyre developed. Strong currents flowed northward along the western coast, turned eastward when reaching the Upper Gulf and southward when reaching the east coast, completing a gyre. On 5 March 2000, currents were weak. Two anticyclonic eddies were formed, one at the upper Gulf, the other at the lower Gulf. After that the currents were strengthened again and formed a large-scaled gyre as illustrated on 10 March 2000. No eddy was found when currents were intense. On 11 March 2000, the anticyclonic eddy was formed at the lower Gulf and lived for 2 days before disappearing when flows were intensified. Anticyclonic eddies of September 2000 event had longer time scale of 2 weeks as depicted in Figure 4.13 and Figure 4.14. Anticyclonic eddy was formed on 12 September and lives until 26 September. On 23 September, a cyclonic eddy was formed south of the anticyclonic eddy. Together they formed a dipole eddy and live for 4 days. Figure 4.15 shows a sequence of cyclonic eddy of January 2001 event presented by daily averaged surface current. On 1 January 2001, a cyclonic eddy was formed and lived for 3 days, then disappeared on 4 January 2001.

This study found that eddies were generated and decayed over a short time in the Gulf but they were recurring phenomena. Analysis of monthly-mean current (see Appendix C) can provide information on those eddies which frequently occur. During 2000, there were two main areas where eddies were present;

Area I - The upper Gulf (latitude  $10-11^{\circ}$  N, longitude  $101-102^{\circ}$  E) where anticyclonic eddies were found all year round except when NE monsoon wind caused a basin-scale cyclonic flow early in the season (November and December 2000). The size of eddy varied depending on the strength of large scale flow. The diameter was about 50-200 km.

Area II - The lower Gulf (latitude  $8-9^{\circ}$  N, longitude  $101.5-102.5^{\circ}$  E) where anticyclonic eddy of 200-km diameter was found in late NE monsoon season (January, February and March). Its strength and size decreased when the mean circulation was

weak in the following transition months. When SW monsoon began, it was still present but was deflected more to the west coast. Its size was shrunk, its strength was weakened. This area is actually the deepest spot in the Gulf of Thailand.

No eddy was found in the Inner gulf. This may be attributed to the present model which has relatively coarse grids (approximately 11 km) compare to the dimension of the Inner Gulf (100 km x 100 km). Accordingly, the model might not adequately resolve dynamical processes in the Inner Gulf. Most likely, the very coarse resolution of wind (approximately 120 km) derived from global numerical weather prediction could not provide spatial variation of wind in the Inner Gulf.

Mostly, the eddy patterns were more distinct below the surface. This may arise from the fact that surface currents are directly influenced by the wind stress. According to Ekman theory, surface currents are deflected to 45 degree to the right of the wind direction in northern hemisphere. Thus surface currents are characterized as inflow to the Gulf during NE monsoon and outflow of the Gulf during SW monsoon.

Eddies in the Gulf were barotropic type. Theirs currents flew in the same direction over the entire column even in SW monsoon season when stratification developed and the mean flow exhibited an estuarine circulation with mean current flowing out of the Gulf in the upper layer and compensating by inflow in the lower layer.

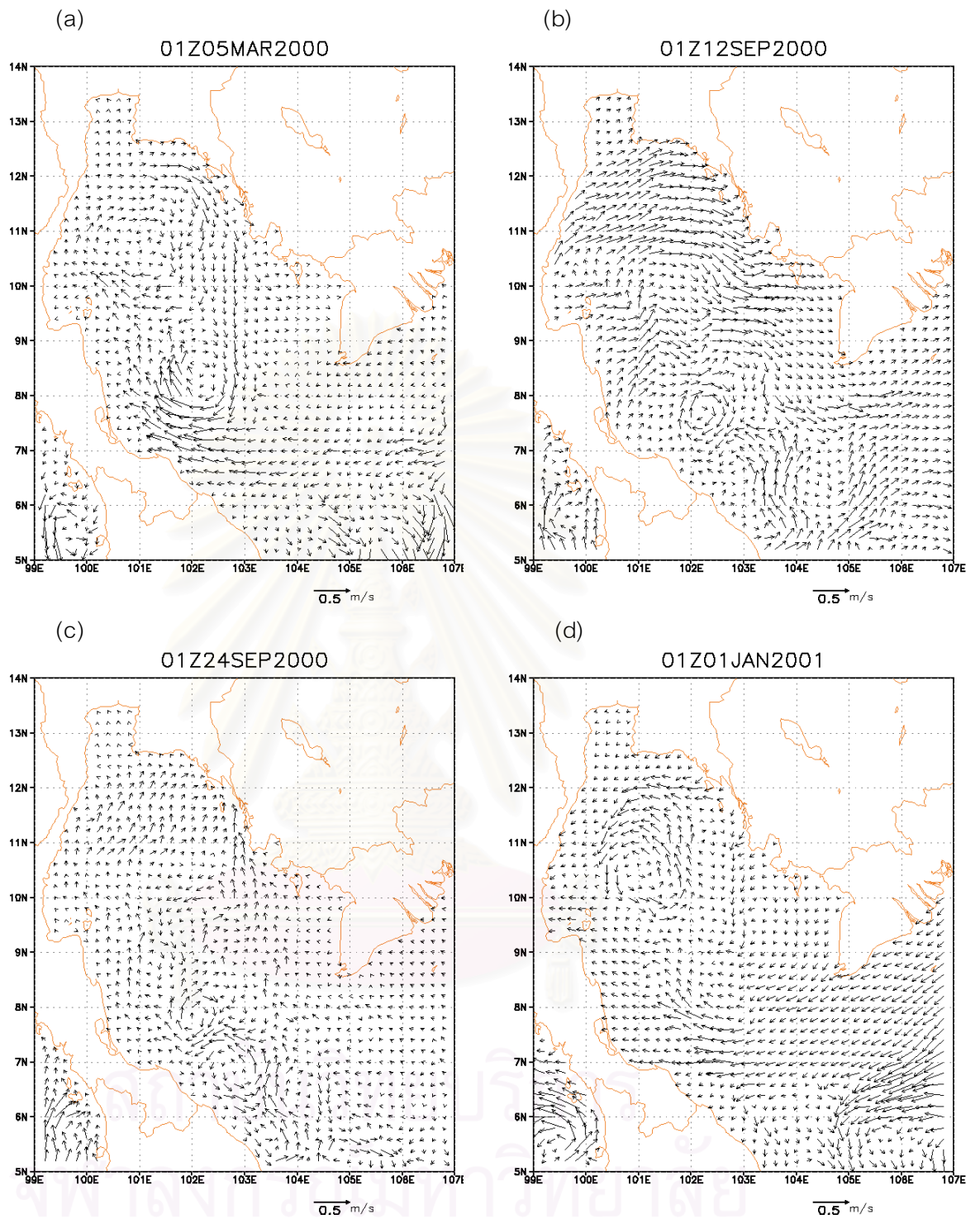


Figure 4.10 Simulated daily averaged surface current driven by NOGAPS wind and composite M2, S2, K1 and O1 tides at open boundaries on (a) 5 March 2000 where two anticyclonic eddies are found (b) 24 September 2000 where a dipole eddy is present (c) 1 January 2001 where a cyclonic eddy is present and (d) 26 January 2001 where an anticyclonic eddy is found.

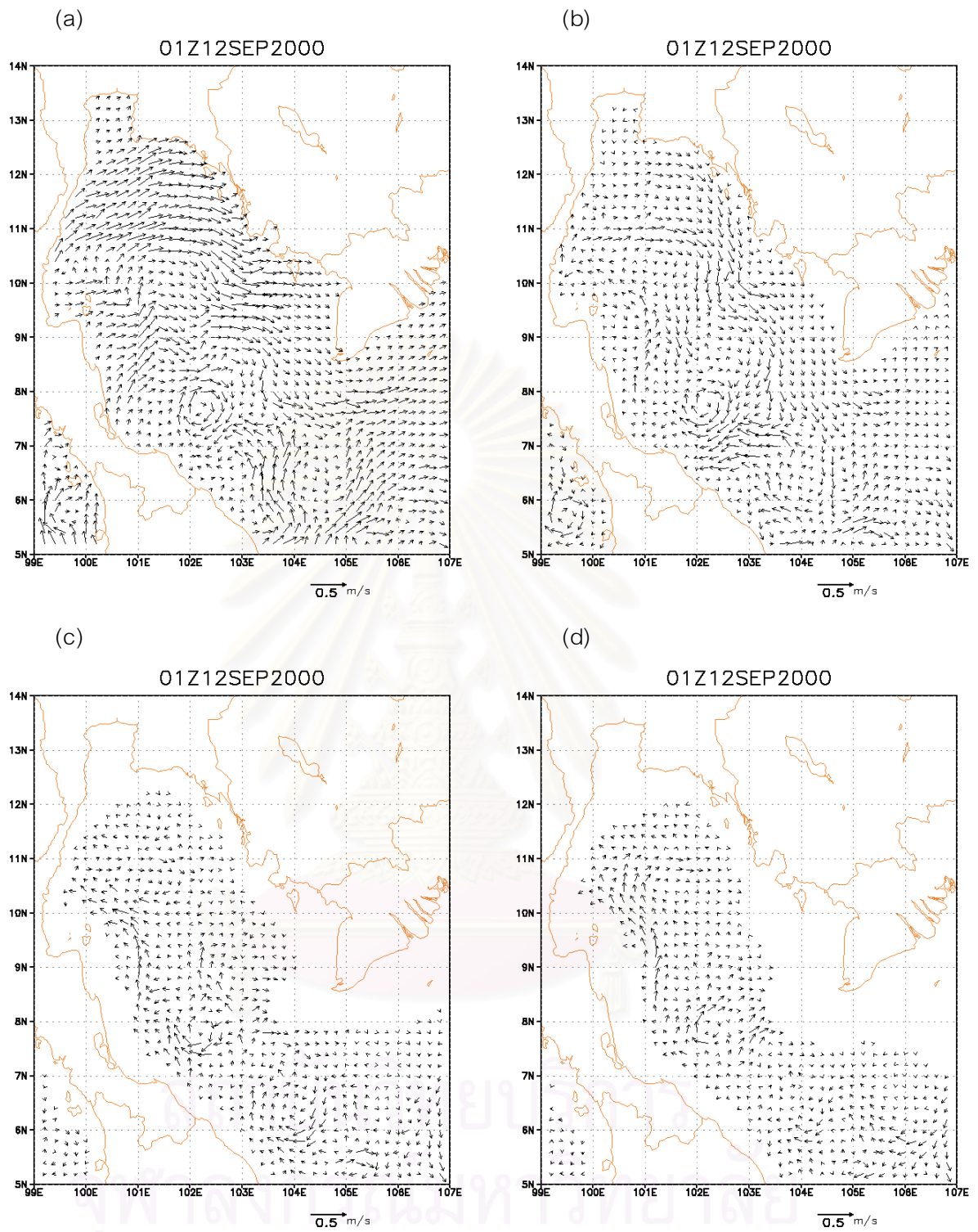


Figure 4.11 Vertical structure of an anticyclonic eddy on 12 September 2000

(a) surface (b) 10 m depth (c) 30 m depth (d) 40 m depth



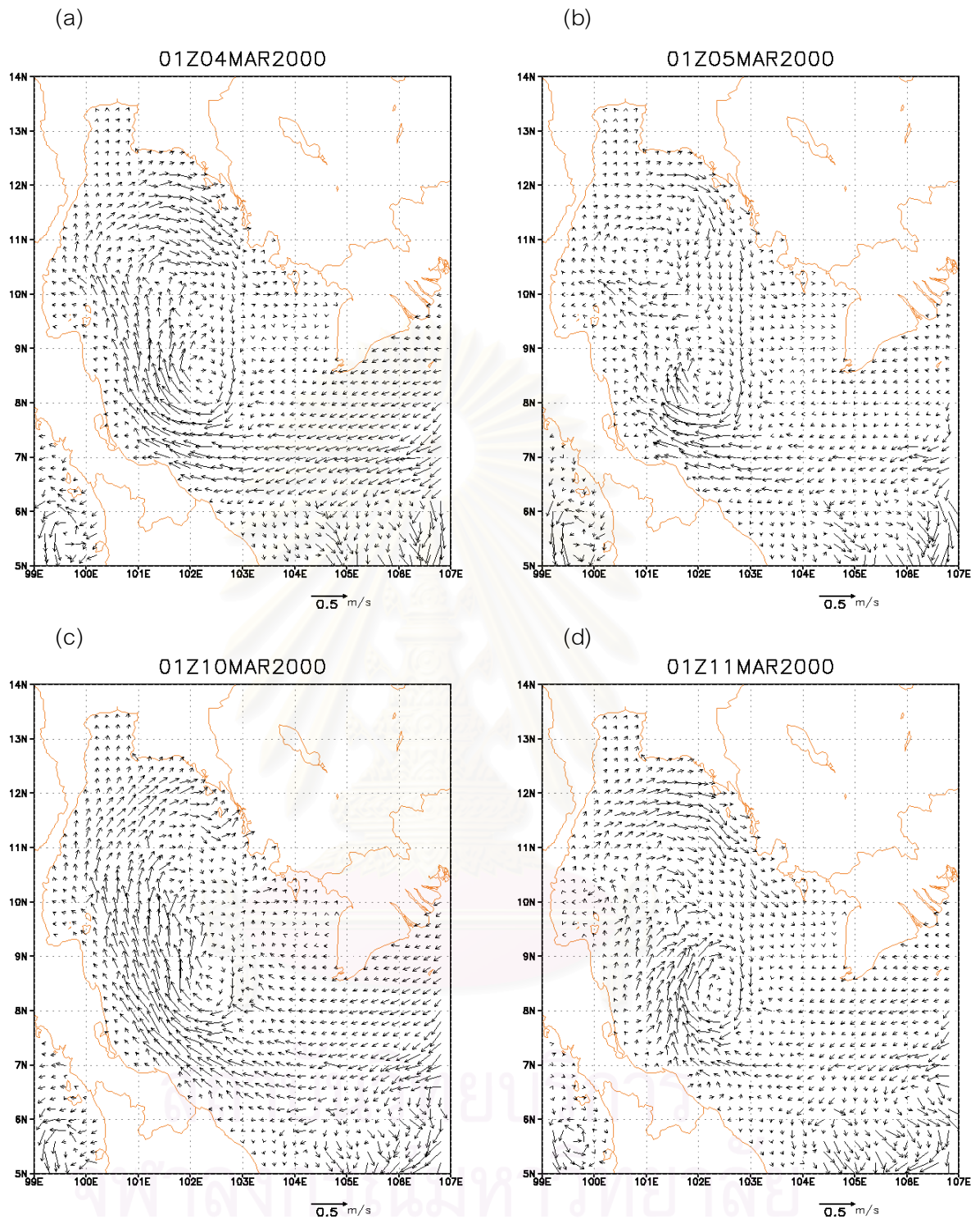


Figure 4.12 A time series of anticyclonic eddies in March 2000 presented by simulated daily averaged surface current driven by NOGAPS wind and composite M2, S2, K1 and O1 tides at open boundaries on (a) 4 March 2000 (b) 5 March 2000 (c) 10 March 2000 and (d) 11 March 2000

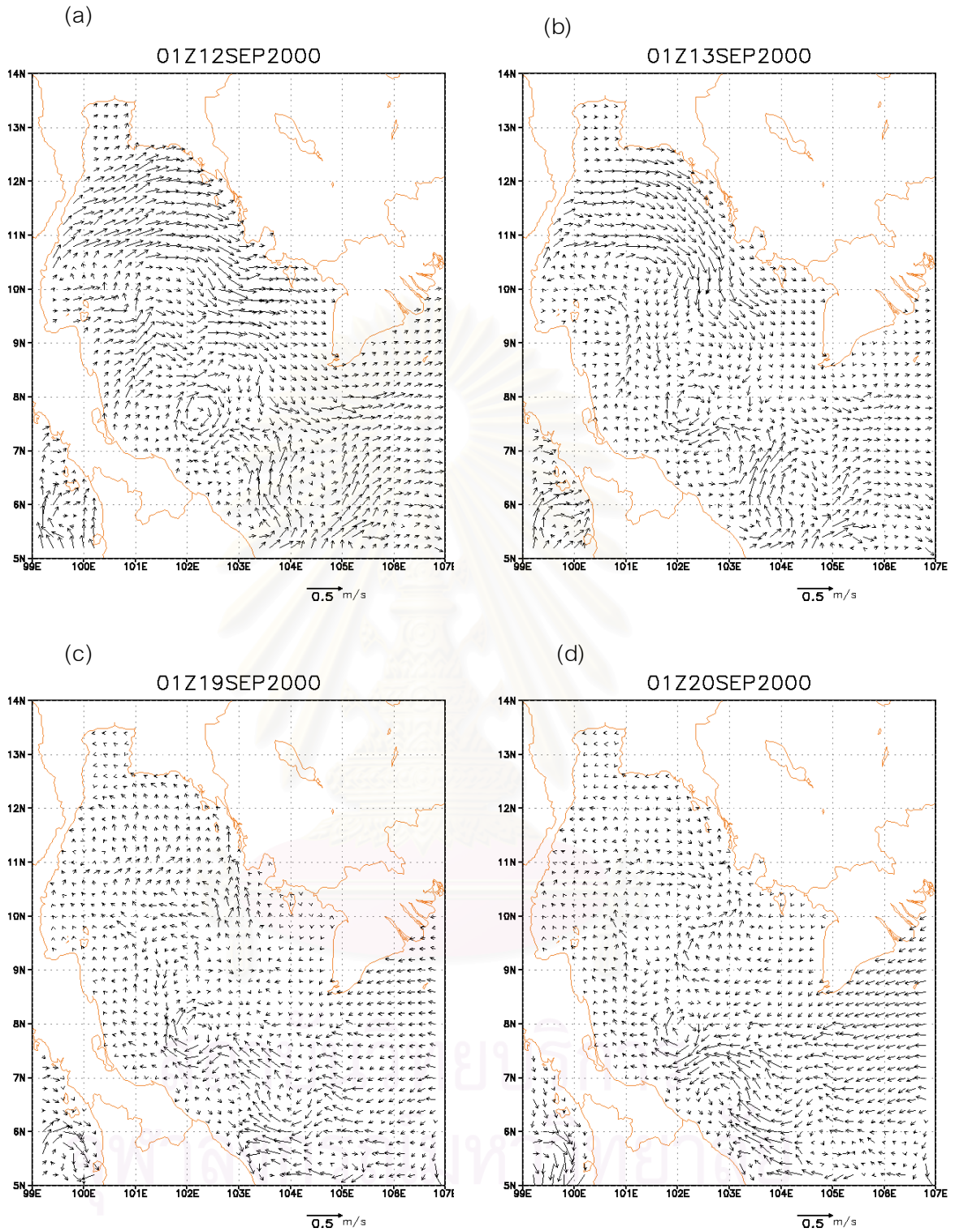


Figure 4.13 A time series of anticyclonic eddies in September 2000 presented by simulated daily averaged surface current driven by NOGAPS wind and composite M2, S2, K1 and O1 tides at open boundaries on (a) 12 September 2000 (b) 13 September 2000 (c) 19 September 2000 and (d) 20 September 2000

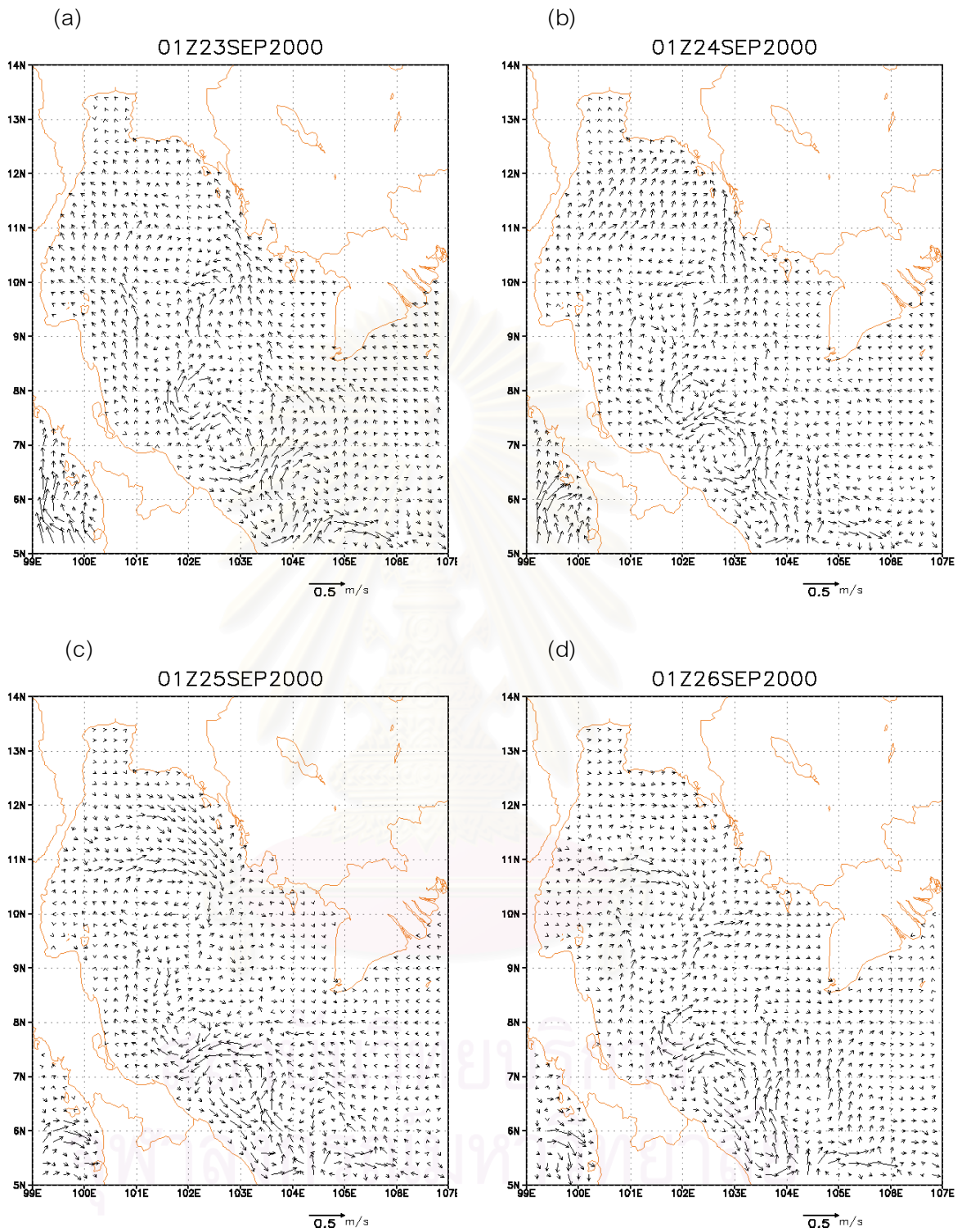


Figure 4.14 A time series of a dipole eddy in September 2000 presented by simulated daily averaged surface current driven by NOGAPS wind and composite M2, S2, K1 and O1 tides at open boundaries on (a) 23 September 2000 (b) 24 September 2000 (c) 25 September 2000 and (d) 26 September 2000

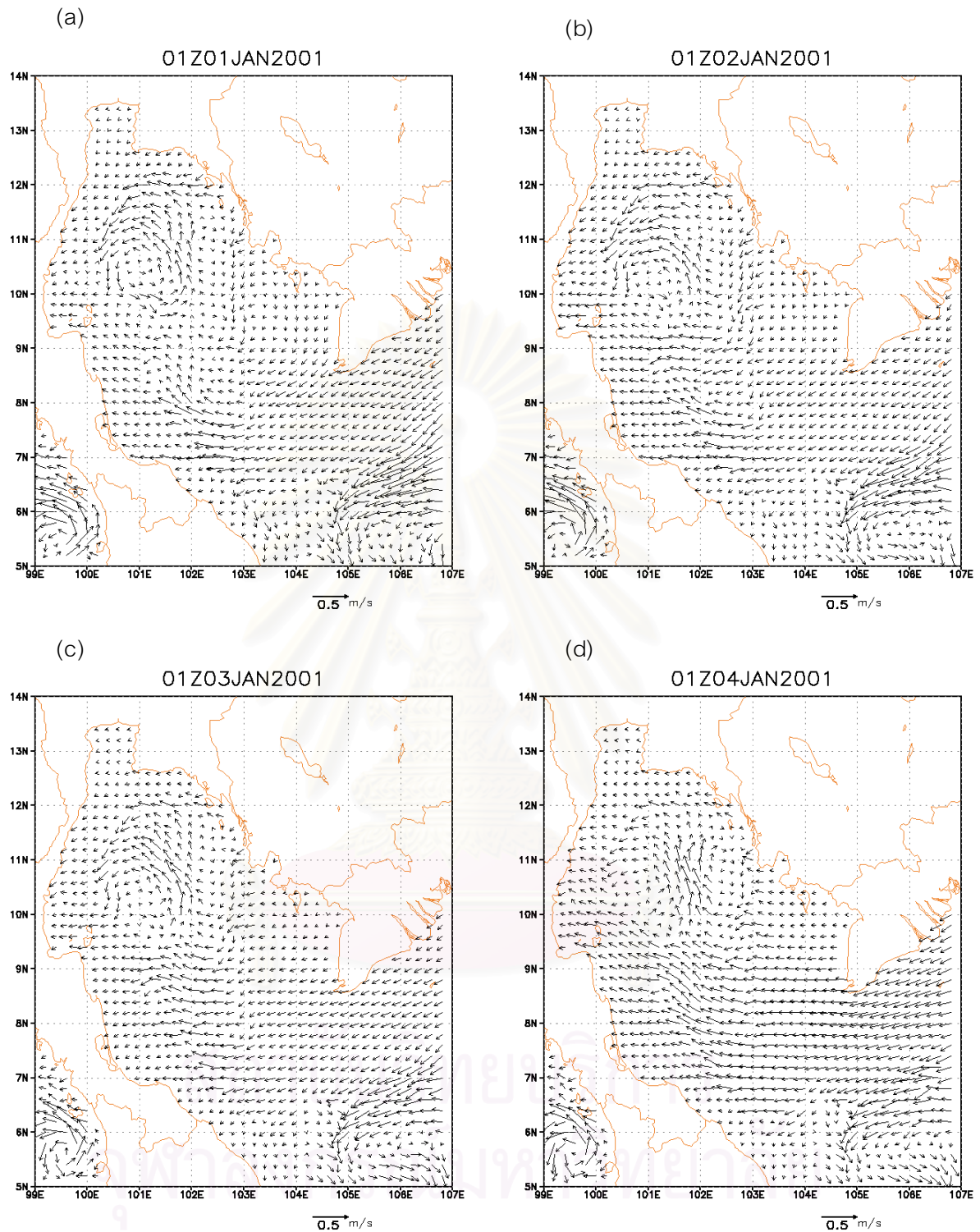


Figure 4.15 A time series of a cyclonic eddy in January 2001 presented by simulated daily averaged surface current driven by NOGAPS wind and composite M2, S2, K1 and O1 tides at open boundaries on (a) 1 January 2001 (b) 2 January 2001 (c) 3 January 2001 and (d) 4 January 2001

#### 4.2.2 Eddy inferred from ocean color images

Of nearly 400 SeaWiFS scenes under the period of consideration from January 2000 – February 2001, only one-fourth of those were cloud free and were processed for images of chlorophyll\_a concentration. By treating phytoplankton and sediment as tracers of eddies, eddies were identified by area of higher or lower chlorophyll\_a concentration than surrounding water. No eddy was found from those images. Selected scenes are present in Figure 4.16 - 4.19. All images are color-scaled ranging from 0.01 – 64  $\mu\text{g}/\text{m}^3$ . The regions covered by clouds are masked with white color. Land is masked by gray color. On 13 March 2000 (Figure 4.16) in which most part of the Gulf were cloud-free, no particular area of higher or lower Chlorophyll\_a than the surroundings was observed. On 3 April 2000 (Figure 4.17) a circular patch of high chlorophyll\_a was seen north of Samui Island. On 20 June 2000 (Figure 4.18) a patch of high chlorophyll\_a was seen on the east side of the Gulf near Cambodia. On 25 February 2000 (Figure 4.19) a patch of high chlorophyll\_a was seen at the mouth of the Gulf crossing from southern tip of Vietnam to Malay Peninsular. This path might arise from high chlorophyll\_a concentration at the mouth of Mekong river carried by surface current flowing from northeast consistent with circulation pattern in northeast monsoon season. Area of high chlorophyll\_a concentration was again seen north of Samui Island.

Inability to detect eddy from ocean color images arises from many reasons. The most obvious obstacle is high frequency of cloud cover over the Gulf. This fact reduces the intended sampling frequency from everyday by its orbit path to only 2-3 times a month practically.

In summary, this study found that using chlorophyll\_a concentration derived from satellite images is not an appropriate mean for studying eddy in the Gulf of Thailand.

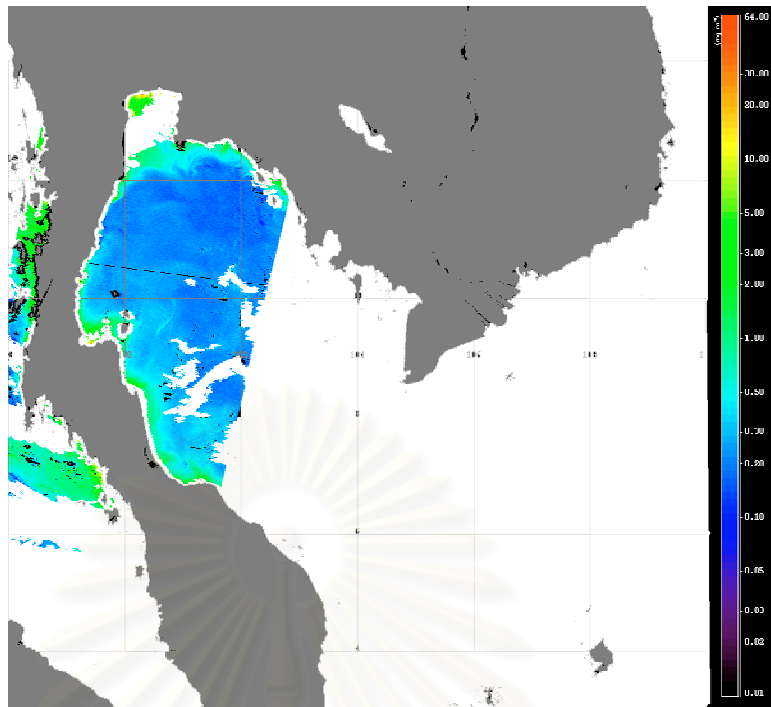


Figure 4.16 Chlorophyll\_a concentration derived from SeaWiFS on 13 March 2000

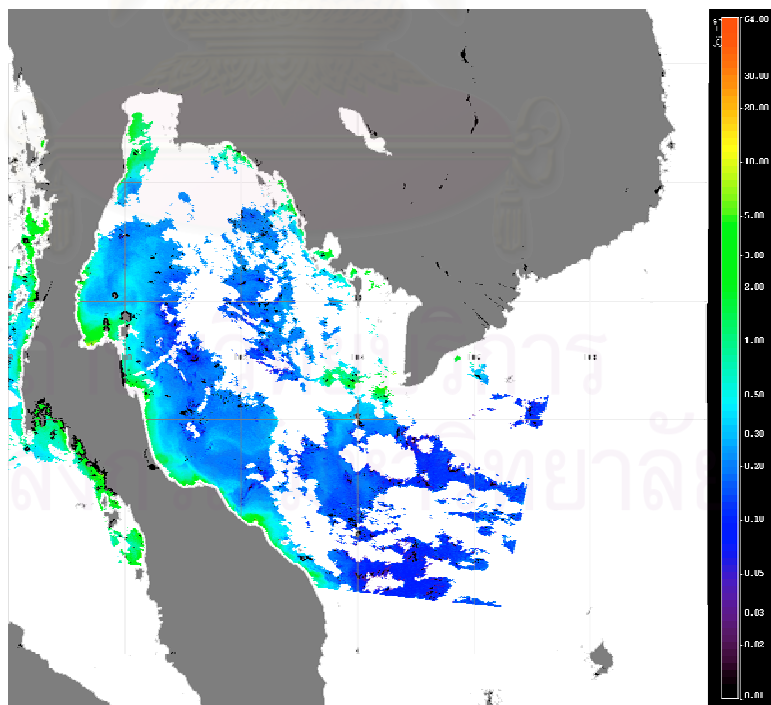


Figure 4.17 Chlorophyll\_a concentration derived from SeaWiFS on 4 April 2000

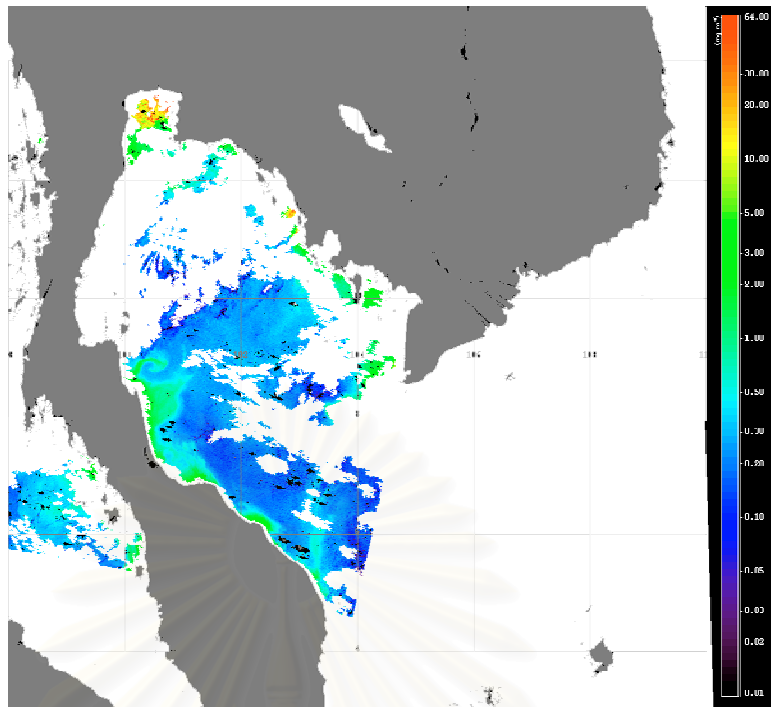


Figure 4.18 Chlorophyll\_a concentration derived from SeaWiFS on 20 June 2000

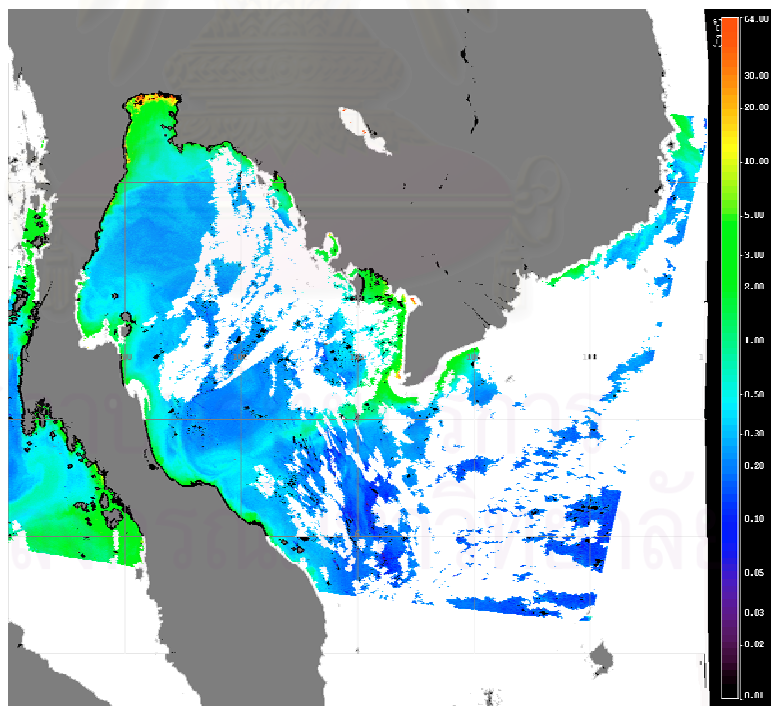


Figure 4.19 Chlorophyll\_a concentration derived from SeaWiFS on 25 February 2001

### 4.3 Eddy generation mechanisms in the Gulf of Thailand

#### 4.3.1 Contribution from tide

To investigate the contribution of tide on eddy generation in the Gulf of Thailand, the model was run by forcing wind stress calculated from NOGAPS wind at the surface boundary while excluding tidal calculation at the open boundaries (experiment EM1). The model results were compared with those from experiment EC which were driven by both wind and tide. Figure 4.20 compares the currents on 5 March 2000 on which an anticyclonic eddy occurred in both experiments.

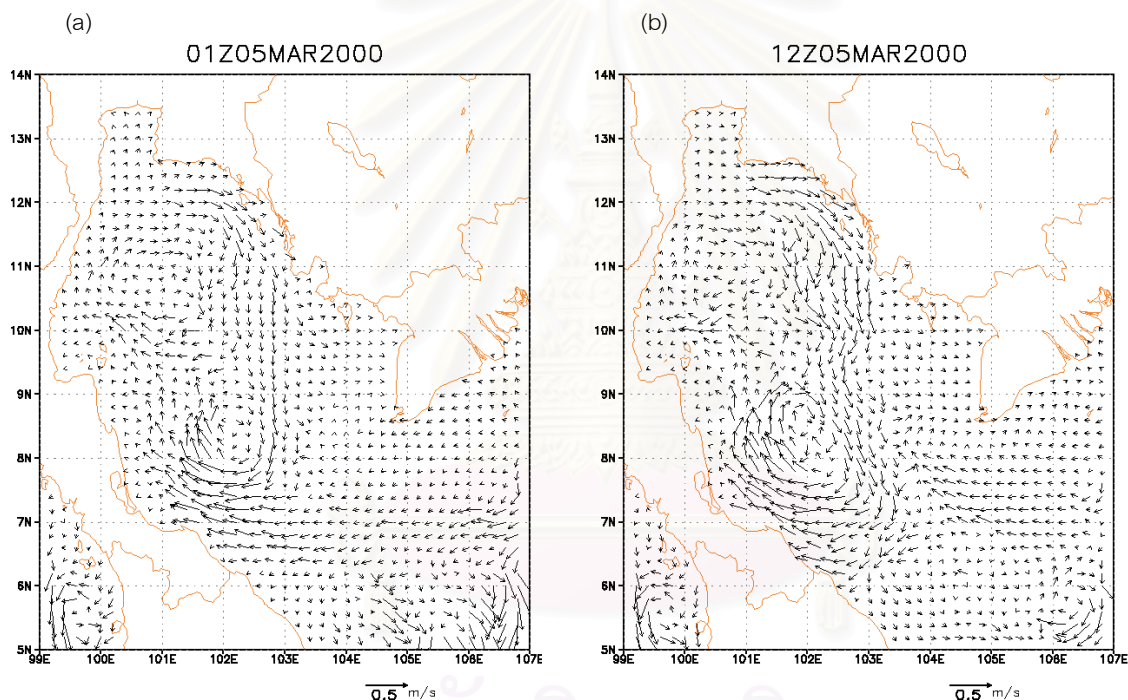


Figure 4.20 Comparison of simulated (a) wind-tidally driven current and (b) wind-driven current on 5 March 2000

However, an anticyclonic eddy on 12 September 2000 occurred in wind-tidally driven simulation (experiment EC) was not developed in wind-driven simulation (experiment EM1) until 13 September 2000 as depicted in Figure 4.21. The position of eddy also shifted toward the Malay Peninsular.



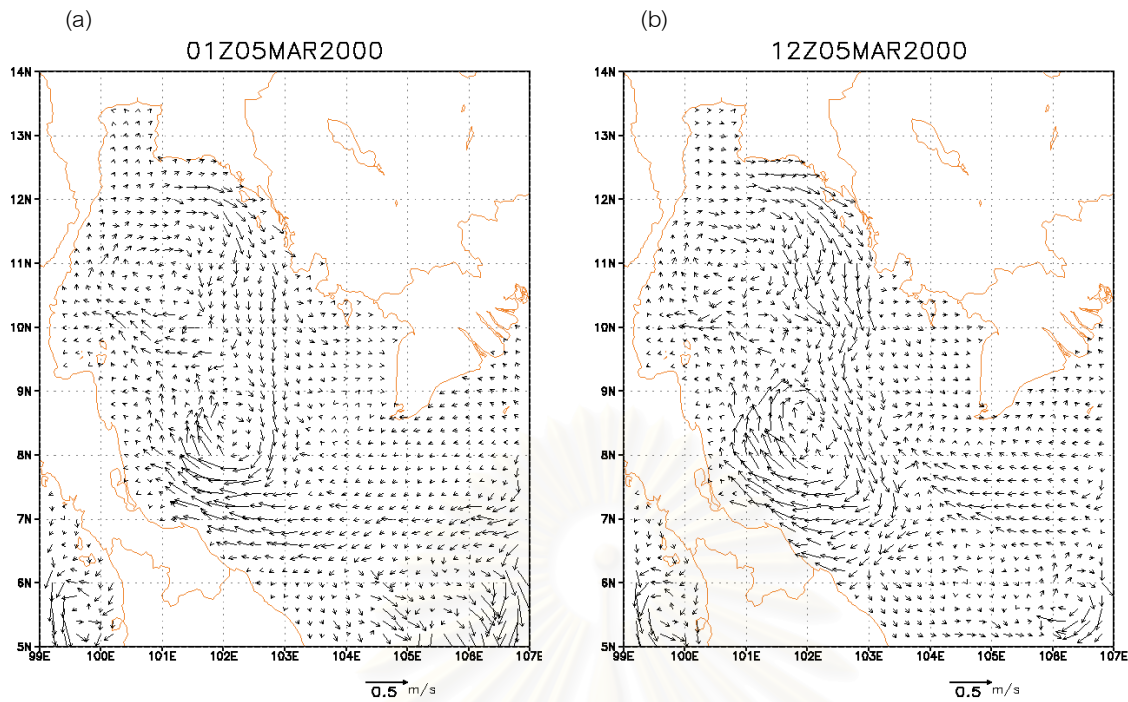


Figure 4.21 Comparison of simulated (a) wind-tidally driven current and (b) wind-driven current on 12 September 2000

#### 4.3.2 Contribution from wind

To investigate the contribution of wind on eddy generation in the Gulf of Thailand, the model was run by prescribing tide at the open boundaries without forcing wind stress at the surface boundary (experiment EM2). A residual flow which is an average current velocity over main tidal period (a half day, one day, or 15 days) (Yanagi, 1999), in this case over 25 hours, were used to compare with the wind-tidally driven currents (experiment EC). Figure 4.22 compares the tidally-driven current with that of driven by wind and tide. It can be seen that without wind forcing, current in the Gulf hardly developed eddies. Note that vortex arising near southern boundary is the result of boundary effect, thereby was not considered in this study.

สถาบันวิทยบริการ  
จุฬาลงกรณ์มหาวิทยาลัย

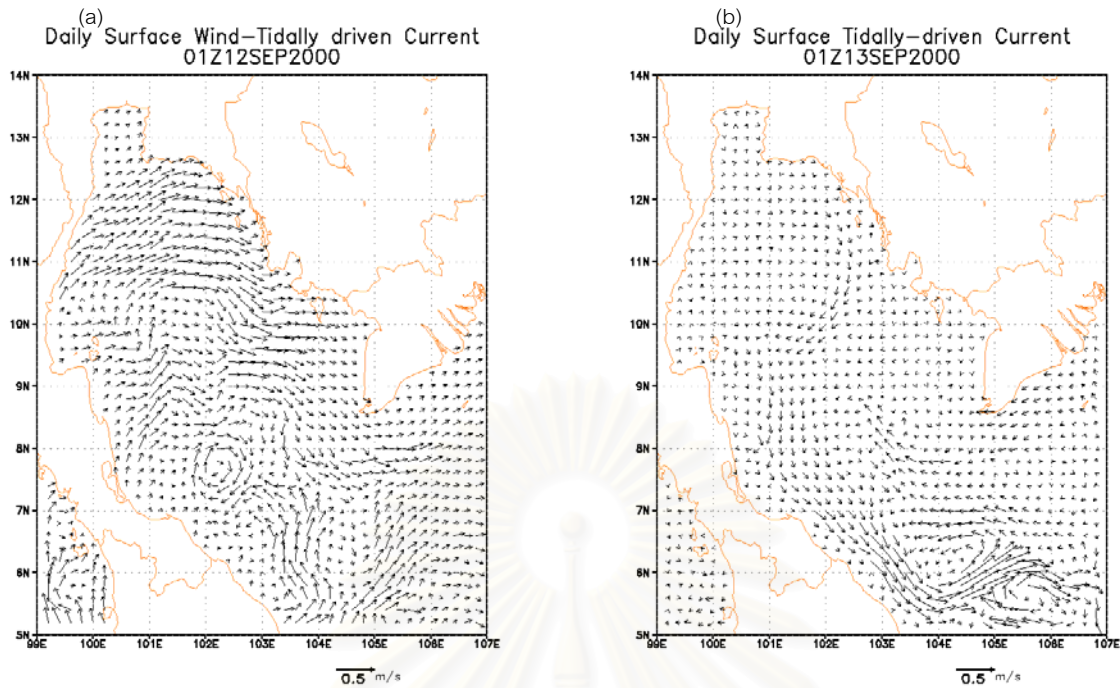


Figure 4.22 Comparison of simulated (a) wind-tidally-driven current on 12 September 2000 and (b) tide-induced residual current on 13 September 2000

#### 4.3.3 Uniform wind experiments

To investigate wind characteristics which could generate eddy, maps of wind stress from NOGAPS which is used to drive the model during the periods when eddies occur were plotted. Most eddies occurred when wind stress were weak except the cyclonic eddy on January 2001. During strong wind stress, surface currents generally exhibit uni-directional flow type. Figure 4.23 - 4.25 are presented to illustrate the wind stress condition when eddies were found. Comparisons of the days on which larger magnitude of wind stress under the same prevailing wind direction occurred are also given.

Wind stress on 5 March 2000 on which two anticyclonic eddies were present is depicted in Figure 4.23 (a) Mean wind speed was 2 m/s. Directions of wind were variable. Comparing to wind stress on 25 March 2000 (Figure 4.23 (b)) on which mean wind speed was 5 m/s, no eddy was formed while surface currents were strong and flew towards the west coast under the influence of northeasterly-easterly winds.

Figure 4.24 (b) depicts the wind stress on 24 September 2000 on which a dipole eddy was present. Again, mean wind speed was 2 m/s. In comparison, mean westerly wind speed on 10 September 2000 (Figure 4.24 (a)) was 5 m/s. Surface currents were strong and flew southeastward out of the Gulf. Even though meanders were seen, no closed eddy was found.

Figure 4.25 (b) depicts the wind stress on 1 January 2001. Mean northeasterly wind speed was 4.5 m/s. Despite quite strong wind, a cyclonic eddy was present. Comparing of wind stress on 20 December 2000 (Figure 4.25 (a)) which had the same mean wind speed but slightly different pattern at the lower Gulf where winds were more from the east, no eddy was found.

From the above mention, it is speculated that eddy is formed when wind stress is weak and that when wind stress is strong, surface currents tend to flow in a one-directional pattern thus eddy is not formed. To investigate further, the model was driven by idealized steady uniform wind of different magnitude and direction without prescribing tide at the open boundary. Experiments were performed for the case of wind blowing from northeast, east, southeast and west as they represented the actual prevailing direction of wind in northeast monsoon season, the transition period and the southwest monsoon season respectively. For each wind direction, two experiments were carried out for wind magnitude of 2 m/s and 5 m/s representing the weak and strong wind conditions actually occurred. Current at the 15<sup>th</sup> day after integration were analyzed for eddy generation mechanism.

In general, current patterns driven by 2 m/s wind were similar to that of 5 m/s except that they are lesser in magnitudes. Steady and uniform northeasterly wind of 5 m/s drove the current southwestward to the west coast (Figure 4.26). The piling water at the coast generated a southward flowing current below the surface (10 m). At this depth, flow in the Upper Gulf deflected more to the right of surface current according to Ekman theory resulted in a northward flowing current which separates into a cyclonic eddy and an anticyclonic eddy. Steady and uniform easterly wind of 5 m/s drove the current northwestward into the Gulf (Figure 4.27). Eddies and meanders were seen in current at

10 m depth. Steady and uniform southeasterly wind of 5 m/s and 2 m/s generated similar current patterns to that of driven by easterly wind. Steady and uniform westerly wind of 5 m/s drove the current to the east coast at the Upper Gulf (Figure 4.28). Constrained by topography, the currents flow southeastward along the coast and out of the Gulf. Current at 10 m depth developed an anticyclonic gyre at the Upper Gulf.

These experiments suggest that currents in the Gulf of Thailand exhibit shallow water type of Ekman transport where surface currents tend to flow in the same direction as the wind. In addition, currents in the Gulf are constrained by topography and affected by Coriolis force. Exerted by strong wind of 5 m/s, surface currents tend to flow in or out of the Gulf. Meanders often occur, but no gyre or eddy is formed. More vigorous eddies are found in current at 10 m depth when driven by wind of 5 m/s. Likewise, eddies are found when driving with wind of 2 m/s, but they are weaker compared to that driven by stronger wind. When strong winds prevail, it is not likely that eddy occurs. Rather, surface currents are characterized by unidirectional flows. However, it can be seen from the experiments that eddies are better formed at 10 m depth which correspond to the wind-tidally driven simulation (experiment EC) in that eddies are found in greater numbers below the surface (see monthly mean current at surface, 10 m and 40 m at Appendix C). In reality, winds in the Gulf are not steady, their magnitude change considerably from time to time. Thus when weaker winds prevail, eddies which exist in the layer lower from the surface can manifest themselves on sea surface current.

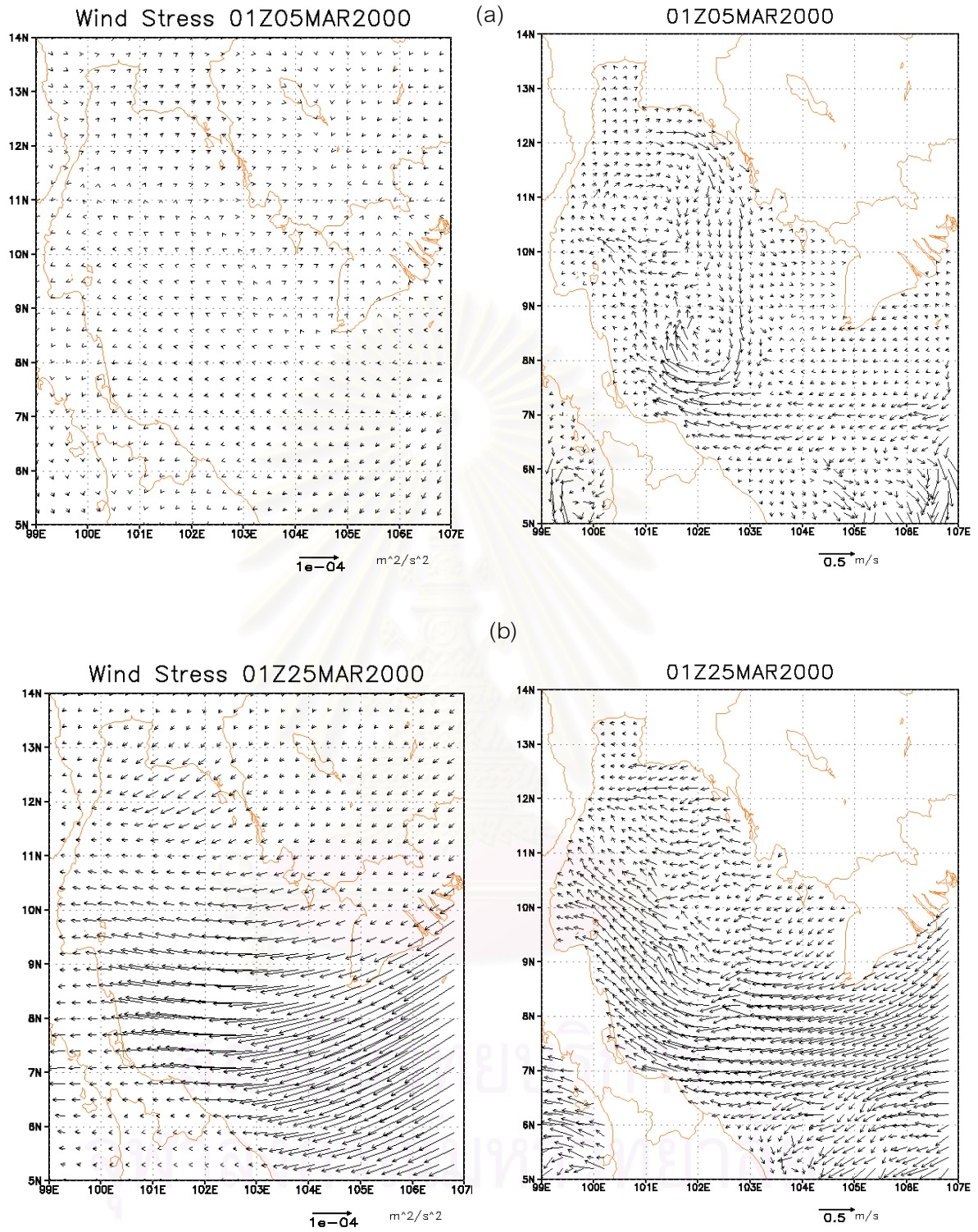


Figure 4.23 Wind stress from NOGAPS and simulated current in March 2000 when an anticyclonic eddy was present and absent (a) on 5 March 2000 when an anticyclonic eddy occurred (b) on 25 March 2000 when no eddy occurred

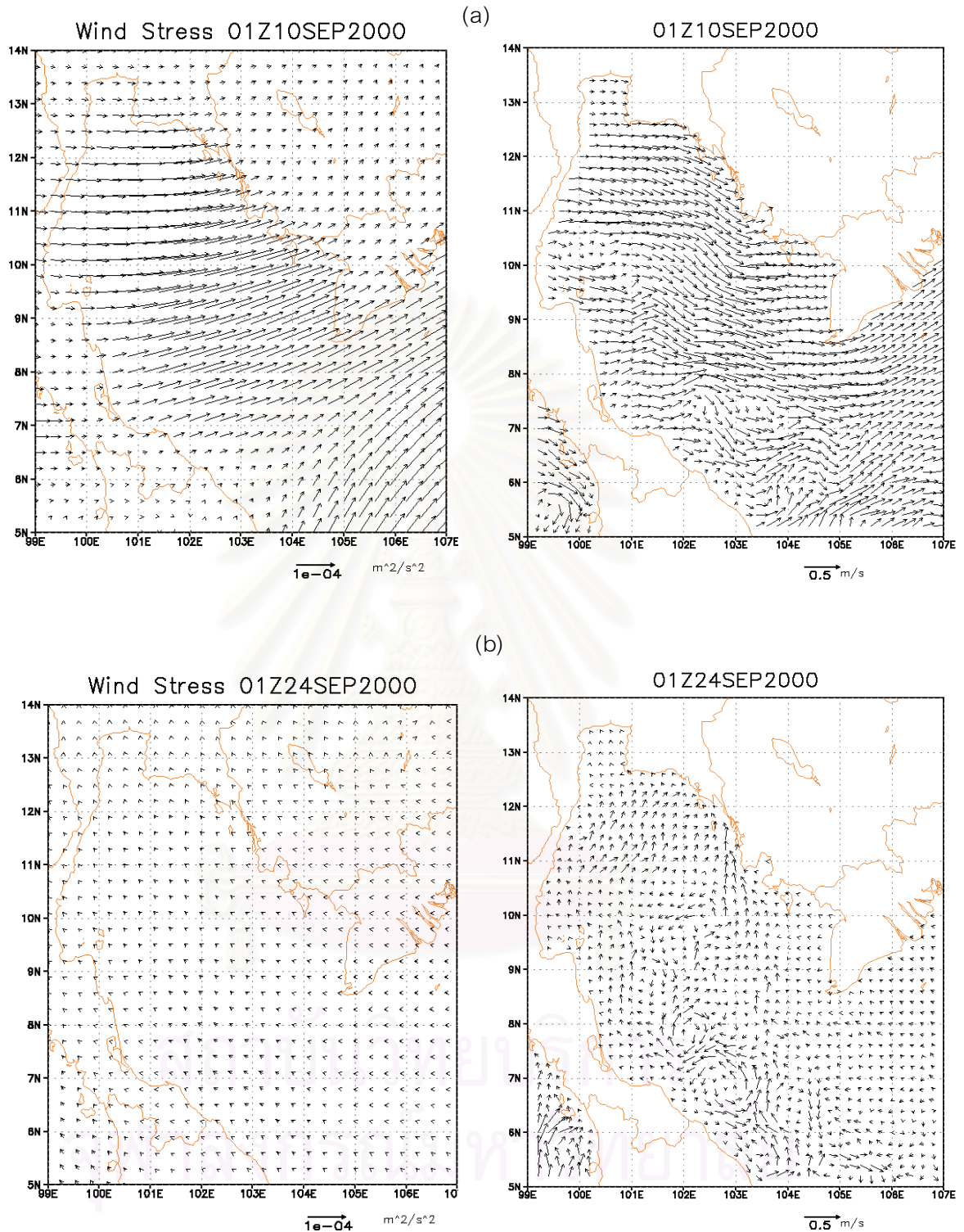


Figure 4.24 Wind stress from NOGAPS and simulated current in September 2000 when a dipole eddy was present and absent. (a) on 10 September 2000 when no eddy occurred (b) on 24 September 2000 when an anticyclonic eddy and a cyclonic eddy were present

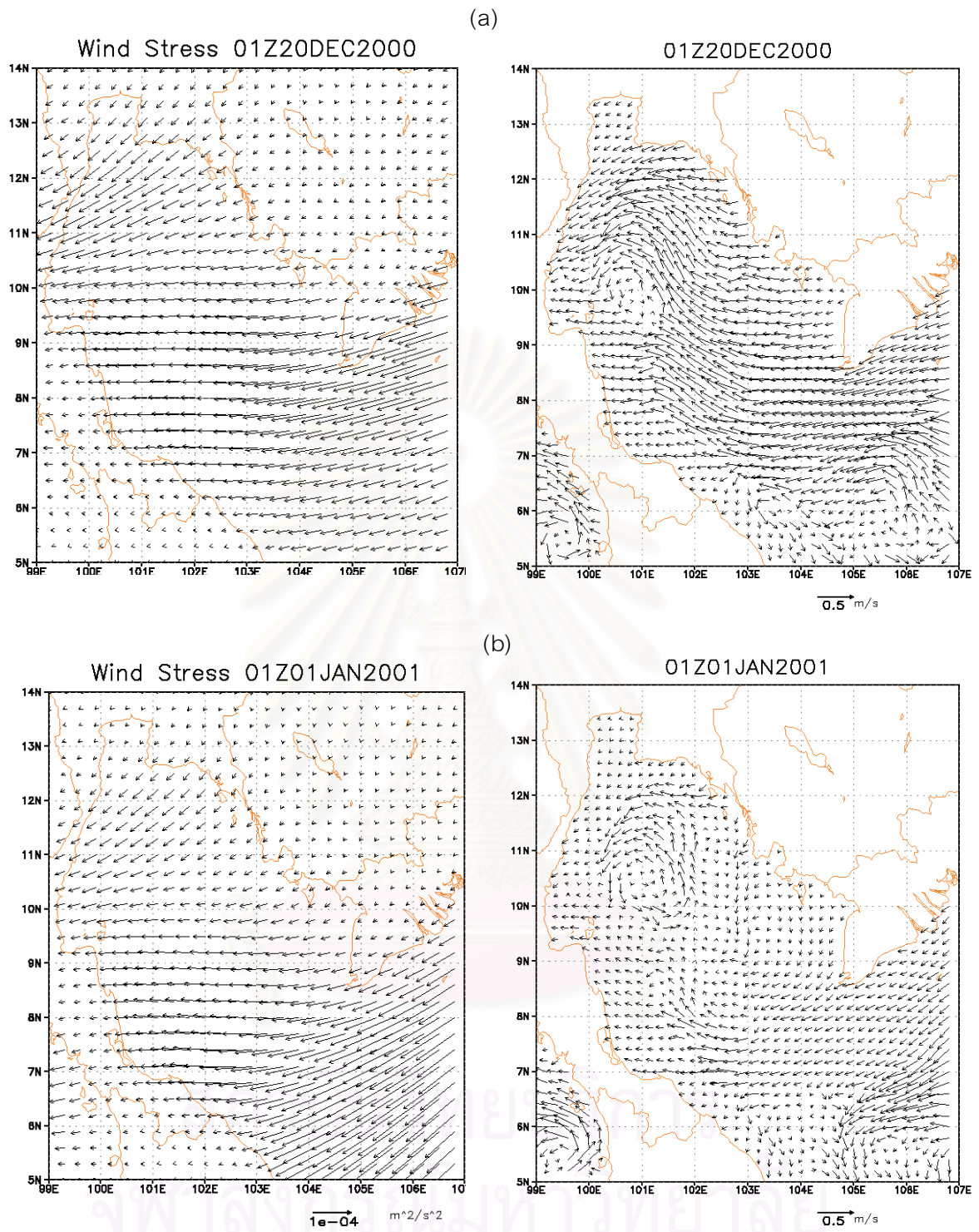
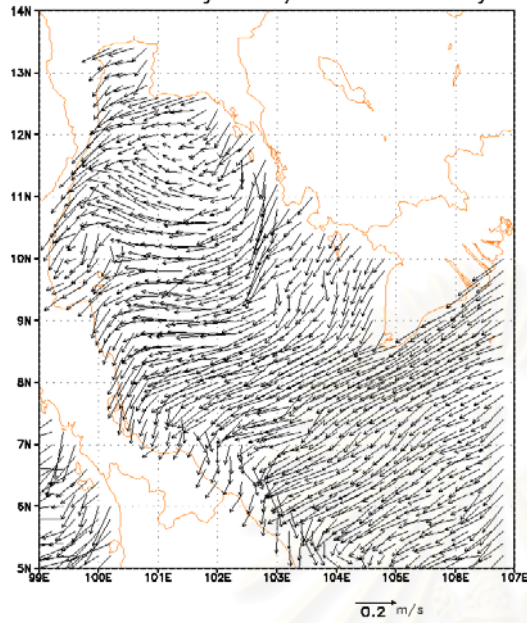


Figure 4.25 Wind stress from NOGAPS and simulated current in December 2000 when a cyclonic eddy was present and absent (a) on 20 December 2000 when no eddy occurred (b) on 1 January 2001 when a cyclonic eddy occurred

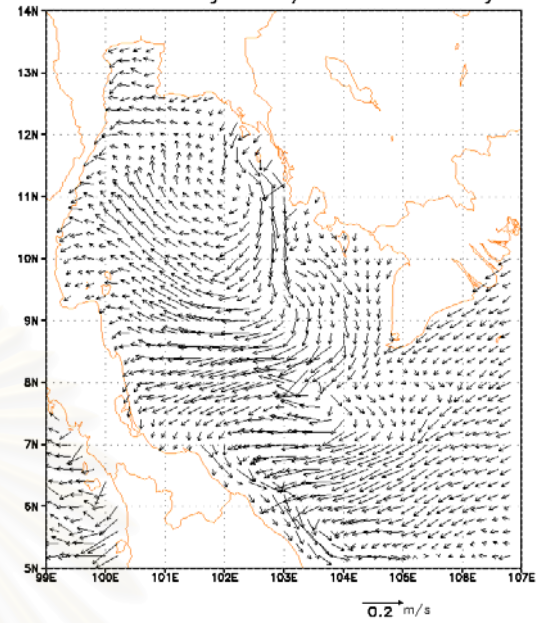
(a)

Current driven by 5 m/s northeasterly wind

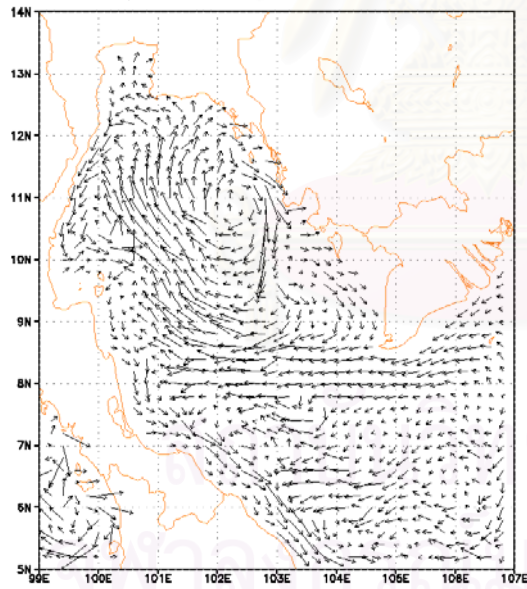


(b)

Current driven by 2 m/s northeasterly wind



(c)



(d)

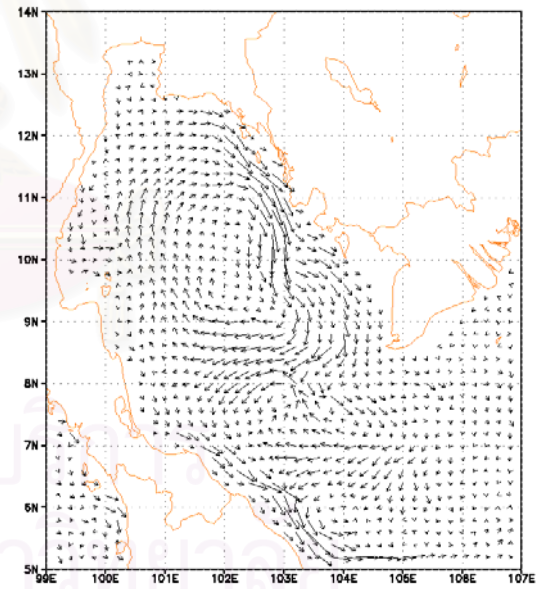


Figure 4.26 Current driven by steady and uniform northeasterly wind

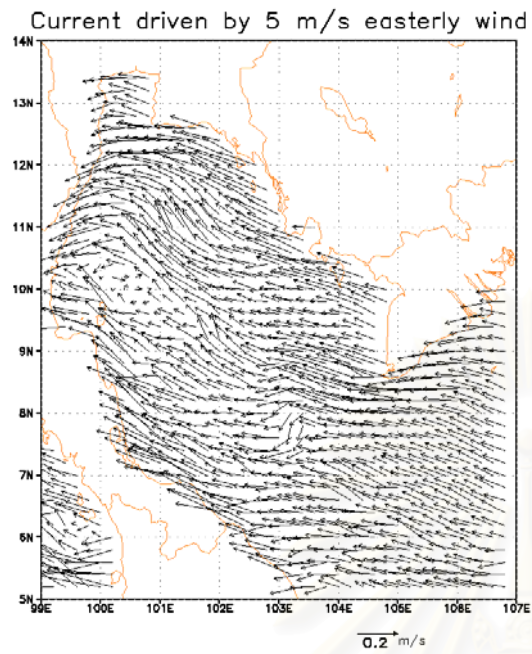
(a) current at surface driven by 5 m/s wind (b) current at surface driven by 2m/s wind

(c) current at 10 m depth driven by 5 m/s wind (d) current at 10 m depth driven by

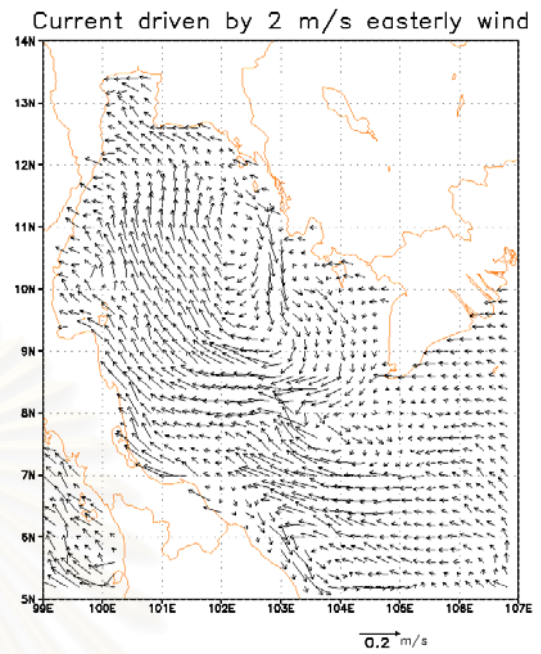
2 m/s wind



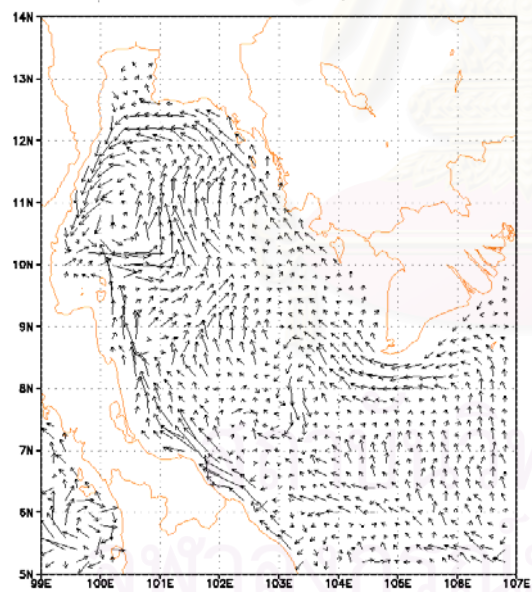
(a)



(b)



(c)



(d)

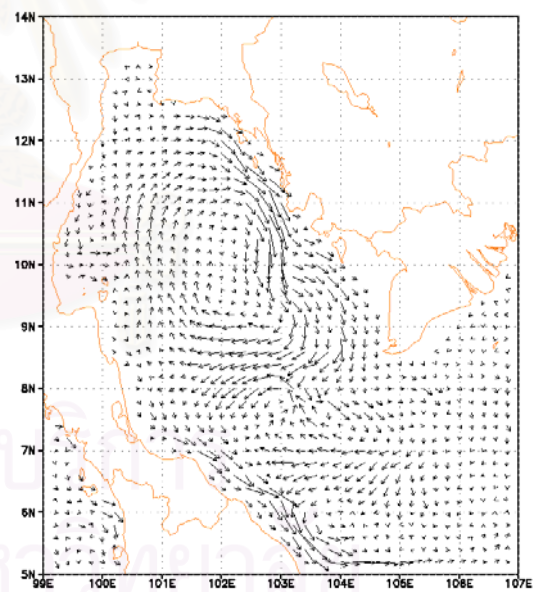


Figure 4.27 Current driven by steady and uniform easterly wind

- (a) current at surface driven by 5 m/s wind (b) current at surface driven by 2 m/s wind  
 (c) current at 10 m depth driven by 5 m/s wind (d) current at 10 m depth driven by 2 m/s wind

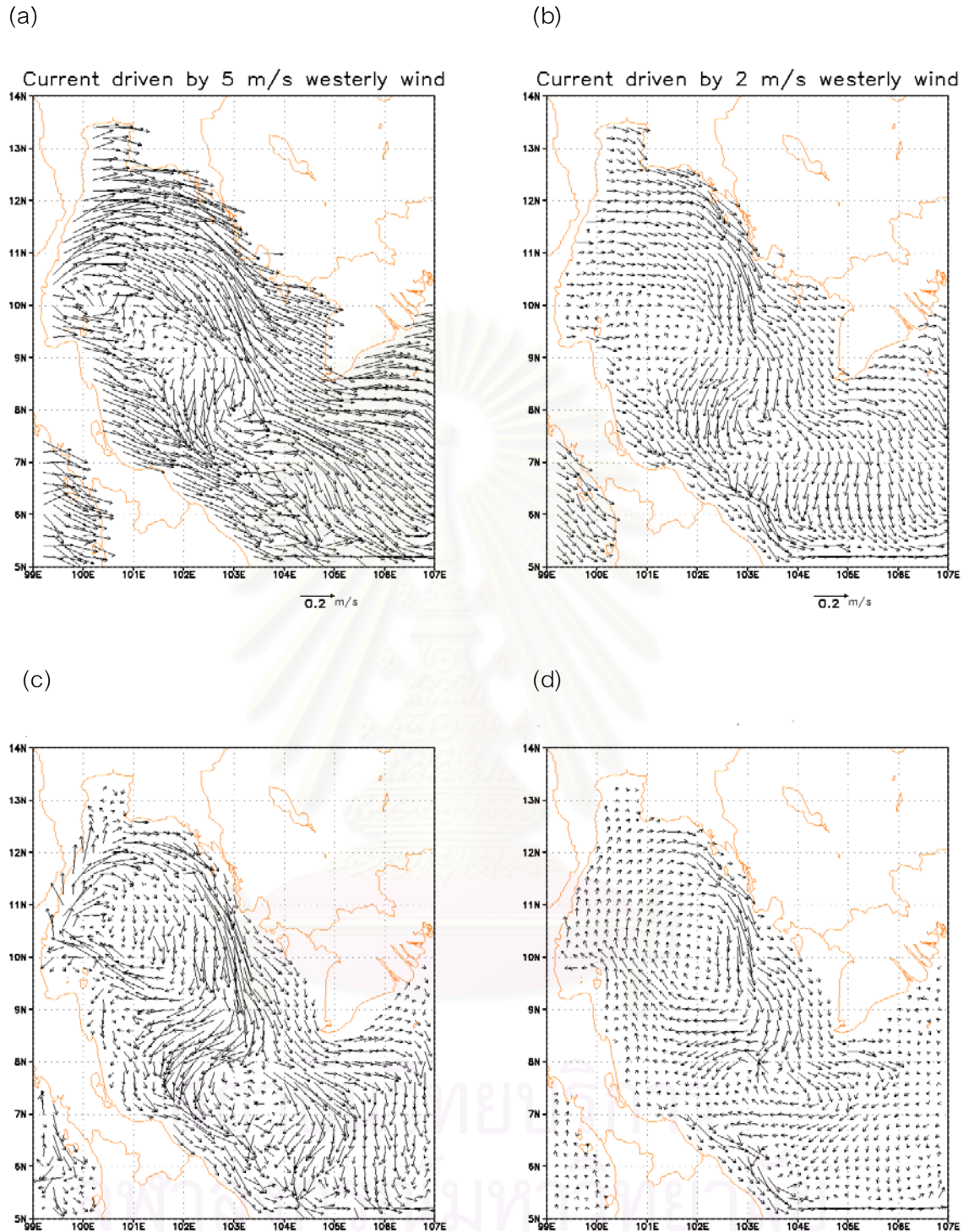


Figure 4.28 Current driven by steady and uniform westerly wind

(a) current at surface driven by 5 m/s wind (b) current at surface driven by 2m/s wind  
 (c) current at 10 m depth driven by 5 m/s wind (d) current at 10 m depth driven by  
 2 m/s wind

## CHAPTER 5

### DISCUSSION

#### 5.1 Model verification

In general, the model can reasonably reproduce observed current patterns as demonstrated by current comparisons at Ko Chang (Figure 4.7) in southwest monsoon season and Huahin (Figure 4.8) and Ko Sichang (4.9) in the northeast monsoon season. However the model cannot reproduce fast changing currents observed at Ko Sichang (Figure 4.6) in southwest monsoon season. This may be accountable by many factors. Most importantly, currents in the model were driven by wind field which, for this study, were derived from global numerical weather prediction model which has coarse resolution (1 degree) resulting in almost uniform wind field over the Inner Gulf. Observed currents are anticipated to be driven by locally non-uniform and unsteady wind. Secondly, this model do not account for the presence of islands at Ko Sichang, while observed currents experience lateral shear with the islands. Thirdly, the phase shifts between observed and calculated currents may result from the fact that discrepancies between observed and calculated tidal elevation do exist when driving the model solely with co-oscillation tide. As tidal current is sensitive to spatial gradient of sea surface elevation, discrepancies between calculated and observed time of highest amplitude of M2, S2, K1 and O1 as mentioned in section 4.1.1 may result in phase shift of tidal current which contributes to the observed current at oceanographic buoy. Discrepancies in calculation of tidal amplitude may arise from the fact that the model was driven by only 4 largest tidal constituents - M2, S2, K1 and O1- while tidal waves in the real ocean are driven by the astronomical forces which result in many more tidal constituents. Discrepancies in phase comparisons with those from observed tide gauges eventhough the model calculated correct patten of cotidal charts seem to occur from prescribed starting phases at open boundaries. Lastly, the present model only response to prescribed tide, wind and initial horizontal density gradient and stratification in the water column, other governing processes which are not consider by this model may cause such discrepancy in current pattern such as fresh water discharge. It should be pointed out that observations were congregated to only near the head of the Gulf.

Observations from upper part and lower part of the Gulf were not available during the period under consideration. This prevents further investigation of the model response at the other parts of the Gulf.

### 5.1 Eddy characteristics

The only extensive observation which mentioned about eddies in the Gulf dates back to 1959 (Robinson, 1974). It was reported that downwelling occurred in all months in the central part of the Gulf which corresponds with the result that simulated anticyclonic eddies were found more frequently than cyclonic eddies. Besides, the reported areas where downwelling occurred correspond to the two areas where anticyclonic eddies are frequently found in numerical results (see Appendix C). The first one locates at approximately between latitude 10-11 °N longitude 101-102 °E. The other locates at approximately between latitude 8-9 °N longitude 101.5-102.5 °E. Both areas lie in the middle of the Gulf with bottom depth exceeding 60 m and the second area is indeed the deepest spot of the Gulf. In addition, it was reported that a weak counter-clockwise eddy at the surface was better developed at 30 and 50 meters. Similar eddy pattern of better developed at sub-surface was also found in the numerical results. The more distinct eddy pattern at sub-surface may arise from the fact that surface currents are directly under the influence of wind which generally blows in one particular direction. While lower from the surface, inertia of fluids slow the response to the wind and bottom topography has more control on the current.

### 5.2 Eddy generation mechanism

As wind and tide are the two major circulation driving terms in the Gulf of Thailand, experiments were performed to investigate the contribution of individual term to eddy generation. Comparison of simulated wind-tidally driven current (experiment EC) and wind-driven current (experiment EM1) in Figure 4.20 and Figure 4.21 show that without tidal forcing at the open boundaries, eddies still occurred. This fact points out that tide is not essential to eddy generation in the Gulf of Thailand. However the shift of eddy position when taking out tidal forcing depicted in Figure 4.21 suggests that

interaction of wind and tidal forcing may account for the location and scale of eddy. It should be noted that the finding from this study that tide is not the main contributor to eddy generation contradicts to previous numerical simulation done by Yanagi and Takao (1998) which found many small-scale eddies in tide-induced residual current generated by 4 major tidal constituents (M2, S2, K1 and O1) even though both models have similar resolution (10 km). This is another aspect where further investigation should be done.

Comparison of simulated wind-tidally-driven (experiment EC) and tide-induced residual current (experiment EM2) in Figure 4.22 shows that without wind forcing, eddy hardly developed. This fact points out that wind is the major contributor to eddy generation in the Gulf of Thailand. To investigate the wind condition under which eddy is generated, three events where eddies occurred from wind-tidally driven current (experiment EC) were selected consisting of the anticyclonic eddy on 5 March 2000, the dipole eddy on 24 September 2000 and the cyclonic eddy on 1 January 2001. The three eddies occurred under different prevailing winds which are easterly, westerly and northeasterly respectively. Numerical experiments EM3 driven by steady and uniform wind were carried out. Only the cyclonic eddy on 1 January 2001 can be reproduced from the numerical experiment. When exerted with northeasterly wind of 5 m/s, currents at 10 m depth developed a cyclonic eddy and an anticyclonic eddy at the upper Gulf (Figure 5.1 (a)). This pattern arises from Ekman current which deflect to the right of northeasterly wind resulting in northward current. When it encountered the coast in the north, the current diverged into a cyclonic eddy and an anticyclonic eddy. This process indeed occurred when northeasterly wind blew over the upper Gulf in December 2000. Subsurface current developed two eddies similar to the experiment (Figure 5.1 (b)). Later the cyclonic eddy could be seen at the surface. However the anticyclonic eddy on 5 March 2000 could not be reproduced from steady and uniform easterly or southeasterly wind. Currents in the experiments tended to form a large anticyclonic gyre rather than eddy. Likewise, the dipole eddy on 24 September could not be reproduced from steady and uniform westerly wind experiment. When consider the pattern of winds during the two-eddies formations, it was found that winds were weak and variable. This

fact points out that direct steady and constant wind forcing may not be accountable for the presence of these two eddies. In reality, wind varies over the space and time scales which may result in wind stress curl or inertial motion. The fact that the two main areas where eddies frequently occurred are the deepest parts in the Gulf suggests that bottom topography might play a role in eddy generation. Other mechanisms such as shear between strong currents may also be plausible. The present model also includes horizontal density gradient and stratification effect, these two mechanisms may induce instability between fronts of two water masses. However, for this study, there is insufficient evidence pertaining to these mechanisms.

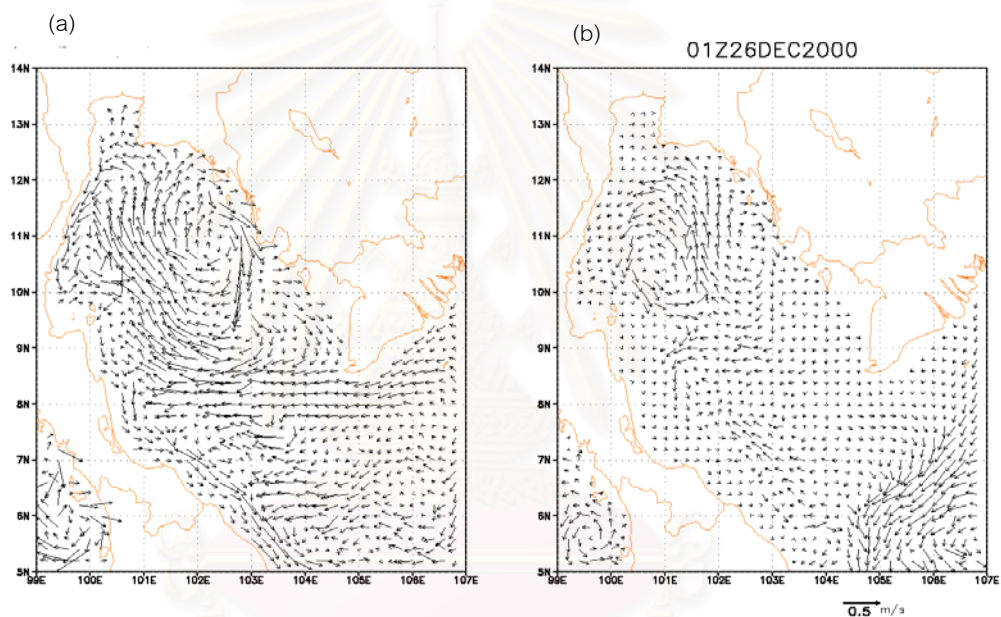


Figure 5.1 (a) current at 10 m depth driven by steady and uniform westerly wind of 5 m/s. (b) current at 10 m depth driven by NOGAPS wind on 26 December 2000

### 5.3 Detection of eddy by ocean color

This study applied ocean color to eddy detection by treating chlorophyll<sub>a</sub> concentration as a tracer, thus it is based on the assumption that cyclonic eddies may cause surface divergence thereby bringing water from below to the surface. And that upwelled water may contain higher nutrients thereby higher chlorophyll<sub>a</sub> concentration. As most eddies found in the simulation are anticyclonic, chlorophyll<sub>a</sub> may not be a good tracer.

## CHAPTER 6

### CONCLUSIONS AND RECOMMENDATIONS

#### 6.1 Conclusions

Numerical simulation of current in the Gulf of Thailand driven by the combination of wind stress from numerical weather prediction, co-oscillation tide and initial climatological horizontal density gradient and stratification were carried out during the period of January 2000-February 2001. The findings are as follows;

1. Both cyclonic and anticyclonic eddies are found in the Gulf of Thailand. Eddies spatial scales are in the order of 100-200 km. Eddies time scales are in the order of 2 days to 2 weeks.
2. There are two main areas where eddies frequently occur. The first one locates at approximately between latitude  $10-11^{\circ}$  N longitude  $101-102^{\circ}$  E. The other locates at approximately between latitude  $8-9^{\circ}$  N longitude  $101.5-102.5^{\circ}$  E. Both areas lie in the middle of the Gulf where bottom depth exceeding 60 m and the second area is indeed the deepest part of the Gulf.
3. Numerical experiments show that wind is the major contributor to eddy generation in the Gulf of Thailand, while tide is not the essential causative term to eddy generation. However, interaction between wind and tide may account for the location and scale of eddies.

## 6.2 Recommendations

1. More observations are obviously needed to verify the characteristics of eddies.
2. As wind plays a significant role in eddy generation, better accuracy of eddy simulation can be achieved by using local numerical weather prediction data which should yield better spatial variability than the present global wind data.
3. Simulation of eddy in the Gulf of Thailand can be improved by employing finer resolution model which should better resolve eddy of smaller-scale in the near shore area.
4. The accuracy of the present model can be improved by various ways. The model response to co-oscillation tide is very sensitive to the model bathymetry. Apart from the four major constituents (M2, S2, K1 and O1), inclusion of other constituents which have noticeable amplitude in the Gulf of Thailand (e.g. P1, Q1, J1, T2, K2) may improve the model accuracy. Simulation of tidal response in this study is done with initial climatological temperature and salinity. Although this initialization makes the model resemble to true ocean, it nevertheless includes additional processes which may arise from stratification such as internal tide. Thus further investigation on influence of stratification on tidal current should be explored.
5. Further investigation on eddy generation mechanisms should consider the inertial motion in the Gulf of Thailand.
6. Ocean color sensor should be used incorporation with other sensors such as microwave sensor to alleviate the high frequency of cloud coverage over the Gulf of Thailand and provide better resolution in both space and time.



## REFERENCES

- Aristegue, J., et al. 1997. The influence of island-generated eddies on chlorophyll distribution: A study of mesoscale variation around Gran Canaria. Deep-Sea Research Part I 44: 71-96.
- Blumberg, A. F., and G. L. Mellor. 1987. A description of a three-dimensional coastal ocean circulation model. In N. Heaps (ed.), Three-Dimensional Coastal Ocean Models, pp. 1-16. Washington, D.C.: American Geophysical Union.
- Bograd, S. J., P. J. Stabeno, and J. D. Schumacher. 1994. A census of mesoscale eddies in Shelikof Strait, Alaska, during 1989. Journal of Geophysical Research 99 (C9): 18,243-18,254.
- Buranapratheprat, A. 1997. Hydrodynamic model for investigation of oil spill in the Gulf of Thailand. Master's Thesis, Department of Marine Science, Faculty of Science, Chulalongkorn University.
- Choi, B. H., D. G. Kim, and D. H. Kim. 1997. A numerical tidal model for the Southeast Asian Seas. In H. Yu, K. S. Low, N. M. Son, and D.-Y. Lee (eds.), Oil spill modelling in the East Asian Region, pp. 38-53. Quezon City, Philippines: GEF/UNDP/IMO Regional Programme for the Prevention and Management of Marine Pollution in the East Asian Seas.
- Davies, P. A., J. M. Dakin, and R. A. Falconer. 1995. Eddy formation behind a coastal headland. Journal of Coastal Research 11: 154-167.
- Egbert, G. D., and S. Y. Erofeeva. 2002. Efficient inverse modeling of barotropic ocean tides. Journal of Atmospheric and Oceanic Technology 19: 183-204.
- Enriquez, A. G., and C. A. Friehe. 1995. Effect of wind stress and wind stress curl variability on coastal upwelling. Journal of Physical Oceanography 25: 1,651-1,671.

- Fang, G., Y. K. Kwok, K. Yu, and Y. Zhu. 1999. Numerical simulation of principal tidal constituents in the South China Sea, Gulf of Tonkin and Gulf of Thailand. Continental Shelf Research 19: 845-869.
- Flather, R. A. 1988. A numerical model investigation of tides and diurnal-period continental shelf waves along Vancouver Island. Journal of Physical Oceanography 18: 115-139.
- Galperin, B., and G. L. Mellor. 1990. A time-dependent, three-dimensional model of the Delaware Bay and river system Part 1: Description of the model and tidal analysis. Estuarine, Coastal and Shelf Science 31: 231-253.
- Han, G. 2000. Three-dimensional modeling of tidal currents and mixing quantities over the Newfoundland Shelf. Journal of Geophysical Research 105(C5): 11,407-11,422.
- Hatamaya, T., T. Awaji, and K. Akitomo. 1996. Tidal currents in the Indonesian Seas and their effect on transport and mixing. Journal of Geophysical Research 101 (C5): 12,353-12,373.
- Ho, C. R., N. J. Kuo, Q. Zheng, and Y. S. Soong. 2000. Dynamically active areas in the South China Sea detected from TOPEX/POSEIDON satellite altimeter data. Remote Sensing of Environment 71: 320-328.
- Hogan, T. F., and T. E. Rosmond. 1991. The description of the Navy Operational Global Atmospheric Prediction System. Monthly Weather Review 119: 1,786-1,815.
- Hwang, C., and S.-A. Chen. 2000. Circulation and eddies over the South China Sea derived from TOPEX/Poseidon altimetry. Journal of Geophysical Research 105 (C10): 23,943-23,965.
- Ikeda, M., L. A. Mysak, and W. J. Emery. 1984. Observation and modeling of satellite-sensed meanders and eddies off Vancouver Island. Journal of Physical Oceanography 14: 3-21.

- Johannessen, J. A., E. Svendsen, S. Sandven, O. M. Johannessen, and K. Lygre. 1989. Three-dimensional structure of mesoscale eddies in the Norwegian Coastal Current. Journal of Physical Oceanography 19: 3-19.
- Kamenkovich, V. M., M. N. Koshlyakov, and A. S. Monin. 1986. Synoptic eddies in the ocean. Dordrecht, Netherland : D.Reidel.
- Kantha, L. H., and C. A. Clayson. 2000. Numerical models of oceans and oceanic processes. San Diego: Academic Press.
- Kempler, S. 2000. Sea-viewing Wide Field-of-view Sensor (SeaWiFS) Level 1A and Level 2 HDF Dataset Guide Document Version 2.0 [Online]. Maryland: NASA Goddard Space Flight Center. Available from: [http://daac.gsfc.nasa.gov/DATASET\\_DOCS/SeaWiFS\\_L1A2\\_Guide.html](http://daac.gsfc.nasa.gov/DATASET_DOCS/SeaWiFS_L1A2_Guide.html) [2000, April 5]
- Lee, S. H., and R. C. Beardsley. 1999. Influence of stratification on residual tidal currents in the Yellow Sea. Journal of Geophysical Research 104(C7): 15,679-15,701.
- Levitus, S., R. Burgett, and T. P. Boyer. 1994. World ocean atlas 1994 Volume 3: Salinity. NOAA atlas NESDIS 3. Washington D.C.: U.S. Department of Commerce.
- Levitus, S. and T. P. Boyer. 1994. World ocean atlas 1994 Volume 4: Temperature. NOAA atlas NESDIS 4. Washington D.C.: U.S. Department of Commerce.
- Liu, Z., H. Yang, and Q. Liu. 2001. Regional dynamics of seasonal variability in the South China Sea. Journal of Physical Oceanography 31: 272-284.
- Longhurst, A. 1993. Seasonal cooling and blooming in tropical oceans. Deep-Sea Research Part I 40: 2,145-2,165.
- Lowwittayakorn, S. 1998. Analysis of sea surface temperature and salinity from oceanographic bouys with circulation patterns in the Gulf of Thailand from

mathematical model. Master's Thesis, Department of Marine Science, Faculty of Science, Chulalongkorn University.

Mellor, G. L. 1996. Users guide for a three-dimensional, primitive equation, numerical Ocean Model. rev. ed. New Jersey: Princeton University.

Mellor, G. L., and T. Yamada. 1982. A hierarchy of turbulence closure models for planetary boundary layers. Journal of Atmospheric Science 31: 1,791-1,896. Cited in Mellor, G. L. 1996. Users guide for a three-dimensional, primitive equation, numerical Ocean Model. rev. ed. New Jersey: Princeton University.

Millero, F. J., and A. Poisson. 1981. International one-atmosphere equation of state of sea-water. Deep-Sea Research Part I 27: 255-264. Cited in Pond, S., and G.L. Pickard. 1983. Introductory Dynamical Oceanography. Oxford: Pergamon Press.

Namba, T. 2000. The circulation in the upper and intermediate layers of the South China Sea. Doctoral dissertation, Department of Engineering, Kyushu University.

Open University Course Team. 1989. Ocean circulation. Great Britain: BPCC Wheatons.

O'Reilly, J. E., *et al.* 2000. SeaWiFS postlaunch calibration and validation analyses, Part 3. In S. B. Hooker, and E. R. Riestone (eds.), NASA Tech. Memo. 2000-206892. Vol. 11, pp. 11-12. Greenbelt, Maryland: NASA Goddard Space Flight Center.

Pares-Sierra, A., W. B. White, and C.-K. Tai. 1993. Wind-driven coastal generation of annual mesoscale eddy activity in the California Current. Journal of Physical Oceanography 23: 1,110-1,121.

Pugh, D. T. 1987. Tides, surges and mean sea-level. Great Britain: Bath Press.

Qu, T. 2000. Upper-layer circulation in the South China Sea. Journal of Physical Oceanography 30: 1,450-1,460.

Rachev, N. H., and E. V. Stanev. 1997. Eddy processes in semiclosed seas: A case study for the Black Sea. Journal of Physical Oceanography 27: 1,581-1,601.

- Robinson, A. R. 1983. Eddies in marine science. Berlin: Springer-Verlag.
- Robinson, M. K. 1974. The physical oceanography of the Gulf of Thailand, Naga Expedition. In E. Brinton, W. A. Newman (eds.), Naga report, Volume3, Part 1, pp. 5-110. La Jolla, California: The University of California, Scripps Institution of Oceanography.
- Siripong, A. 1985. The hydrography of the South China Sea and the Gulf of Thailand. Vol. 4: Wave, tide, and current. Bangkok: United Nations Environmental Programme.
- Smagorinsky, J. 1963. General circulation experiment with the primitive equations, I. The basic experiment. Monthly Weather Review 91: 99-164. cited in Mellor, G. L. 1996. Users guide for a three-dimensional, primitive equation, numerical Ocean Model. rev. ed. New Jersey: Princeton University.
- Snidvongs, A. 1998. The oceanography of the Gulf of Thailand: Research and management priorities. In D.M. Johnston (ed.), SEAPOL Integrated studies of the Gulf of Thailand Vol.1, pp. 5-68. Bangkok: Southeast Asian Programme in Ocean Law, Policy and Management.
- Snidvongs, A., and P. Sojisuorn. 1997. Numerical simulations of the net current in the Gulf of Thailand under different monsoon regimes. In Proceeding of the first technical seminar on marine fishery resources survey in the South China Sea, Area I: Gulf of Thailand and Peninsular Malaysia, pp. 54-72. Samutprakarn, Thailand: Training Department, Southeast Asian Fisheries Development Center.
- Tomczak, M. 1996. An introduction to physical oceanography [On line]. Available from: <http://www.es.flinders.edu.au/~mattom/IntroOc/index.htm> [2003, April 10]
- Unesco. 1981. Tenth report of the Joint Panel on Oceanographic Tables and Standards. Unesco Technical Papers in Marine Science, No. 36. Cited in Pond, S., and G.L. Pickard. 1983. Introductory Dynamical Oceanography. Oxford: Pergamon Press.

- Wyrski, K. 1961. NAGA report. Vol. 2. La Jolla, California: The University of California, Scripps Institution of Oceanography.
- Yanaki, T. 1999. Coastal oceanography. Tokyo: Terra Scientific.
- Yanaki, T., T. Takao, and A. Morimoto. 1997. Co-tidal and co-range charts in the South China Sea derived from satellite altimetry data. La mer 35: 85-93.
- Yanaki, T., and T. Takao. 1998. Seasonal variation of three-dimensional circulations in the Gulf of Thailand. La mer 36: 43-55.
- Yanaki, T., S. I. Sachoemar, T. Takao, and S. Fujiwara. 2001. Seasonal variation of stratification in the Gulf of Thailand. Journal of Oceanography 57: 461-470.
- Yokouchi, K., K. Takeshi, I. Matsumoto, G. Fujiwara, H. Kawamura, and K. Okuda. 2000. OCTS-derived chlorophyll-a concentration and oceanic structure in the Kuroshio Frontal Region off the Joban/Kashima Coast of Japan. Remote Sensing of Environment 73: 188-197.



สถาบันวิทยบริการ  
จุฬาลงกรณ์มหาวิทยาลัย



สถาบันวิทยบริการ  
จุฬาลงกรณ์มหาวิทยาลัย

## APPENDIX A

International Equation of State of Sea Water, 1980

The equation of state that is now commonly used is presented by Millero and Poisson (1981, cited in Pond and Pickard, 1983) and also given in UNESCO Technical Paper in Marine Science Number 36 (UNESCO, 1981, cited in Pond and Pickard, 1983). The density of sea water (in  $\text{kg m}^{-3}$ ) as a function of temperature  $T$  ( $^{\circ}\text{C}$ ), salinity  $S$  (psu), and pressure  $p$  (bars) over the typical oceanic range of  $-2$  to  $40$   $^{\circ}\text{C}$  temperature,  $0$  to  $42$  psu salinity, and  $0$  to  $1000$  bars pressure is given to a precision of  $3.5 \times 10^{-3} \text{ kg m}^{-3}$  by

$$\rho(T, S, p) = \rho(T, S, 0)[1 - p / K(T, S, p)]^{-1} \quad (\text{A.1})$$

where  $K(T, S, p)$  is the secant bulk modulus.

The polynomial expressions for  $\rho(T, S, 0)$  and  $K(T, S, p)$  are given below.

For the IES 80, the density of sea water at one standard atmosphere pressure ( $p = 0$ ) is given by:

$$\begin{aligned} \rho(T, S, 0) = & \\ & + 999.842\,594 & + 6.793\,952 \times 10^{-2} T \\ & - 9.095\,290 \times 10^{-3} T^2 & + 1.001\,685 \times 10^{-4} T^3 \\ & - 1.120\,083 \times 10^{-6} T^4 & + 6.536\,332 \times 10^{-9} T^5 \\ & + 8.244\,93 \times 10^{-1} S & - 4.089\,9 \times 10^{-3} TS \\ & + 7.643\,80 \times 10^{-5} T^2 S & - 8.246\,7 \times 10^{-7} T^3 S \\ & + 5.387\,50 \times 10^{-9} T^4 S & - 5.724\,66 \times 10^{-3} S^{1.5} \\ & + 1.022\,70 \times 10^{-4} TS^{1.5} & - 1.654\,6 \times 10^{-6} T^2 S^{1.5} \\ & + 4.831\,40 \times 10^{-4} S^2 & \end{aligned} \quad (\text{A.2})$$



For the IES 80, the secant bulk modulus is given by:

$$\begin{aligned}
 K(T, S, p) = & \\
 & + 19\,652.21 \\
 & + 148.420\,6 \quad T \quad - 2.327\,105 \quad T^2 \\
 & + 1.360\,477 \times 10^{-2} \quad T^3 \quad - 5.155\,288 \times 10^{-5} \quad T^4 \\
 & + 3.239\,908 \quad p \quad + 1.437\,13 \times 10^{-3} \quad Tp \\
 & + 1.160\,92 \times 10^{-4} \quad T^2 p \quad - 5.779\,05 \times 10^{-7} \quad T^3 p \\
 & + 8.509\,35 \times 10^{-5} \quad p^2 \quad - 6.122\,93 \times 10^{-6} \quad Tp^2 \\
 & + 5.278\,7 \times 10^{-8} \quad T^2 p^2 \\
 & + 54.674\,6 \quad S \quad - 0.603\,459 \quad TS \\
 & + 1.099\,87 \times 10^{-2} \quad T^2 S \quad - 6.167\,0 \times 10^{-5} \quad T^3 S \\
 & + 7.944 \times 10^{-2} \quad S^{1.5} \quad + 1.648\,3 \times 10^{-2} \quad TS^{1.5} \\
 & - 5.300\,9 \times 10^{-4} \quad T^2 S^{1.5} \quad + 2.283\,8 \times 10^{-3} \quad pS \\
 & - 1.098\,1 \times 10^{-5} \quad TpS \quad - 1.607\,8 \times 10^{-6} \quad T^2 pS \\
 & + 1.910\,75 \times 10^{-4} \quad pS^{1.5} \quad - 9.934\,8 \times 10^{-7} \quad p^2 S \\
 & + 2.081\,6 \times 10^{-8} \quad Tp^2 S \quad + 9.169\,7 \times 10^{-10} \quad T^2 p^2 S
 \end{aligned}
 \tag{A.3}$$

The above polynomials are taken from UNESCO Technical Papers in Marine Science No. 36, 1981.

## APPENDIX B

## Location of tide gauge stations and oceanographic buoys

Table B.1 Location of tide gauge stations and oceanographic buoys

No.	Station	Latitude (° N)	Longitude (° E)	observed data
T1	Hatien	10.37	104.47	tidal elevation
T2	Kampong Som	10.63	103.48	tidal elevation
T3	Laem Ngob	10.17	102.40	tidal elevation
T4	Laem Sing	12.47	102.07	tidal elevation
T5	Rayong	12.67	101.28	tidal elevation
T6	Ao Sattahip	12.65	100.88	tidal elevation
T7	Ko Si Chang	13.15	100.82	tidal elevation
T8	Bang Pakong	13.50	100.98	tidal elevation
T9	Bangkok Bar	13.43	100.58	tidal elevation
T10	Tachin	13.53	100.27	tidal elevation
T11	Mae Klong	13.38	100.00	tidal elevation
T12	Huahin	12.57	99.97	tidal elevation
T13	Ko Lak	11.80	99.82	tidal elevation
T14	Ko Mattaphon	10.45	99.25	tidal elevation
T15	Ko Prap	9.27	99.43	tidal elevation
T16	Songkla	7.22	100.58	tidal elevation
T17	Pattani	6.88	101.25	tidal elevation
T18	Bang Nara	6.43	101.83	tidal elevation
B1	Huahin	12.50	100.16	current at 3.5 m depth
B2	Ko Si Chang	13.25	100.75	current at 3.5 m depth
B3	Ko Chang	12.00	102.20	current at 3.5 m depth

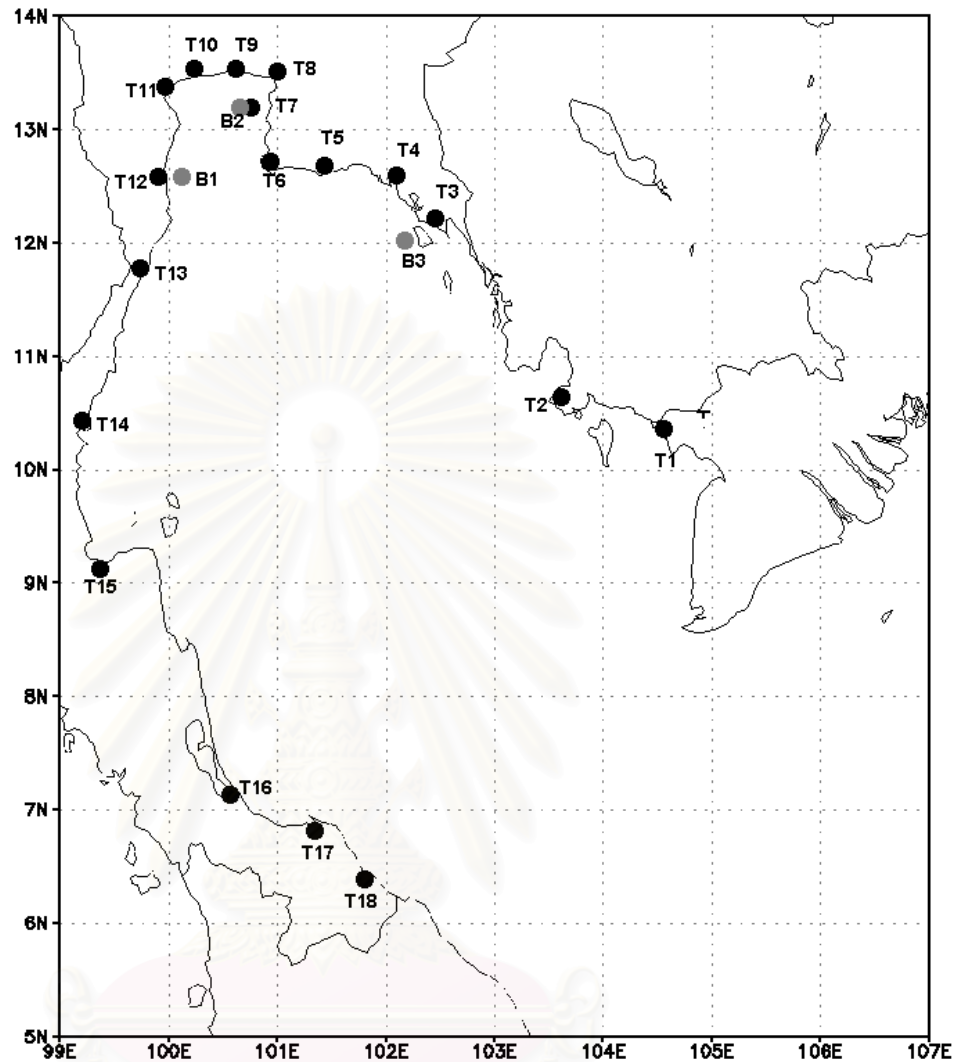


Figure B.1 Location of tide gauge stations (black circle) and oceanographic buoys (gray circle)

## APPENDIX C

## Monthly mean wind stress and current

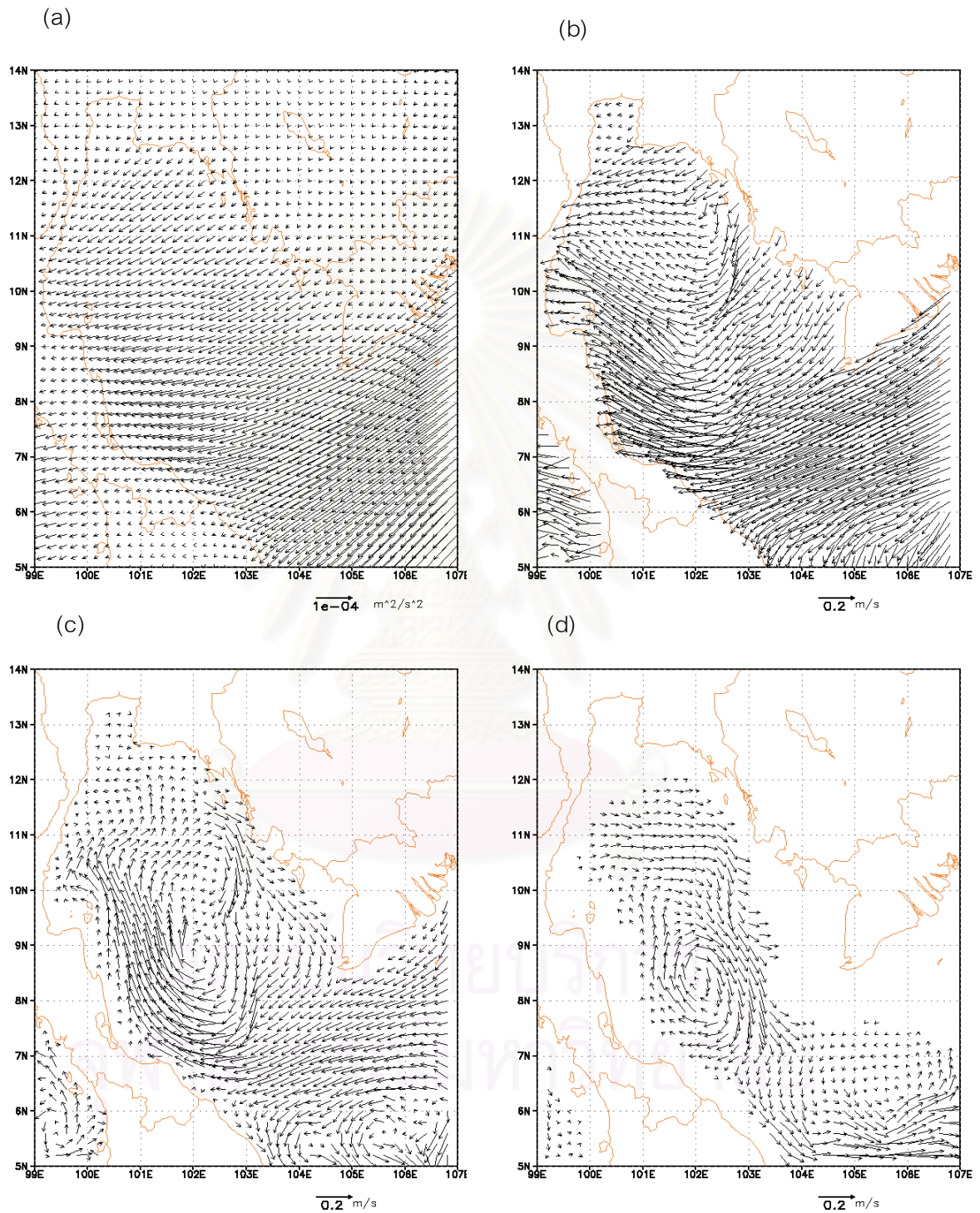


Figure C.1 Monthly mean wind stress and simulated current in January 2000 driven by NOGAPS wind and composite M2,S2, K1 and O1 tides at open boundaries (a) wind stress from NOGAPS (b) surface current (c) current at 10 m depth (d) current at 40 m depth

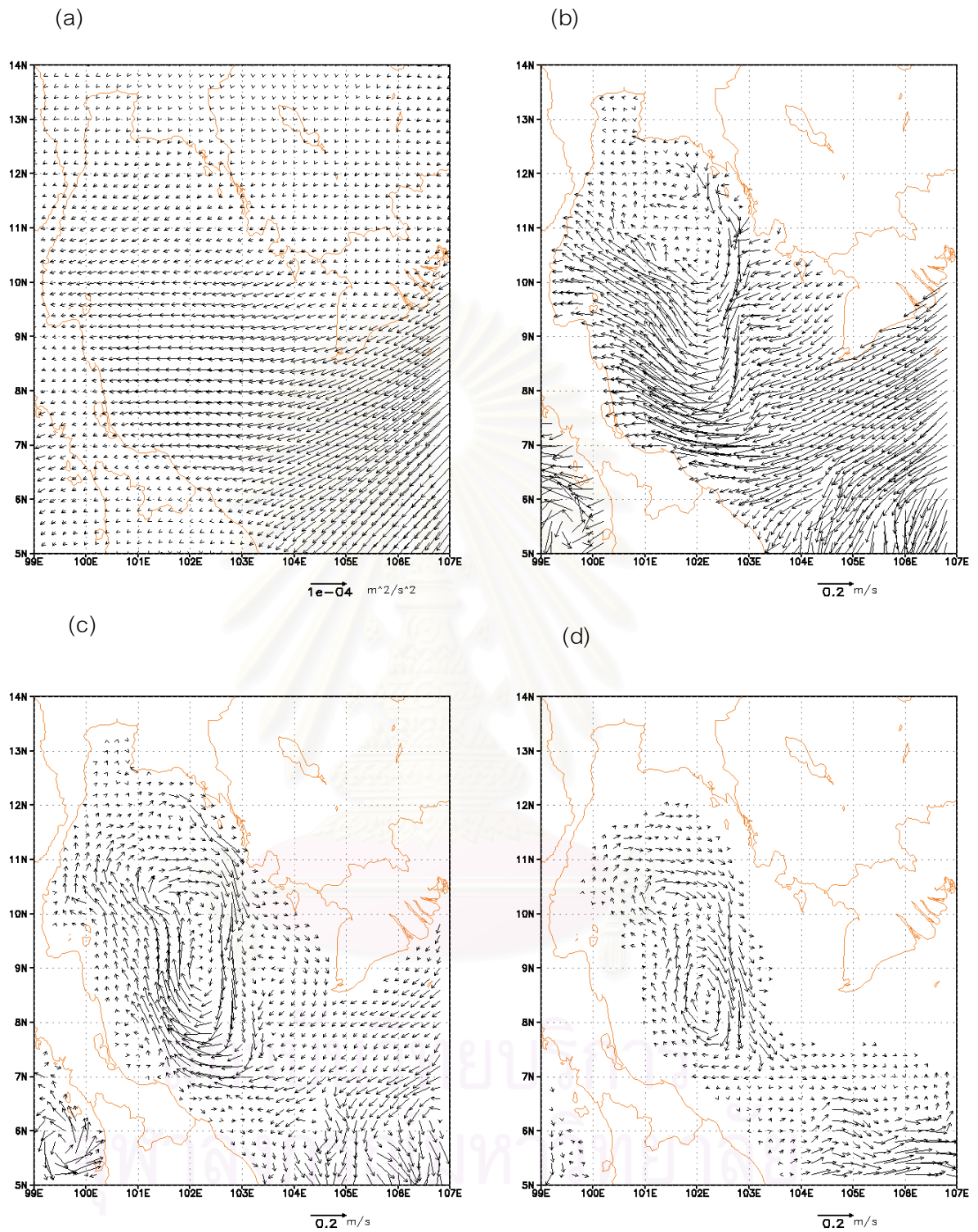


Figure C.2 Monthly mean wind stress and simulated current in February 2000 driven by NOGAPS wind and composite M2,S2, K1 and O1 tides at open boundaries (a) wind stress from NOGAPS (b) surface current (c) current at 10 m depth (d) current at 40 m depth

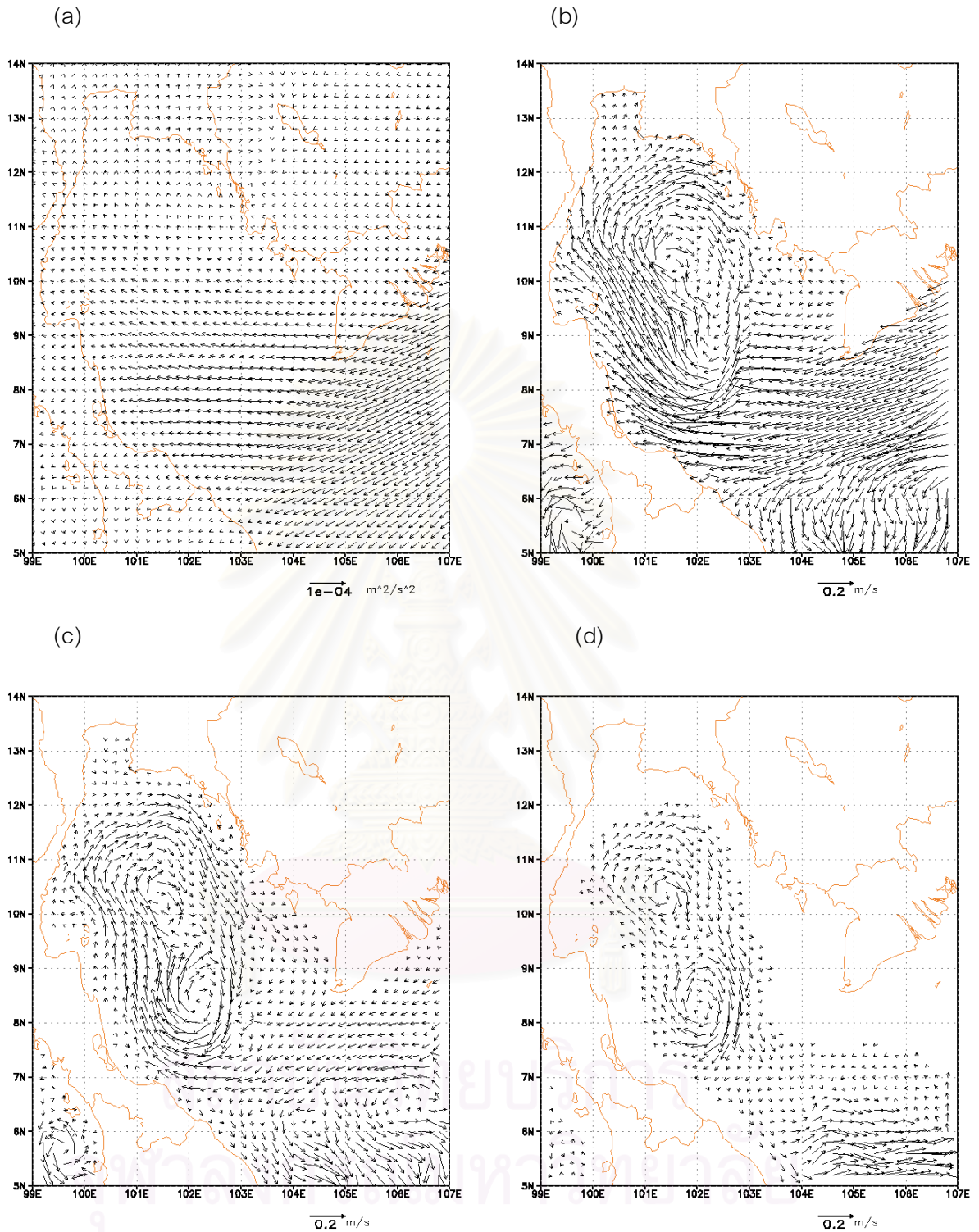


Figure C.3 Monthly mean wind stress and simulated current in March 2000 driven by NOGAPS wind and composite M2,S2, K1 and O1 tides at open boundaries (a) wind stress from NOGAPS (b) surface current (c) current at 10 m depth (d) current at 40 m depth

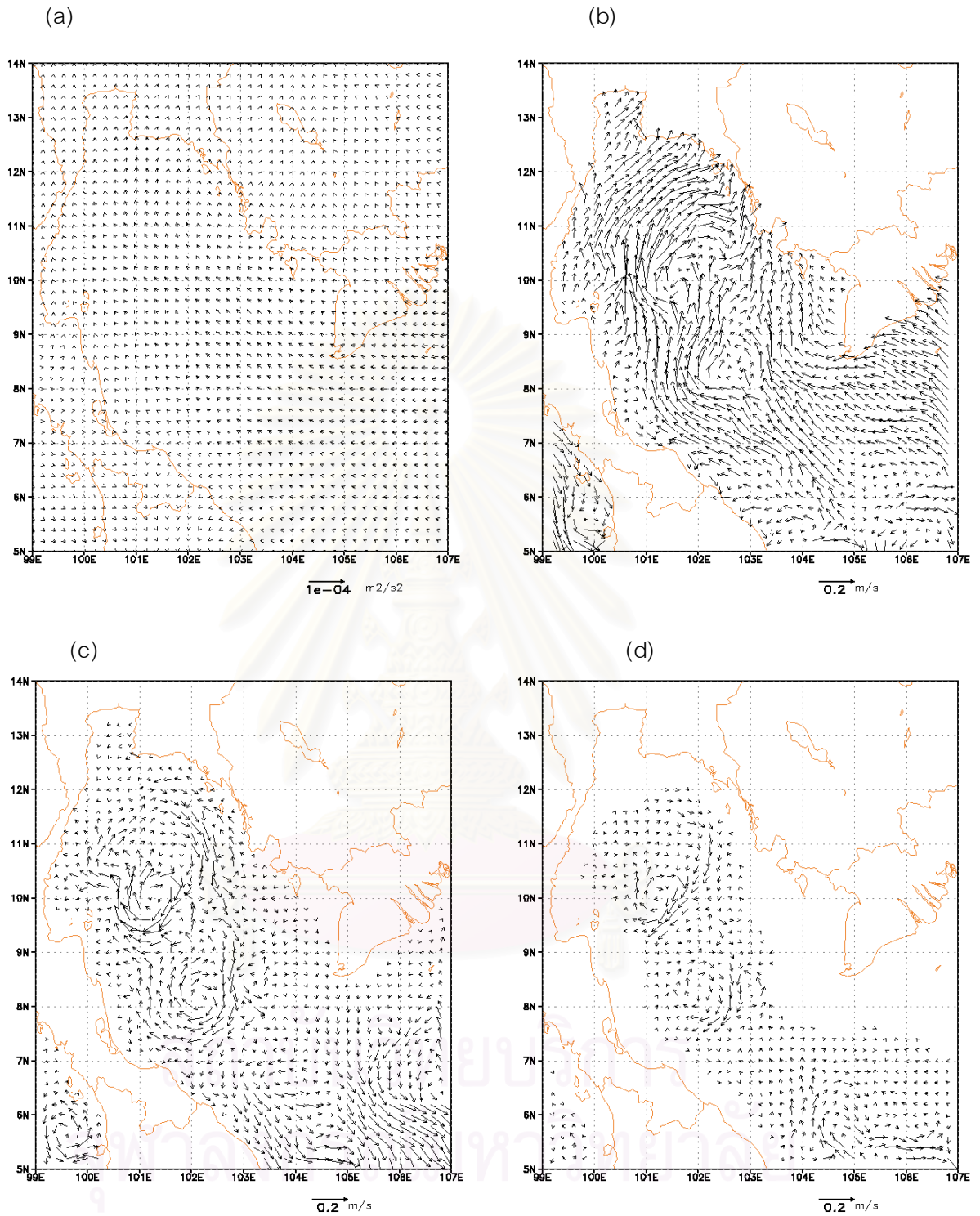


Figure C.4 Monthly mean wind stress and simulated current in April 2000 driven by NOGAPS wind and composite M2, S2, K1 and O1 tides at open boundaries (a) wind stress from NOGAPS (b) surface current (c) current at 10 m depth (d) current at 40 m depth

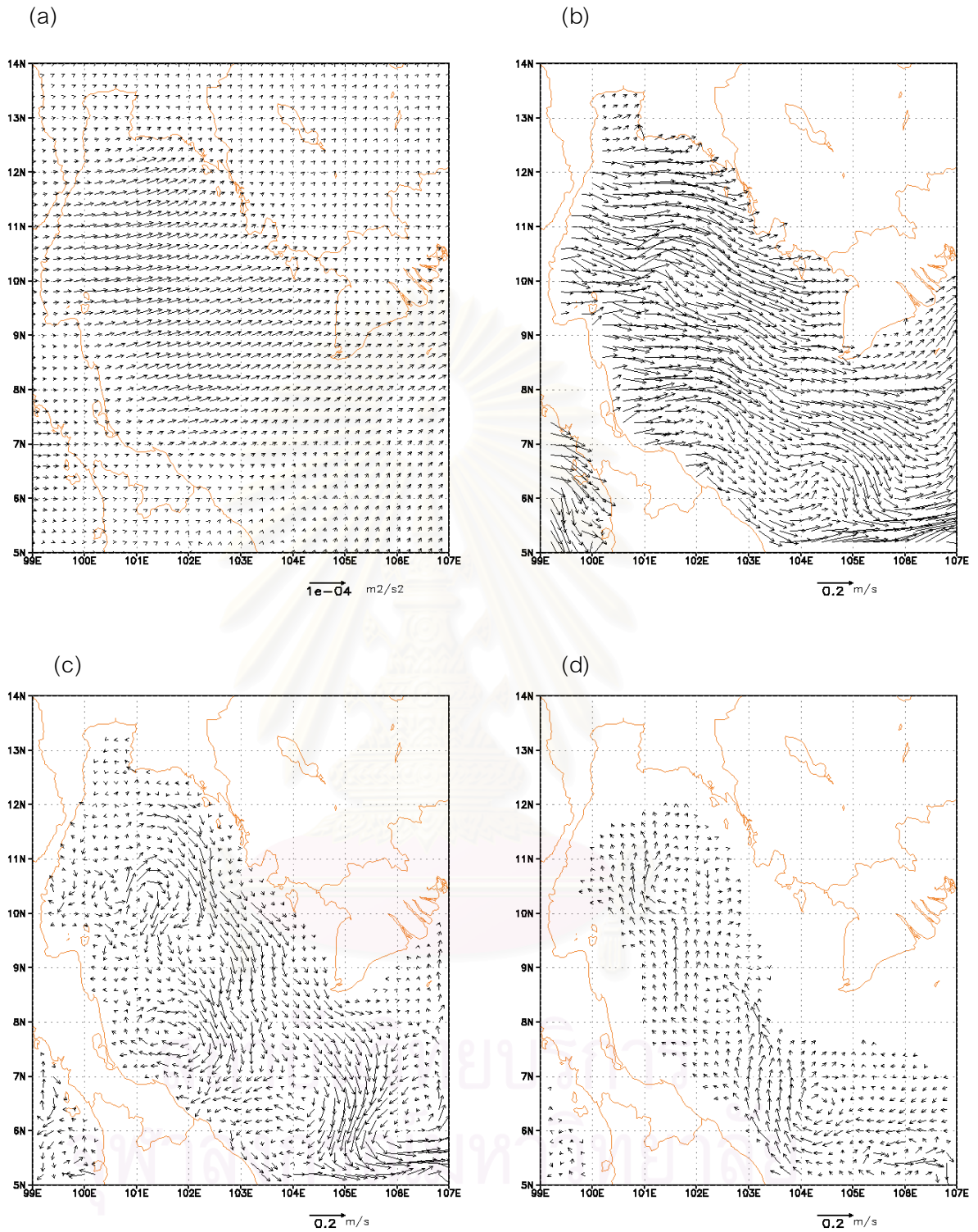


Figure C.5 Monthly mean wind stress and simulated current in May 2000 driven by NOGAPS wind and composite M2,S2, K1 and O1 tides at open boundaries (a) wind stress from NOGAPS (b) surface current (c) current at 10 m depth (d) current at 40 m depth



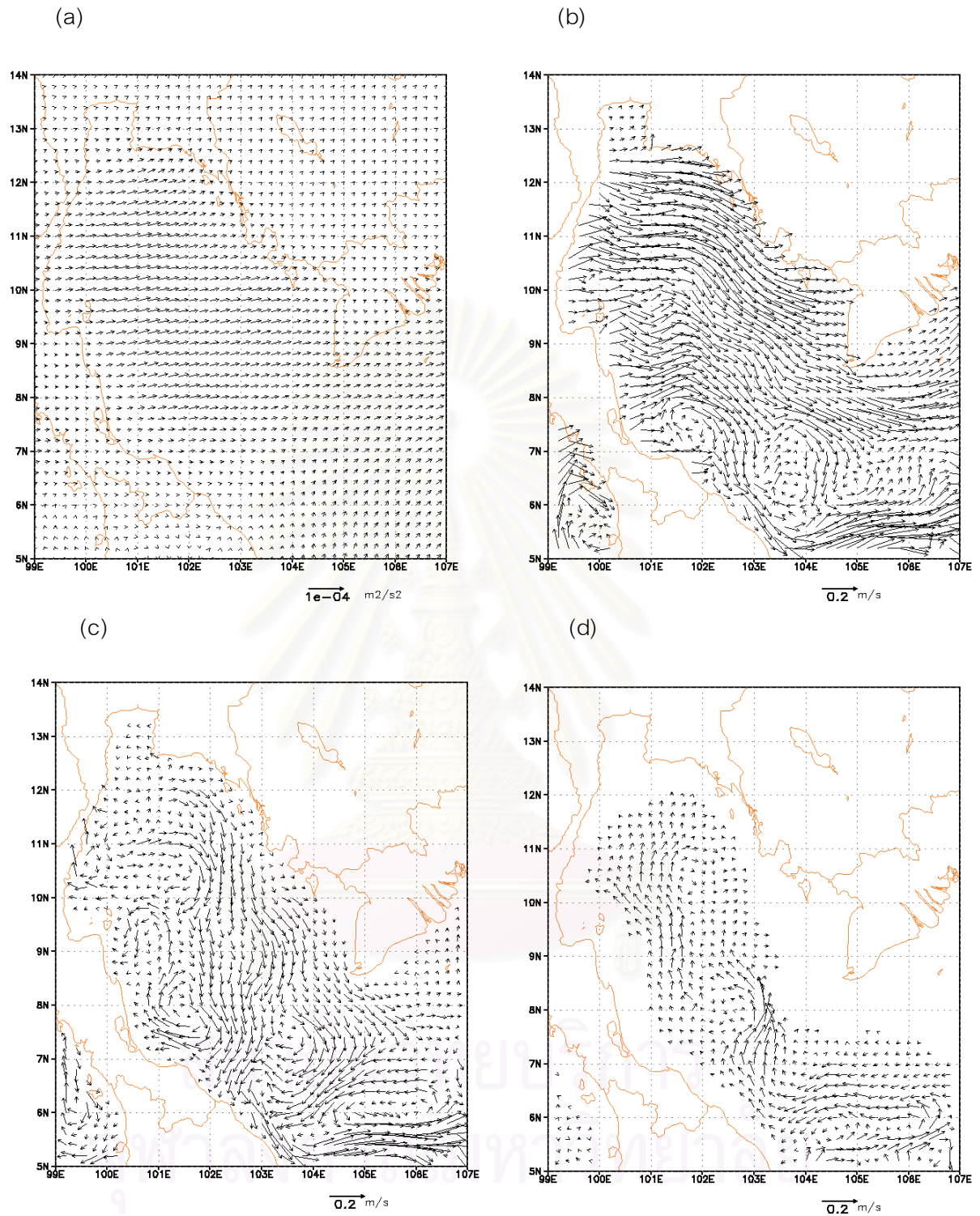


Figure C.6 Monthly mean wind stress and simulated current in June 2000

driven by NOGAPS wind and composite M2, S2, K1 and O1 tides at open boundaries

(a) wind stress from NOGAPS (b) surface current (c) current at 10 m depth (d) current at 40 m depth

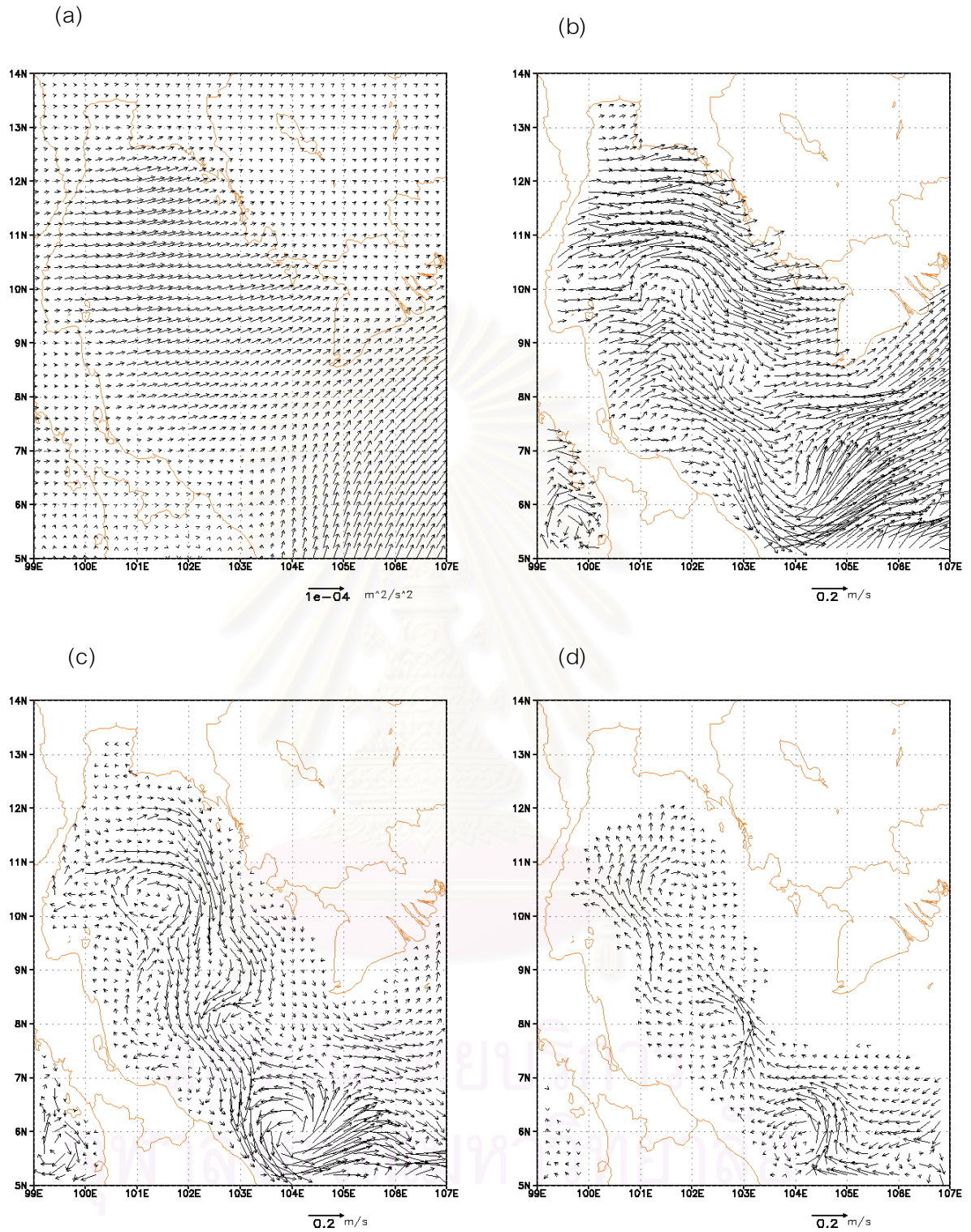
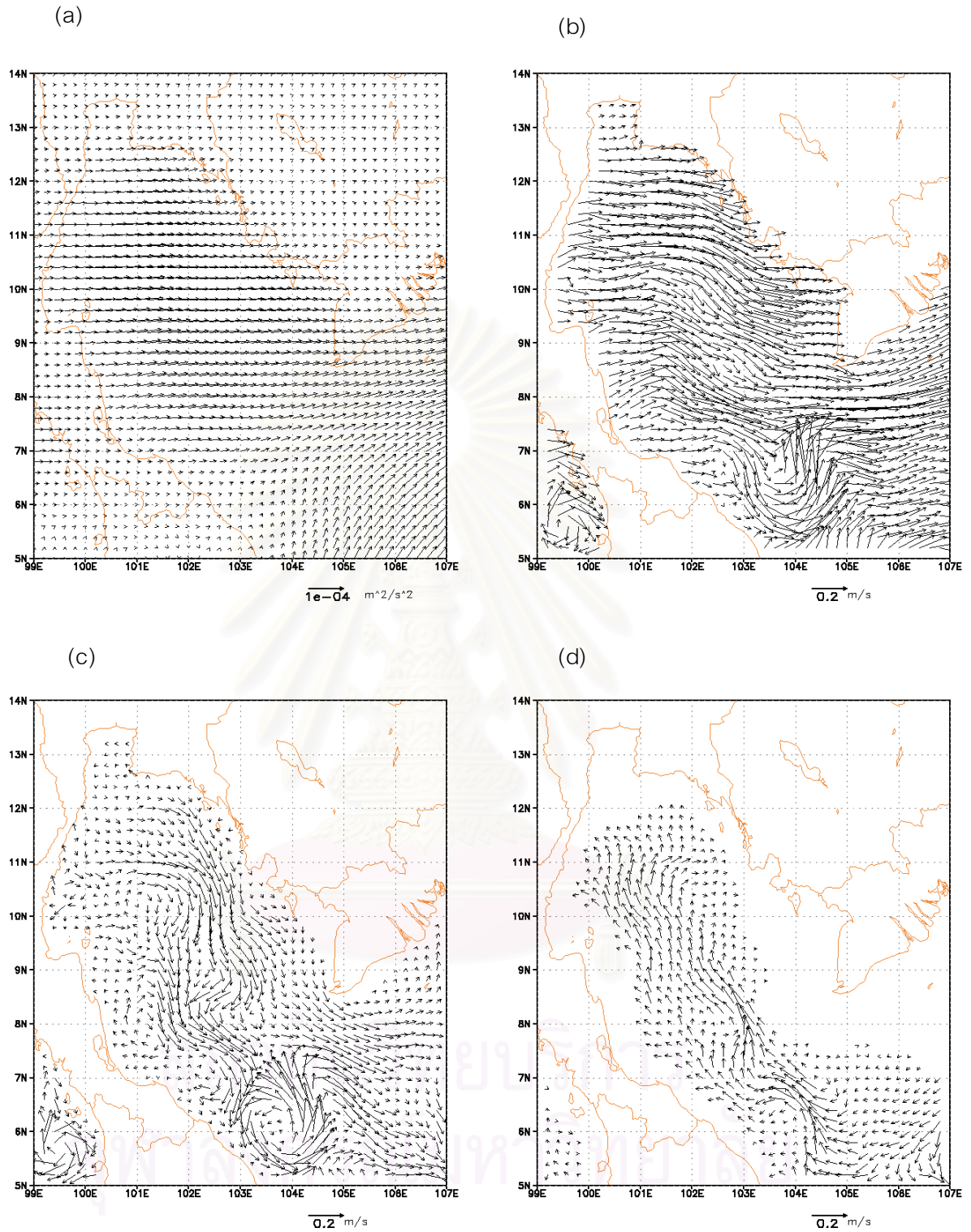


Figure C.7 Monthly mean wind stress and simulated current in July 2000

driven by NOGAPS wind and composite M2, S2, K1 and O1 tides at open boundaries

(a) wind stress from NOGAPS (b) surface current (c) current at 10 m depth (d) current at 40 m depth



**Figure C.8 Monthly mean wind stress and simulated current in August 2000**  
 driven by NOGAPS wind and composite M2,S2, K1 and O1 tides at open boundaries  
 (a) wind stress from NOGAPS (b) surface current (c) current at 10 m depth (d) current  
 at 40 m depth

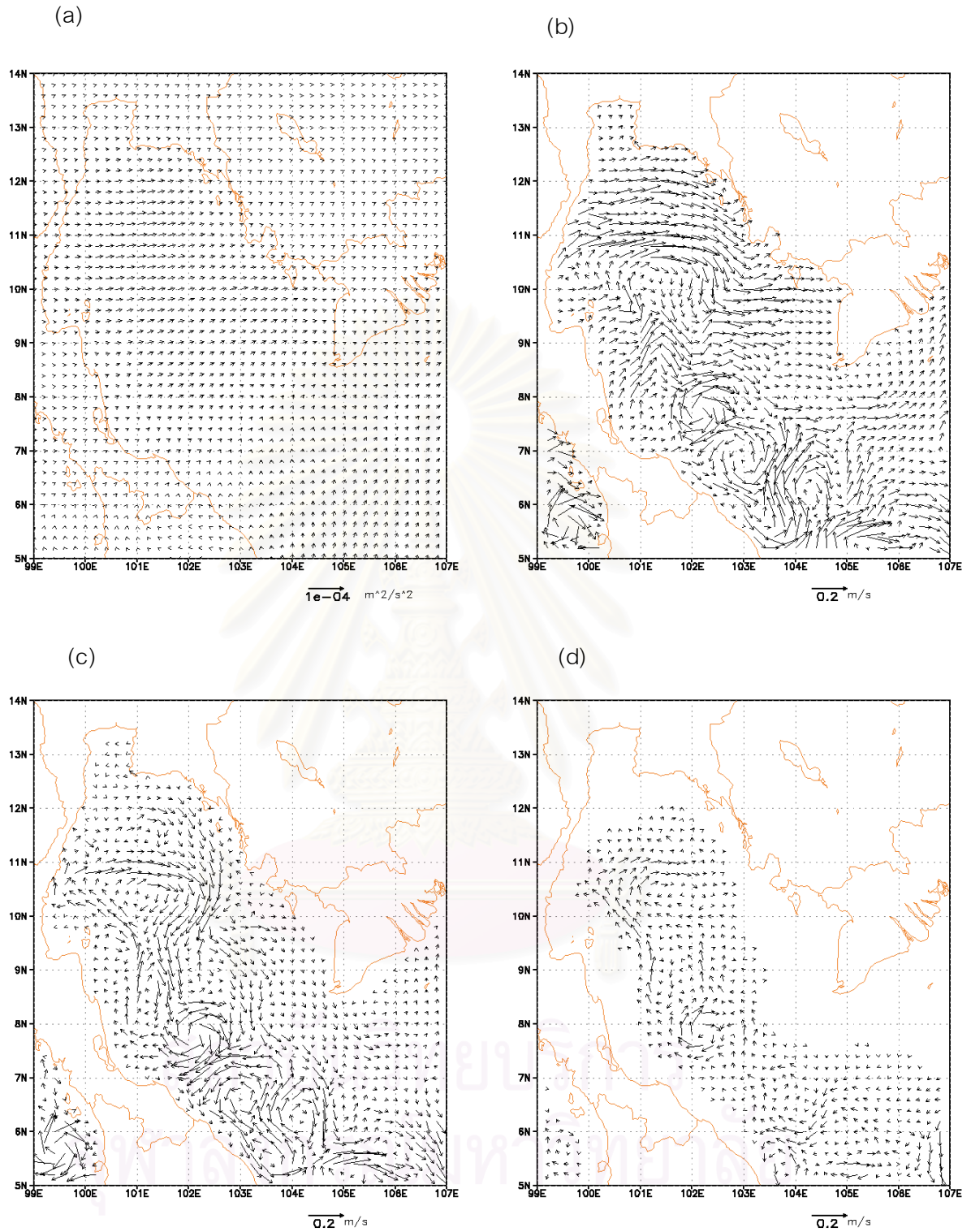


Figure C.9 Monthly mean wind stress and simulated current in September 2000 driven by NOGAPS wind and composite M2,S2, K1 and O1 tides at open boundaries (a) wind stress from NOGAPS (b) surface current (c) current at 10 m depth (d) current at 40 m depth

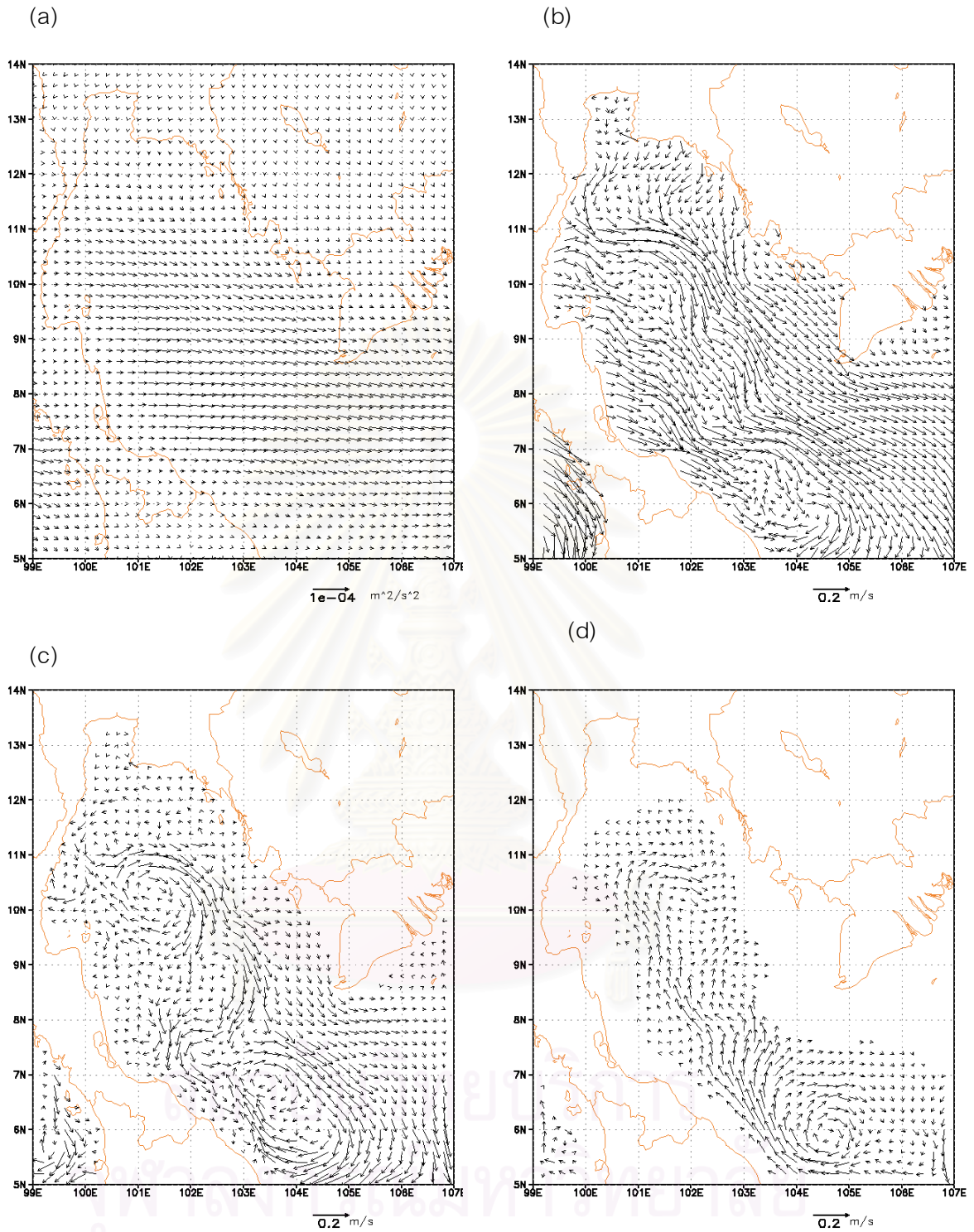


Figure C.10 Monthly mean wind stress and simulated current in October 2000 driven by NOGAPS wind and composite M2,S2, K1 and O1 tides at open boundaries (a) wind stress from NOGAPS (b) surface current (c) current at 10 m depth (d) current at 40 m depth

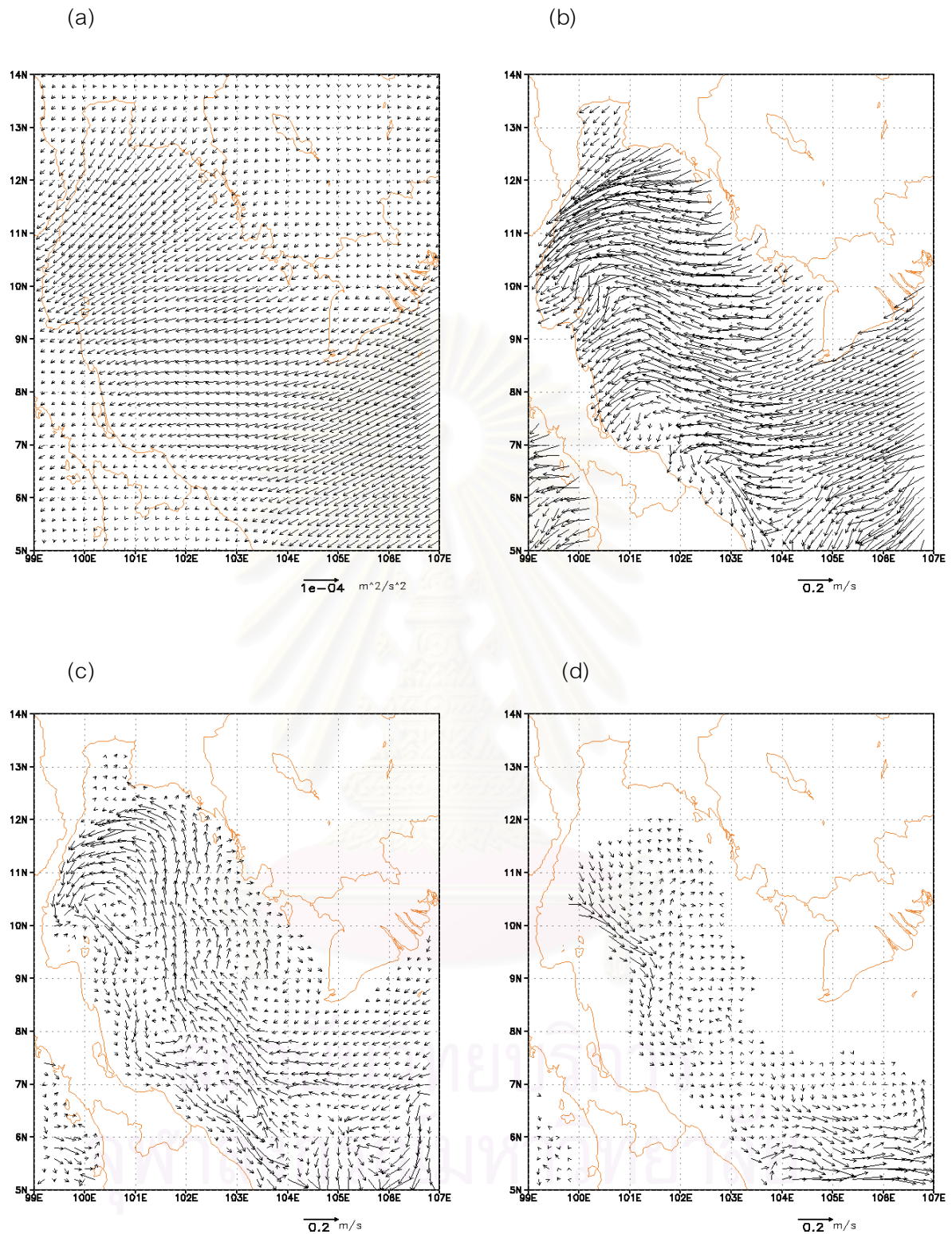


Figure C.11 Monthly mean wind stress and current in November 2000

driven by NOGAPS wind and composite M2, S2, K1 and O1 tides at open boundaries

(a) wind stress from NOGAPS (b) surface current (c) current at 10 m depth (d) current at 40 m depth

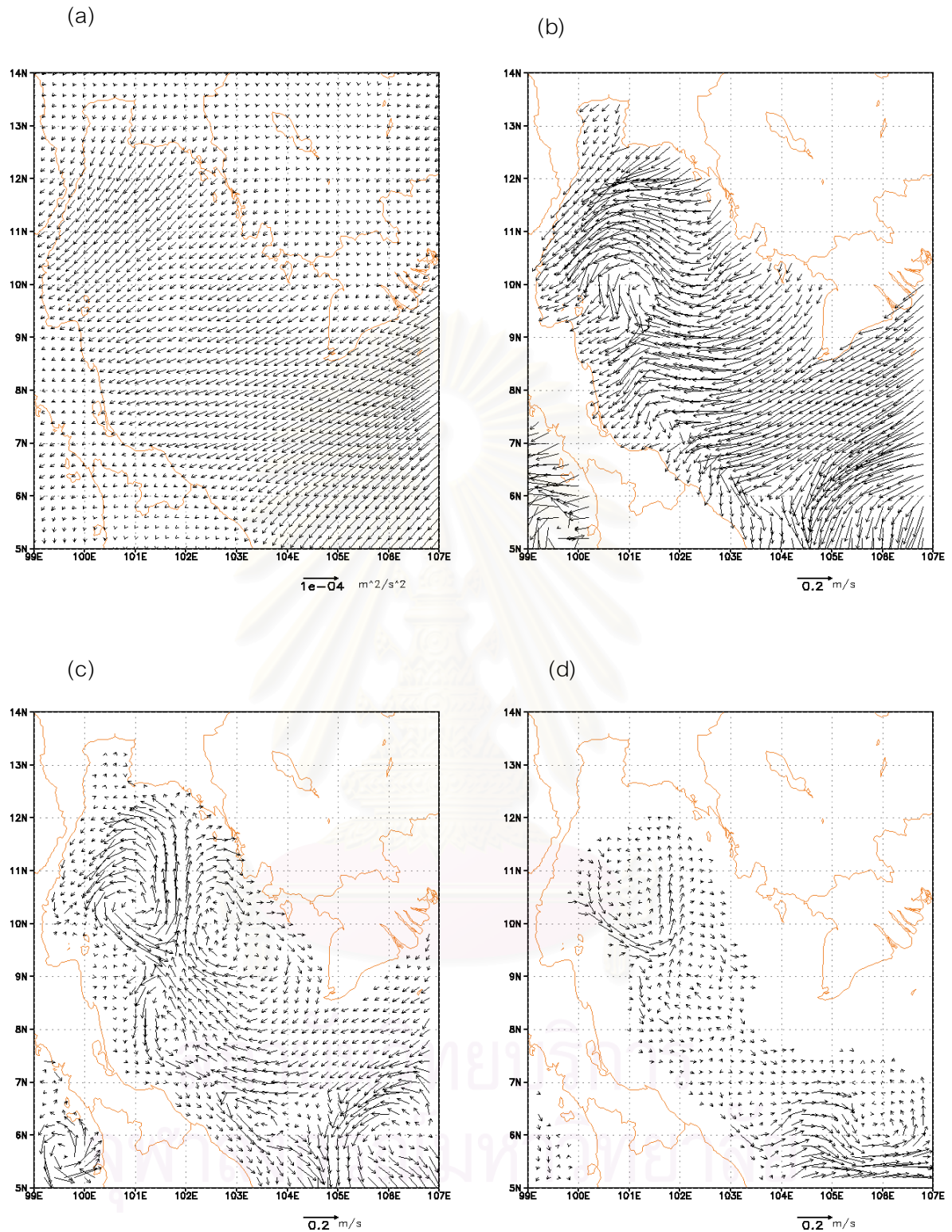


Figure C.12 Monthly mean wind stress and simulated current in December 2000 driven by NOGAPS wind and composite M2, S2, K1 and O1 tides at open boundaries  
 (a) wind stress from NOGAPS (b) surface current (c) current at 10 m depth (d) current at 40 m depth

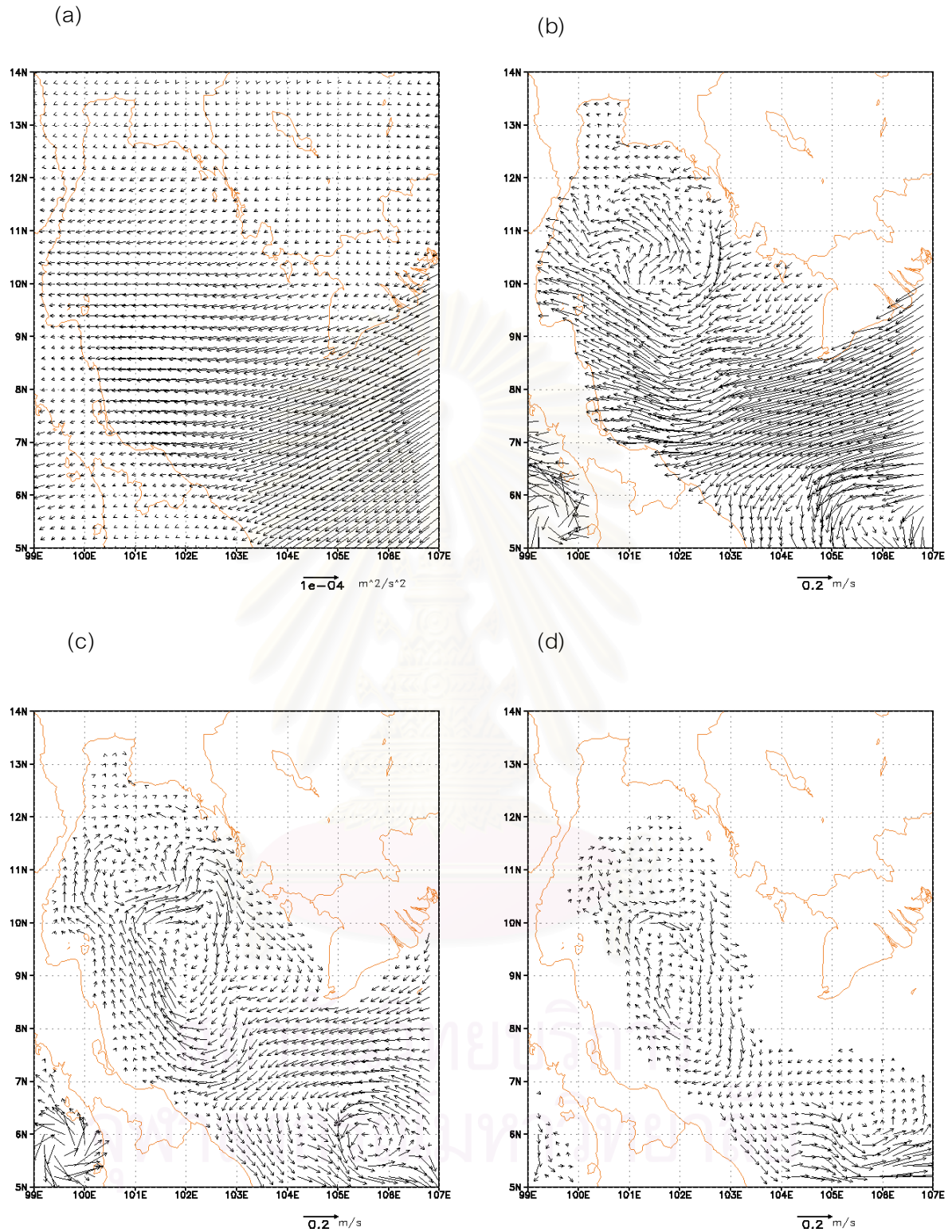


Figure C.13 Monthly mean wind stress and simulated current in January 2001 driven by NOGAPS wind and composite M2, S2, K1 and O1 tides at open boundaries (a) wind stress from NOGAPS (b) surface current (c) current at 10 m depth (d) current at 40 m depth



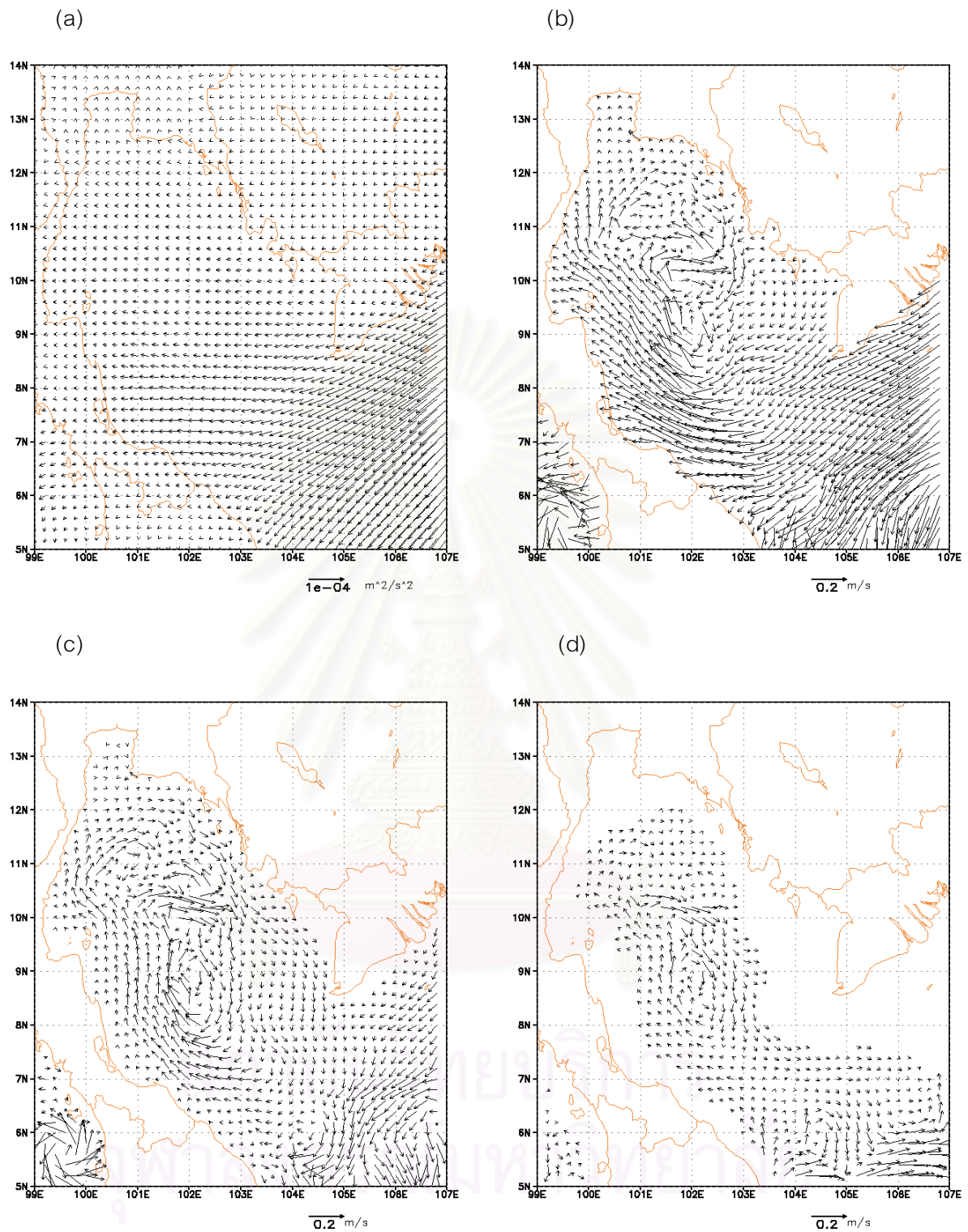


Figure C.14 Monthly mean wind stress and simulated current in February 2001 driven by NOGAPS wind and composite M2, S2, K1 and O1 tides at open boundaries (a) wind stress from NOGAPS (b) surface current (c) current at 10 m depth (d) current at 40 m depth

## BIOGRAPHY

Patama Singhruck was born on 18 August 1974 in Phitsanuloke. She received a Bachelor degree of Engineering in Electrical Engineering from King Mongkut's Institute of Technology North Bangkok in 1996. After graduation, she worked as an engineer for an energy conservation consultant company. In 1999, she entered a Master degree program at Department of Marine Science, Faculty of Science, Chulalongkorn University. She received the scholarship from Ministry of University Affairs in 2001.



สถาบันวิทยบริการ  
จุฬาลงกรณ์มหาวิทยาลัย